

APPLICATIONS TECHNOLOGY SATELLITE

HUGHES

HUGHES AIRCRAFT COMPANY
SPACE SYSTEMS DIVISION

FEBRUARY 1968

ATS POWER SUBSYSTEM RADIATION EFFECTS STUDY PHASE I/FINAL REPORT

NASA Contract NAS 5-3823

GPO PRICE \$ _____

CFSTI PRICE(S) \$ _____

Hard copy (HC) 3.00

Microfiche (MF) .65

ff 653 July 65

FACILITY FORM 602

N 68-23 889 (THRU)

127 (PAGES)

01-94612 (NASA CR OR TMX OR AD NUMBER)

(CODE)

31 (CATEGORY)

SSD 80089R

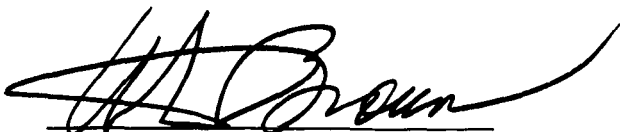
FEBRUARY 1968

APPLICATIONS TECHNOLOGY SATELLITE

ATS POWER SUBSYSTEM RADIATION EFFECTS STUDY

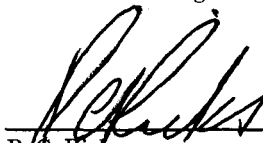
PHASE I/FINAL REPORT

NASA Contract NAS 5-3823



W. D. Brown
Task Force Manager

Approved: _____



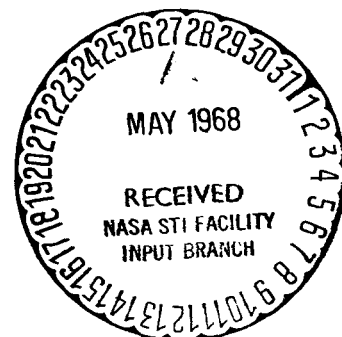
P. C. Ricks
Manager, Power System Department



T. A. Savo
ATS Senior Project Engineer
Engineering Laboratories

HUGHES

HUGHES AIRCRAFT COMPANY
SPACE SYSTEMS DIVISION



FOREWORD

This technical report presents the results of a special 2-month task force study conducted to analyze the anomalous degradation of the ATS-F1 solar cell arrays. The subject study was conducted by the Hughes Aircraft Company, Space Systems Division, El Segundo, California, for the NASA Goddard Space Flight Center under Contract NAS 5-3823. The work was administered under the direction of Mr. R. J. Darcey, ATS Project Manager, NASA Goddard. Mr. E. O. Marriott was the cognizant Hughes Aircraft Project Manager.

This report is being published and distributed prior to NASA review of the final draft. Its publication, therefore, does not constitute approval by NASA of the findings or conclusions contained herein. It is published solely for the exchange of technical information.

PRECEDING PAGE BLANK NOT FILMED.

ACKNOWLEDGMENT

The assistance of Dr. E. Stofel and Mr. L. Rachal of the Aerospace Corporation in the conduct of the proton irradiation tests and the cooperation of Dr. R. C. Waddel of NASA Goddard in supplying data from the ATS-F1 solar cell experiment are gratefully acknowledged. The authors assume full responsibility for the interpretation of these various data and apologize for any possible misinterpretations. The time constraints associated with this study precluded a careful cross-check of all reduced data and some errors were no doubt missed.

Principal Hughes Task Force Members

E. Angle	L. Macca
D. Cohen	A. Moses
R. Ellars	R. Parfitt
L. Goldhammer	A. Spreen
G. Hodgman	R. Steinhauer
S. Klapman	G. Todd
M. Lyon	

PRECEDING PAGE BLANK NOT FILMED.

SUMMARY

The first Applications Technology Satellite (ATS-F1) was launched into synchronous orbit in early December of 1966. The experiment complement included a special solar cell experiment designed by Dr. R. C. Waddel of NASA Goddard to evaluate the effect of the synchronous radiation environment on the electrical performance of several types of solar cells. Initial results from this experiment, covering the first 120 days of operation, indicated performance degradations which were anomalous in both magnitude and effect.

In an attempt to corroborate Dr. Waddel's finding, a representative sampling of ATS-F1 main array telemetry data, spanning the same 120-day time period, was reduced and evaluated. This preliminary analysis indicated a performance degradation on the order of 20 percent which was more severe by approximately a factor of four than the degradation experienced in the solar cell experiment.

Based on the best available synchronous environment model and the corresponding known radiation effects, a degradation rate on the order of 2 to 4 percent per year was expected as a direct result of the trapped electron environment component. The observed flight performance of the two Hughes spacecraft which have been in synchronous orbit for the longest period, Syncom III (launched August 1964) and Intelsat I (launched April 1965), was in good agreement with the model predictions.

Therefore, the apparent ATS-F1 main array degradation did not correlate with either the solar cell experiment or with predictions based on the synchronous environment model and previous flight experience.

As a result of these anomalies, a 2-month task force study was initiated in November 1967 in a concerted attempt to identify the damage mechanism (s) and to define corrective action for subsequent ATS spacecraft. The results of this task force study are presented in this report.

As the first logical step, all available flight data for six Hughes synchronous satellites and for the special ATS-F1 solar cell experiment were reduced to provide all possible relevant clues. Based on these data, it was apparent that the synchronous environment was having vastly differing effects on the various cells and arrays. Array performance degradations after 1 year in orbit varied from approximately 2 percent for Syncom III and Intelsat I to 32 percent for the ATS-F1 aft solar panel. Since all of the degradations

exhibited a logarithmic time dependence, it was summarily assumed that radiation effects of some type were the basic cause. The inconsistency of the performance data strongly suggested one or more uncontrolled significant variables, probably associated with the solar cells or the solar cell modules.

To identify the critical variable(s), a comparative analysis of component properties was conducted for the various solar cell assemblies. The only variable which appeared to correlate with the observed performance degradations was exposed cell area around the periphery of the coverslides. The Syncom III and Intelsat I arrays, which apparently did not degrade in an abnormal fashion, utilized a shingled solar cell module configuration which essentially prevented the exposure of any bare cell area. The two arrays which degraded at the highest rate, ATS-F1 and Intelsat II-F4, both had significant exposed cell areas.

The effect of penetrating radiation on small exposed areas would be a loss proportional to the fraction of the active cell area exposed. Such a loss would normally be negligible. However, the effect of low-energy proton irradiation of partially shielded cells had not been carefully considered. The first comprehensive model of the trapped low-energy proton environment became available in early 1967 (see Appendix A), but the significance of this environment component was not fully appreciated.

To evaluate this possible new damage mechanism, a laboratory irradiation test program was conducted using proton energies and fluences comparable to those expected in a synchronous orbit. The results dramatically confirmed that low-energy proton damage to exposed cell areas was the primary mechanism responsible for the ATS-F1 and Intelsat II-F4 performance degradations. A new evaluation technique termed "loss function analysis" was developed in the process of evaluating the various data and in performing the required correlation studies. This approach proved invaluable in isolating and identifying the various damage mechanisms.

To protect the cells on in-process ATS arrays, a low-energy proton shield was required which could be economically applied to the cell assemblies. Several candidate coatings were evaluated and a modified epoxy was chosen that is identical to the solar cell adhesive used on the ATS arrays. The details of the test program are presented in Appendix E of this report.

The solar cell experiment data exhibited a marked loss in short-circuit current for virtually all of the cell samples. A cross-correlation of the various data identified the degradation source as a transmission loss in the coverslide assemblies. This loss appeared to be a surface effect, independent of coverglass type, coatings, adhesives, etc. A similar loss appeared to affect the performance of the ATS-F1 aft solar panel, but not the forward panel. Additional flight data spanning a longer time period should be reduced to confirm this observation. Based on the available data, it is concluded that the ATS-F1 aft panel and the solar cell experiment which was mounted on the aft panel were contaminated by some substance which darkened with time under ultraviolet (UV) and/or low-energy proton exposure.

In addition to the transmission loss phenomenon, the solar cell experiment data also exhibited an anomalous maximum power degradation phenomenon which was proportional to coverglass thickness. The loss function analysis approach was applied to this data and the damage mechanism was identified as a shunt loss effect, similar to that resulting from low energy proton damage to small exposed areas. However, it seems improbable that exposed cell area would be related to coverglass thickness. Recommendations for further study of this anomaly are presented in Section 5 of this report.

The optimal modeling technique used to reduce the solar cell experiment data met all expectations. This data reduction technique and the loss function analysis methodology can be profitably applied to further study in several areas, including evaluation of ATS-F3 flight performance data.

CONTENTS

	<u>Page</u>
1.0 INTRODUCTION	1-1
2.0 TECHNICAL APPROACH	
2.1 Rationale	2-1
2.2 Program Plan	2-1
3.0 FLIGHT DATA EVALUATION	
3.1 Summary of Hughes Flight Experience	3-1
3.2 General Power Subsystem Characteristics	3-1
3.3 In-Orbit Performance Results	3-2
4.0 RADIATION EFFECTS ANALYSIS	
4.1 Comparative Evaluation of Component Properties	4-1
4.2 Identification of Possible Damage Mechanisms	4-5
4.3 Correlation Analyses	4-9
5.0 CONCLUSIONS AND RECOMMENDATIONS	
5.1 Conclusions	5-1
5.2 Recommendations	5-3
6.0 REFERENCES	6-1
APPENDICES	
A. SYNCHRONOUS ORBIT RADIATION ENVIRONMENT	A-1
B. ATS TRANSFER ORBIT RADIATION ENVIRONMENT	B-1
C. DATA REDUCTION TECHNIQUES	C-1
D. LOW ENERGY PROTON IRRADIATION TESTS OF SOLAR CELL ASSEMBLIES	D-1
E. LOW ENERGY PROTON SHIELD INVESTIGATION	E-1
F. ANGLE OF INCIDENCE EFFECTS ON THE PERFORMANCE OF CYLINDRICAL SOLAR PANELS	F-1

PRECEDING PAGE BLANK NOT FILMED.

1.0 INTRODUCTION

In early December of 1966, the first Applications Technology Satellite (ATS-F1) was launched into synchronous orbit. The ATS series of spacecraft, developed by Hughes Aircraft Company for NASA Goddard Space Flight Center, are designed to provide versatile earth orbital test vehicles for a wide variety of experiments. The ATS-F1 experiment complement included a solar cell experiment designed by Dr. R. C. Waddel of NASA Goddard to evaluate the effects of the synchronous environment on the electrical performance of several types of solar cell assemblies. Initial results from this experiment covering the first 120 days of operation indicated performance degradations that were anomalous in both magnitude and effect.

Based on the best available model for the synchronous orbit radiation environment (See Appendix A), a maximum power degradation rate in the range of 2 to 4 percent per year was expected as a result of the trapped electron environment. With the exception of solar flare protons, no other component of the environment was believed to be significant. The flight performance data of Syncom III (launched 19 August 1964) and Intelsat I (launched 6 April 1965) were consistent with this model within the error tolerances of the sensors and the associated data reduction techniques. However, during the first 120 days of ATS-F1 operation, a maximum power degradation on the order of 7 percent was observed for similar cell assemblies (N/P, 10 ohm-cm cells with 15-mil, Corning 7940 quartz coverslides) in Dr. Waddel's experiment². The degradation magnitude appeared to correlate with coverglass thickness. Surprisingly, the data indicated an optimum 7940 quartz coverglass thickness of approximately 6 mils with monotonically increasing maximum power degradation for thicker slides. However, the degradation in short-circuit current appeared to be independent of coverslide thickness. Equally anomalous performance was observed for other cell and coverslide types. Qualitatively, the degradation phenomena appeared to exhibit a logarithmic-time-dependence which is characteristic of radiation effects.

In an attempt to corroborate Dr. Waddel's findings, a representative sampling of ATS-F1 main array telemetry data spanning the same 120-day time period was reduced and evaluated. This preliminary analysis indicated a performance degradation on the order of 20 percent which also appeared to be a logarithmic function of time in orbit. Similar cell assemblies (N/P, 10 ohm-cm cells with 30-mil, Corning 7940 quartz coverslides) in the solar cell experiment degraded only about 8 percent. Therefore, the apparent main

array performance did not correlate with either the solar cell experiment or with predictions based on the environment model and previous flight experience.

As a result of these observed flight performance anomalies, a 2-month task force study was initiated in November 1967 in a concerted attempt to identify the damage mechanism(s) and to define corrective action for subsequent ATS spacecraft. The results of this task force study are presented in this report.

2.0 TECHNICAL APPROACH

The extremely short time constraint of 2 months, which resulted from the in-process ATS array fabrication schedules, required that the scope of the study be closely controlled for rapid convergence toward the most probable damage mechanisms. The study rationale and program plan are briefly described in the following subsections.

For clarity, the organization of this report is keyed to the significant study results instead of to the program plan.

2.1 RATIONALE

Based on the logarithmic behavior of the observed degradations as noted in Section 1.0, it was summarily assumed that radiation exposure was the basic damage source. In addition, since the solar cell experiment results were also anomalous, it was assumed that the primary degradation mechanism(s) were associated with solar cell or solar cell module performance, with system influences (e. g., angle of incidence effects associated with cylindrical panels) tending to magnify or reduce the effect relative to apparent array performance. It was also considered highly improbable that the assumed synchronous orbit radiation environment was grossly in error. The inconsistency of the observed flight data strongly suggested one or more uncontrolled, significant variables associated with the solar cells or solar cell modules.

2.2 PROGRAM PLAN

Based on the above assumptions, the task force study was planned and conducted in accordance with the logic flow diagram shown in Figure 2-1. In addition, to ensure that a significant environment component was not being ignored, a careful review of the synchronous orbit radiation environment was conducted. An updated model is presented in Appendix A of this report.

All available synchronous orbit flight data for Hughes spacecraft were reduced to provide as many relevant clues as possible. Based on the observed array performance data, a loss function analysis was conducted to define the required changes in the respective solar cell V-I (voltage-current) relations. A comparative evaluation of array component properties was also conducted

to identify differences in the solar cells and solar cell modules used in the various arrays. These data, combined with the assumed environment, were then utilized in a radiation effects study to identify the probable damage mechanisms. Where possible, the postulated damage mechanisms and the proposed shield design were verified through laboratory tests.

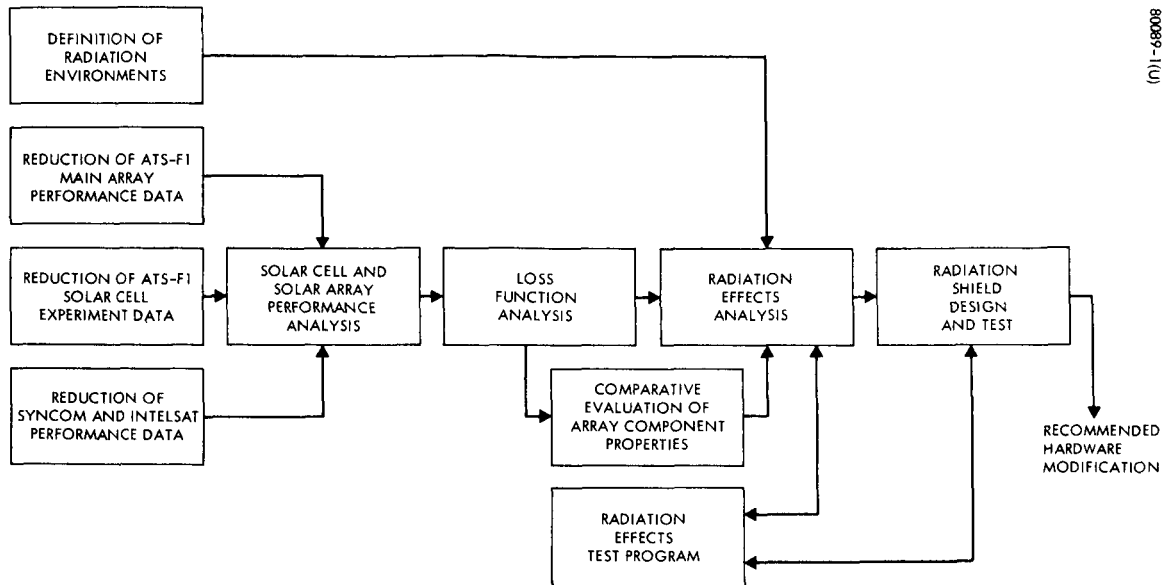


Figure 2-1. ATS Power Subsystem Radiation Effects Study - Logic Flow Diagram

3.0 FLIGHT DATA EVALUATION

3.1 SUMMARY OF HUGHES FLIGHT EXPERIENCE

To date, Hughes Aircraft Company has designed and developed eight synchronous orbiting satellites. These spacecraft are enumerated in Table 3-1 with corresponding launch dates and sponsoring agencies. All are currently operational.

The Syncom series of spacecraft developed by Hughes for NASA Goddard were experimental vehicles designed to demonstrate the feasibility of spin-stabilized, synchronous, communication satellites. The first spacecraft (Syncom I) was lost due to an on-board explosion of a nitrogen control system tank. The following two spacecraft (Syncoms 2 and 3) were completely successful.

Commercial utilization of the new technology resulting from the Syncom project began in early 1965 with the Intelsat I Communications Satellite, developed by Hughes for the Comsat Corporation. Three additional commercial spacecraft have been developed for Comsat in the current Intelsat II program.

A stable, synchronous spacecraft provides an ideal earth orbital experiment platform. The Applications Technology Satellites, developed by Hughes for NASA Goddard, were designed to provide versatile test vehicles for a wide variety of experiments. The Environmental Measurements Experiment (EME) on-board ATS-F1 included a special solar cell experiment that provided the data that motivated the special study covered by this report.

3.2 GENERAL POWER SUBSYSTEM CHARACTERISTICS

All of the Hughes synchronous satellites use cylindrical solar cell arrays as the prime power source with rechargeable nickel-cadmium batteries for eclipse operation. In accordance with the study rationale presented in Section 2.1, the solar array characteristics were given prime consideration. Detailed component property data for the cells and modules used in the various arrays are presented in Table 4-1, Section 4.0 of this report.

TABLE 3-1. HUGHES SYNCHRONOUS ORBITING SPACECRAFT

	Spacecraft	Launch Date	Customer	Comments
1	Syncom 2	26 July 1963	NASA Goddard	Special solar cell experiment
2	Syncom 3	19 August 1964	NASA Goddard	
3	Intelsat I	6 April 1965	Comsat	
4	ATS-F1	6 December 1966	NASA Goddard	
5	Intelsat II-F2	11 January 1967	Comsat	
6	Intelsat II-F3	23 March 1967	Comsat	
7	Intelsat II-F4	28 September 1967	Comsat	
8	ATS-F2	5 November 1967	NASA Goddard	

The only array using p/n cells was Syncom II. Series-connected 5-cell shingled modules were used on the Syncom arrays and the Intelsat I array. All subsequent arrays used a conventional interconnected matrix of flat-mounted cells. With the exception of the ATS spacecraft, all of the arrays used cells with 12-mil quartz coverslides. The ATS arrays used 30-mil shields.

3.3 IN-ORBIT PERFORMANCE RESULTS

With the exception of Syncom II and ATS-F2, array performance data for all of the Hughes synchronous satellites are discussed in following subsections. The Syncom II data were not considered because p/n cells (relative to n/p) exhibit a marked difference in response to radiation exposure. The ATS-F2 spacecraft was just recently launched (5 November 1967) and the relevant flight data are not yet available.

With the exception of ATS-F1, the power subsystems under consideration are poorly instrumented. The only telemetered data are the bus voltages. The electrical loads were assumed to be constant current devices and the total current for any particular load combination was calculated from ground measurements. The mean array temperatures were estimated analytically. If all possible error tolerances were considered, an extremely complex analysis would be required for a meaningful performance evaluation. However, from a practical standpoint, engineering judgment can be applied to weight the significance of data regularity, probable data trends, etc., and to draw meaningful conclusions. In any event, engineering judgment must be considered a primary basis for the performance evaluation of these arrays.

However, both the ATS-F1 power subsystem and the special solar cell experiment have adequate instrumentation (i. e., current sensors, voltage sensors, and temperature sensors) for precise performance analyses.

A summary of the various flight data is presented in the following subsections. A detailed interpretation of the data, including the ATS-F1 solar cell experiment data, is presented in Section 4.0 (Radiation Effects Analysis) of this report.

Syncom III and Intelsat I

The Syncom III and Intelsat I spacecraft (launched 19 August 1964 and 6 April 1965, respectively) have logged the most flight time in synchronous orbit. As shown in Figure 3-1, the solar arrays on both of these satellites have degraded in apparent maximum power at a regular rate of approximately 2 percent per year, which is in reasonable agreement with the minimum limit of the expected degradation due to the time-averaged, trapped electron environment described in Appendix A.

To reduce the flight data, it was necessary to assume a periodic array temperature profile correlated with the season of the year. The convergence or divergence of the calculated temperature profile was found to be extremely sensitive to the assumed rate of array degradation. It is possible that the thermal control surfaces could have degraded significantly with time which would directly influence the apparent array performance. However, it is improbable that such changes would result in a lower mean array temperature. It is also improbable that the load currents would have significantly decreased. Therefore, the apparent degradation rate should be conservative. It should be noted that performance degradations occurring on the order of days after launch could be masked by a greater than expected initial performance.

ATS-F1

As was previously noted, the ATS-F1 solar arrays were well instrumented, and in addition, a special solar cell experiment was included in the spacecraft experiment complement. In general, the data for both the experiment and the spacecraft solar panel are considered valid performance indications for the respective solar cells and arrays.

Solar Cell Experiment

Experiment Description

The ATS-F1 solar cell experiment, designed by Dr. R. C. Waddell of NASA Goddard, was composed of a group of 30 1-by-2 centimeter solar cells, which included several cell types with various coverglass shields. A detailed description of the cell assemblies comprising the experiment is shown in Table 3-2. The Corning 7940 and 0211 coverslides were coated

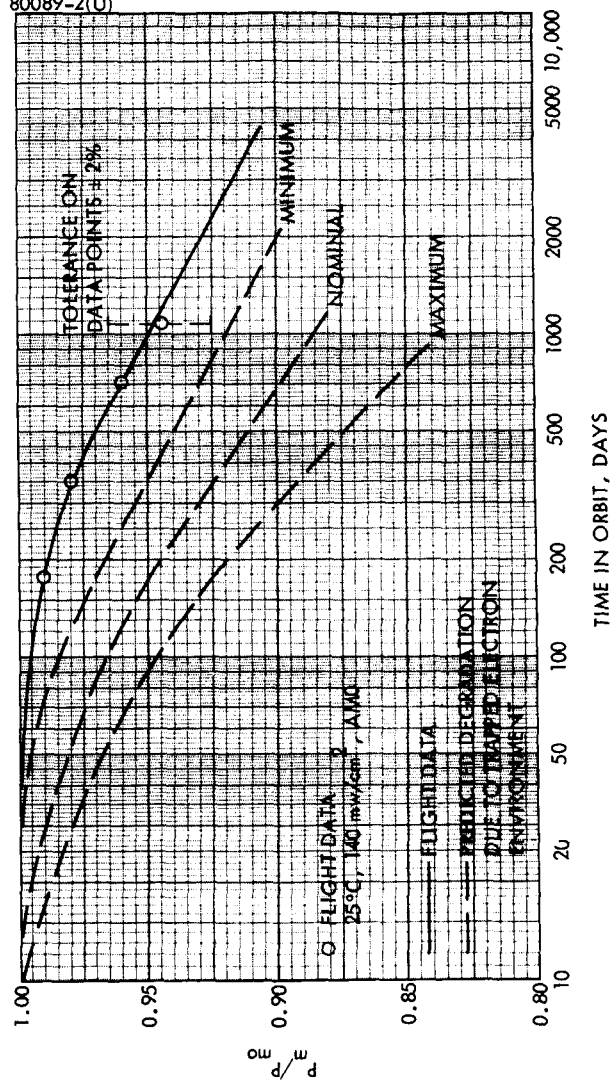


Figure 3-1. Syncom III and Intelsat I In-Orbit Performance

TABLE 3-2. SOLAR CELL DESCRIPTION, ATS-F1 SOLAR
CELL EXPERIMENT ¹

Solar Cell Number	Type	Base Resistivity, ohm-cm	Dopant	Shield Material	Shield Thickness, mils
1, 2	N/P	10	Al	Sapphire	30
3, 4	N/P	13	B	7940 silica	6
5, 6	N/P	10	B	7940 silica	6
7, 8	N/P	7	B	7940 silica	6
9, 10	N/P	3	B	7940 silica	6
11, 12	N/P	Graded	B	7940 silica	6
13	P/N	1	P	None	0
14	N/P	1	B	None	0
15, 16	N/P	10	B	7740 glass	1
17, 18	N/P	10	B	0211 glass	6
19, 20	N/P	10	B	7940 silica	60
21, 22	N/P	10	B	7940 silica	30
23, 24	N/P	10	B	7940 silica	15
25, 26	N/P	10	B	None	0
27, 28	N/P	10	Al	7940 silica	30
29, 30	N/P	10	Al	7940 silica	6

with both a magnesium-fluoride antireflection coating and a "blue" reflecting filter (400-millimicron cutoff). Where used, the coverglass adhesive was Dow Corning XR-634-88. The integral shields (Corning 7740) used neither coatings nor adhesives. Two cells (numbers 1 and 2) had uncoated sapphire shields which were mechanically supported above the cells without the use of an adhesive.

The electronics package associated with the experiment was designed to sequentially connect each of eight fixed load resistors to each cell. A hold circuit was utilized to record the maximum voltage developed across each load resistor during a spacecraft rotation (the ATS-F1 spacecraft is spin-stabilized). Sensor data were also recorded to determine the angle of illumination (1 degree increments). Cell temperatures were monitored by a thermocouple which was located at approximately the center of the 4- by 8-inch magnesium panel (0.125 inch thick). The point temperature readings are considered accurate to within $\pm 1^\circ\text{C}$. Dr. Waddel did not place a specific tolerance on the possible temperature gradients across the mounting plate. However, the plate was thermally isolated, and based on Hughes analysis, a gradient exceeding approximately $\pm 2^\circ\text{C}$ appears improbable.

The maximum possible accuracy permitted by the 8-bit analog-to-digital converter was approximately $\pm 3\text{ mv}$ for telemetered voltages and $\pm 0.3\text{ milliamperes}$ for telemetered currents. The consistency and repeatability of the processed data were such that Dr. Waddel believes the data accuracy to be within these optimal limits (i. e., all other telemetry error sources are believed to be negligible)². The percentage tolerance associated with any given voltage or current is, of course, dependent upon the absolute magnitude of the respective parameter.

Data Reduction Technique

Based on prelaunch calibration data, Dr. Waddel utilized a computer program to correct the primary data to an equivalent illumination intensity of 140 mw/cm^2 (corresponding to the mean earth-sun distance) normal incidence. With a few exceptions (see Table 3-2), there were two identical cell-coverglass assemblies of each type in the experiment. This is not statistically significant but Dr. Waddel observed that the cells of any given pair performed in a very similar fashion². Based on the data plots of Reference 2, it appears that for voltages equal to or less than the maximum power point, the typical current differential between samples of the same type was on the order of 1 milliamperes. Using the 8 voltage-current points for each of the samples (which normally spanned a voltage range from 200 mv to open-circuit), Dr. Waddel estimated a "best fit" average curve for the pair. He did not attempt to perform temperature corrections.

Using the intensity corrected, average V-I data provided by Dr. Waddel^{1, 2, 3, 4}, an independent data reduction and analysis study was conducted by Hughes. The data reduction technique is based on the solar cell mathematical model which is described in detail in Reference 5 and an associated parametric optimization routine which is summarized in

Appendix C. The subject mathematical model analytically simulates the solar cell V-I relation in the power generation region. It is based on the physics of the photovoltaic energy conversion process, and as demonstrated in Reference 5, the model is capable of a remarkably precise match (rms errors on the order of 0.2 to 0.5 percent) to a given V-I curve over a wide range of environmental conditions.

The mathematical relation is solely a function of four parameters: I_{sc} , I_{mp} , V_{mp} and V_{oc} . These parameters are, of course, uniquely defined for any given V-I curve. Therefore, given a set of V-I pairs spanning a reasonable voltage range, there will be a unique set of the four parameters which will result in a V-I relation most nearly matching (e.g., in terms of rms error) the given data pairs. The optimization routine mentioned above uses a gradient technique to define the optimal parameter set. This general data reduction technique is now used as a matter of standard procedure in Hughes ground tests of cell and/or array performance. The program also has appropriate statistical subroutines to calculate the average performance for multiple data sets for either a single cell or a group of cells.

For application to the solar cell experiment, the optimal approach would be to input the eight V-I data sets for each of the two cell samples. The program would then optimally calculate the corresponding average V-I relation. However, time and cost constraints precluded this approach for the current analyses and, as an alternative, nine V-I pairs were selected as input data from each of Dr. Waddel's "average" V-I curves. Temperature corrections were performed based on the assumed temperature coefficients listed in Table 3-3. The voltage coefficients should remain stable under penetrating irradiation⁶. However, the current temperature coefficients are known to increase⁶. The effect of nonpenetrating radiation (e.g., low-energy protons) on these coefficients is virtually unknown. In any event, the uncertainty in the subject coefficients does introduce an additional error. Hopefully, this error will be less than that resulting from no temperature corrections.

TABLE 3-3. ASSUMED TEMPERATURE COEFFICIENTS

$\frac{\Delta I_{sc}}{\Delta T} = 37 \times 10^{-6} \text{ amps/}^\circ\text{C}$	$\frac{\Delta V_{oc}}{\Delta T} = -2.25 \times 10^{-3} \text{ volts/}^\circ\text{C}$
$\frac{\Delta I_{mp}}{\Delta T} = 29 \times 10^{-6} \text{ amps/}^\circ\text{C}$	$\frac{\Delta V_{mp}}{\Delta T} = -2.1 \times 10^{-3} \text{ volts/}^\circ\text{C}$

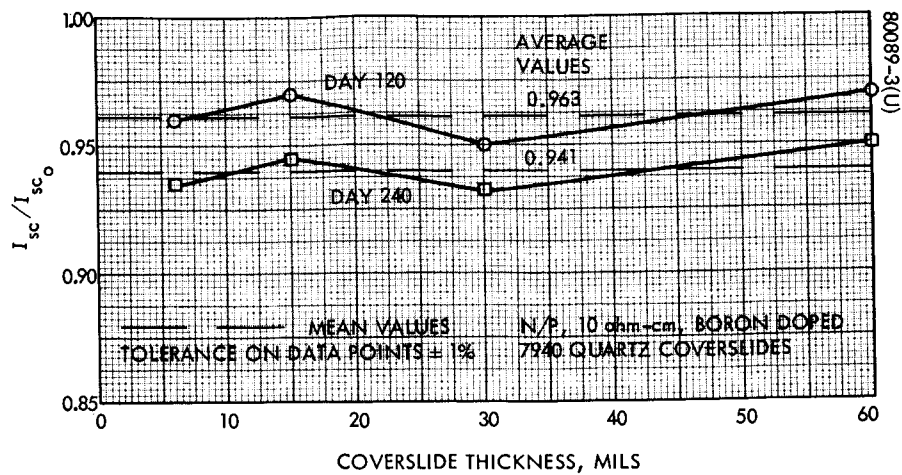


Figure 3-2. Short-Circuit Current Performance as Function of Coverglass Thickness

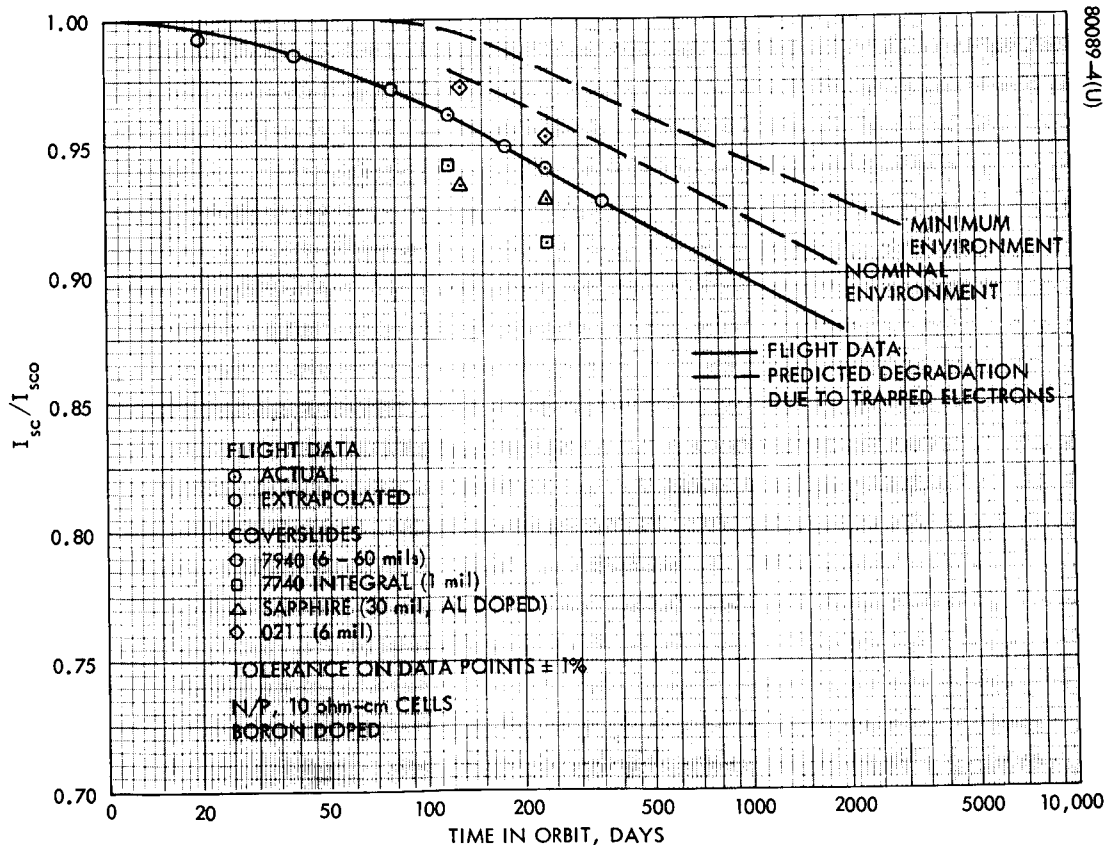


Figure 3-3. Average Short-Circuit Current Degradation as Function of Time

The absolute magnitudes of the performance degradations observed in the experiment were generally in the 1 to 5 percent range. Therefore, the interpretation of the various data is greatly influenced by the assumed tolerances. The telemetry inaccuracies of ± 3 mv for voltages and ± 0.3 milli-ampere for currents result in a nominal tolerance of approximately ± 0.5 percent for both open-circuit voltages and for cell currents in region of most concern between short-circuit and maximum power. Voltage values in the maximum power region would be subject to a greater error on the order of ± 0.77 percent. The extrapolation of the eight V-I points to deduce short-circuit performance and, in particular, maximum-power performance introduces an additional tolerance which is only partially compensated by averaging the data for two cells. Since points off the average V-I curve (including I_{sc} and V_{oc}) were used as input data, the model optimization program would not significantly reduce these errors. The unknown temperature gradients introduce another possible error. The tolerances listed in Table 3-4 were assumed for this study. These values are quite likely optimistic.

For obvious reasons, the performance data presented in this report, which were derived through the techniques described above and which will be subsequently analyzed, constitute a Hughes interpretation of the solar cell experiment data. Due to the time constraints associated with this study, these results and the underlying reduction and analysis techniques have not been completely reviewed by Dr. Waddel, and therefore should not be necessarily assumed to have his concurrence.

Results

For clarity, the experiment results will be discussed in terms of performance in the following operating regions: 1) $V \cong 0$ (short-circuit), 2) $I \cong 0$ (open-circuit), and 3) $V \cong V_{mp}$ (maximum power). Only the first 240 days of in-orbit data are considered.

Short-circuit current data for 10 ohm-cm, boron-doped, N/P cells are shown in Figure 3-2 as a function of coverglass thicknesses between 6 and 60 mils. Two points in time (days 120 and 240) are considered. All of the coverslips are Corning 7940 quartz with an antireflective coating, a blue filter, and Dow XR-634-88 adhesive. Each data point in the 6- to 30-mil thickness range represents a two-cell average. The 60-mil data is for a single cell. The scatter in the data for each of the time periods is within the assumed limits. Therefore, the short-circuit current performance for these cells appears to be independent of coverglass thickness with an average degradation of 3.7 percent at 120 days and 5.9 percent at 240 days. The average data are plotted in Figure 3-3 on a semilog scale.

With reference to Figure 3-3, the extrapolated flight data points were derived through a smooth curve fit to the day 120 and day 240 data on a linear time scale. Short-circuit current data are also shown in Figure 3-3 for 1-mil, 7740 integral coverslips (no coatings, no adhesive); 30-mil sapphire

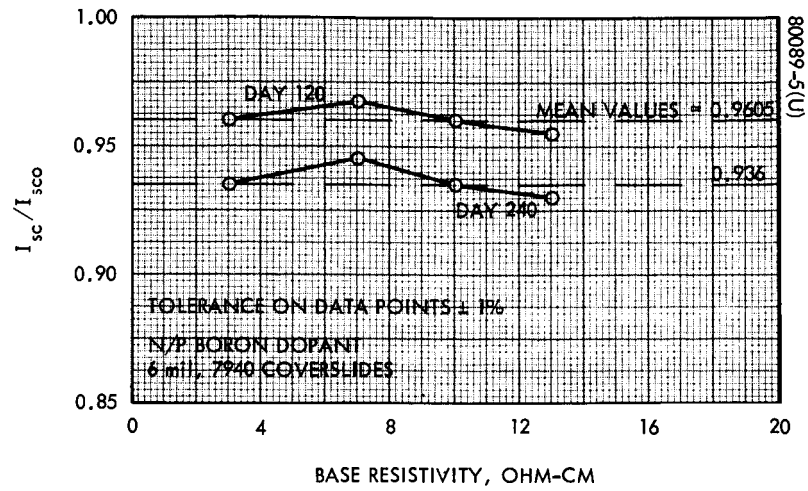


Figure 3-4. Short-Circuit Current Degradation as Function of Base Resistivity

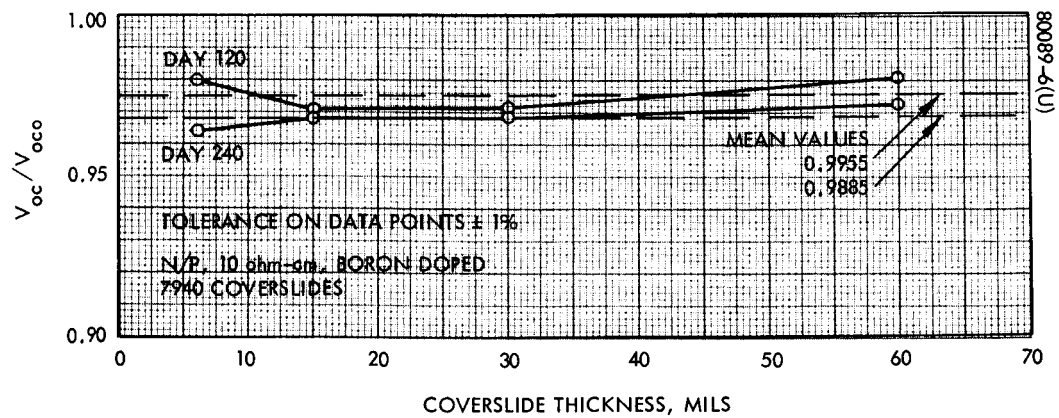


Figure 3-5. Open-Circuit Voltage Degradation as Function of Coverglass Thickness

TABLE 3-4. DATA ACCURACY ASSUMPTIONS

<u>Parameter</u>	<u>Assumed Tolerance, percent</u>
Current	± 0.5
Voltage	± 0.5
Maximum power	± 1.0
Normalized current	± 1.0
Normalized voltage	± 1.0
Normalized maximum power	± 2.0

coverslides (no coatings, no adhesive); and 6-mil, 0211 microsheet coverslides (antireflective coating, blue filter, and XR-634-88 adhesive). The two cells with the sapphire shields were aluminum doped and highly blue sensitive. The long term degradation rate of the 7940, 7740, and 0211 data is in excellent agreement with the nominal trapped electron environment (see Appendix A). However, the sapphire data (assuming that the two data points are reasonably correct) indicates a much lower long-term degradation rate which is consistent with the expected effect of penetrating radiation on a highly blue sensitive cell. The absolute short-circuit current degradation for the 1-mil integral coverslide data appears slightly greater (~ 1 percent), but the differential could be time independent. Additional data spanning a longer time period will be required to resolve this question.

Additional short-circuit performance data are shown in Figure 3-4 as a function of base resistivity. Note that the degradation appears independent of base resistivity and that the mean data for days 120 and 240 respectively are in excellent agreement with the data of Figure 3-2.

Open-circuit voltage degradation data are presented in Figure 3-5 as a function of 7940 coverslide thickness for N/P, 10 ohm-cm, boron doped cells. (Short-circuit current data for these same cells was previously presented in Figure 3-2.) Note that the data scatter for each of the two time points is within the respective error limits. Therefore, the open-circuit voltage degradation also appears to be independent of coverglass thickness with an average loss of 0.45 percent at 120 days and 1.15 percent at 240 days. Assuming a possible temperature error of $\pm 1^\circ\text{C}$ due to gradients, it is conceivable that essentially no loss in V_{oc} occurred during the 240-day period under consideration. However, some degradation due to trapped electron effects is probable with the mean data of Figure 3-5 representing a best estimate. These mean data are plotted in Figure 3-6 on a semilog scale with corresponding degradation predictions based on the trapped electron environment of Appendix A. Note that the flight data is in good agreement

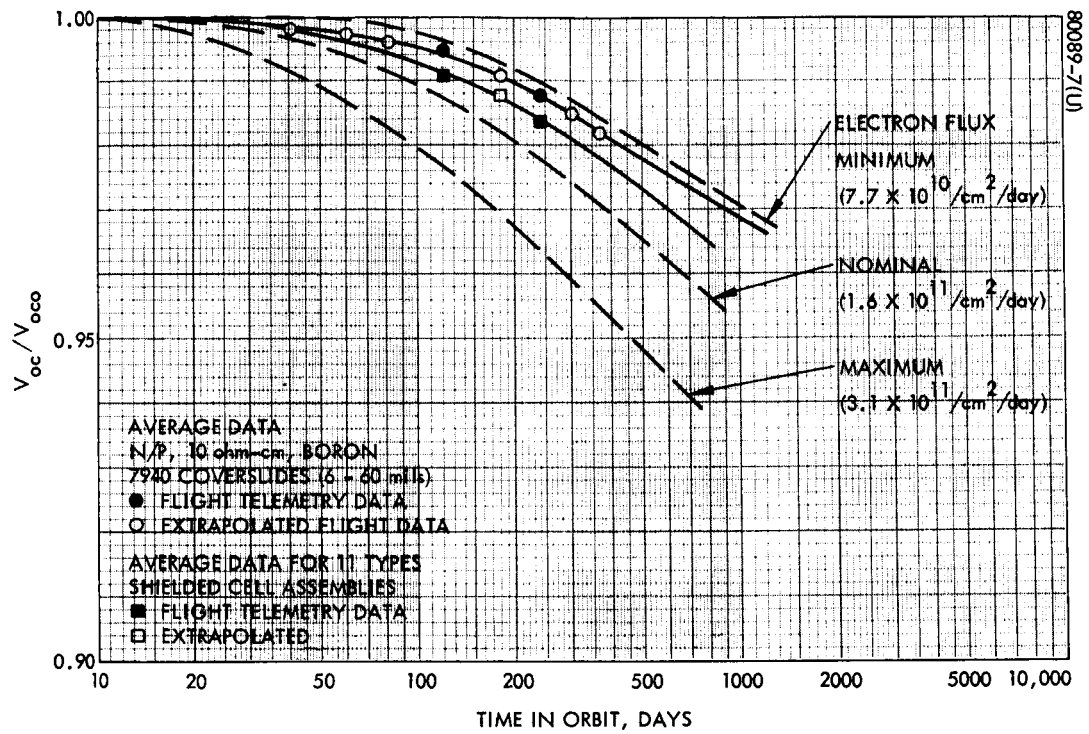


Figure 3-6. Average Open-Circuit Voltage Degradation as Function of Time

with the predicted degradation corresponding to the minimum electron environment. Average open-circuit degradation data for all shielded cells in the experiment (excepting data for the 1-mil, integral shields) is also shown in Figure 3-6. These data correlate with a slightly more severe electron environment, but still significantly below nominal.

The mean 7940 data is compared in Figure 3-7 with corresponding V_{OC} degradation data for 1-mil, 7740 integral shields and 30-mil sapphire shields. The data for the sapphire and 0211 shields correlates precisely with the 7940 data. The cells with the integral 1-mil shields appear to have degraded an additional 1 to 2 percent during the first 120 days with perhaps little or no additional degradation during the following 120-day period. The effect of base resistivity on open circuit voltage degradation is illustrated in Figure 3-8. The data scatter at each of the two time points is within the error limits, and therefore no correlation is evident.

Based on the preceding discussion and the data of Figures 3-2 through 3-8, it appears that (with the exception of cells with integral shields) both the observed short-circuit current degradations and open-circuit voltage degradations are independent of coverglass type, thickness, coatings, and adhesives; semiconductor dopant; and cell base resistivity. The average open-circuit voltage degradation correlates in both magnitude and slope with expected degradation for a near-minimum trapped electron environment. The long term short-circuit current degradation rate correlates with a nominal electron environment, but the total degradation is greater by 4 to 5 percent for time points after approximately 100 days in orbit. It appears that the differential short-circuit current loss is the result of a degradation phenomenon which has essentially an equal effect on all of the coverglass assemblies.

The most interesting anomalies associated with the solar cell experiment were evidenced in maximum power effects. First, the influence of base resistivity and second the influence of coverglass thickness will be considered. Maximum power data are presented in Figures 3-9 and 3-10 as a function of base resistivity. No correlation with maximum power, maximum power voltage, or maximum power current is evident. However, the data scatter for the 7 and 10 ohm-cm samples is outside the assumed limits. This is not considered significant by this evaluator, but it should be noted that Dr. Waddel (Reference 3) did conclude that the maximum power degradation correlated with base resistivity and that 10 ohm-cm appeared nearly optimal. This discrepancy could be the result of a Hughes data reduction error or an error in the tolerance assumptions. Additional analyses will be required to resolve the issue. Pending further evaluation, it is tentatively concluded that the maximum power performance of the subject cells does not correlate with base resistivity.

The influence of coverglass thickness on maximum power performance was evaluated in a more subtle manner, using a differential loss approach. First, it was assumed that the predominate damage mechanisms influencing short-circuit current and open-circuit voltage performance were

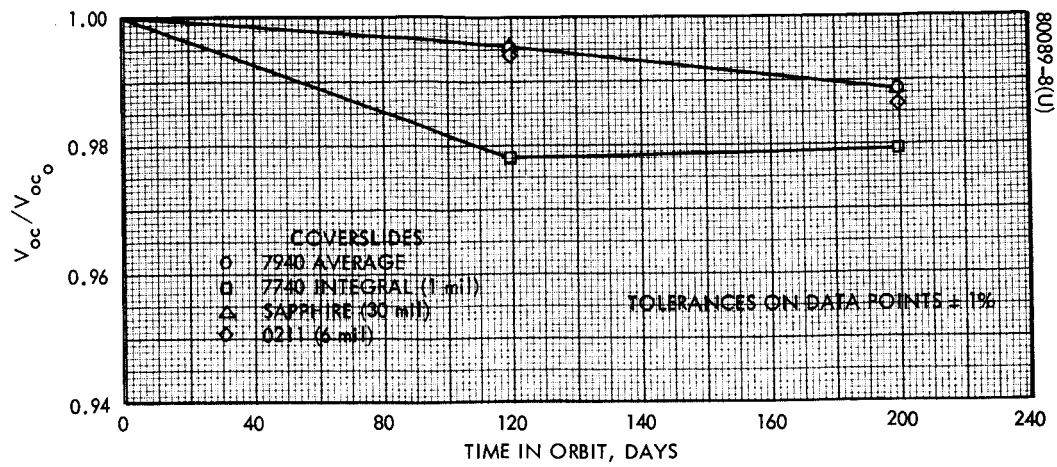


Figure 3-7. Comparison of Open-Circuit Voltage Degradation for Conventional and Integral Shields

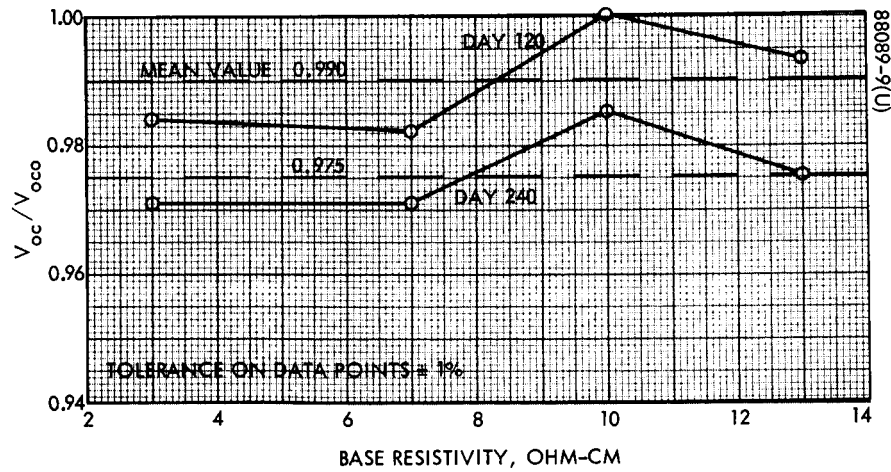


Figure 3-8. Open-Circuit Voltage Performance as Function of Base Resistivity

independent of the mechanisms anomalously affecting maximum power. Since the degradations in both short-circuit current and open-circuit voltage were previously found to be independent of coverglass thickness, the respective average degradation ratios were used to compensate for the effect of these damage mechanisms on maximum power performance and to isolate the effect of the remaining degradation. This compensation is based on the assumption that the ratios I_{mp}/I_{sc} and V_{mp}/V_{oc} are invariant for the predominate damage mechanisms affecting I_{sc} and V_{oc} . The results for normalized maximum power current and normalized maximum power voltage are presented in Figures 3-11 and 3-12 for 7940 coverglass thicknesses between 6 and 60 mils. The ordinate represents the percentage additional degradation beyond that expected from the mean I_{sc} and V_{oc} degradation data. In both cases, a straight line approximation appears reasonable and the functions appear time independent after 120 days. Assuming the straight line approximations for I_{mp} and V_{mp} , the corresponding differential degradation in maximum power is shown in Figure 3-13.

A preliminary differential loss analysis of the aluminum-doped cells indicated an improvement in curve factor with time, apparently as the result of a decreasing effective series resistance. Further analyses will be required to confirm this effect.

Main Array Performance

Unlike the Syncom and Intelsat spacecraft, the ATS-F1 power subsystem is well instrumented and the performance of the two solar panels (hereafter termed "forward" and "aft") could be precisely evaluated over a relatively large operating region. The ATS-F1 was launched on 6 December 1966 and the performance of the solar arrays has been evaluated for the first 10 months of in-orbit operation.

Flight data in the form of voltage-current pairs were not available for voltages below 23 volts or above 33 volts due to charge control and voltage limiting electronics, respectively. However, the available data range was of prime importance since the nominal maximum power voltage is approximately 26 to 27 volts. The solar cell modeling technique summarized in Appendix C was used to optimally reduce the flight data. Mathematical extrapolations to open-circuit voltage and short-circuit current conditions were also attempted. A careful evaluation of the extrapolated short-circuit current data revealed a bias associated with degradations in the maximum power region. This result was expected in that the nonlinearities introduced by the cylindrical array geometry invalidate the physical basis of the mathematical model. For the same reason, the open-circuit voltage extrapolations must also be interpreted with caution. In addition, the open-circuit voltage estimates are extremely sensitive to small errors in both the assumed temperature and the temperature correction technique. All of the telemetry data were corrected to standard conditions (140 mw/cm², AMO equivalent, 25°C) in the manner described in Appendix C.

Typical reduced data for the ATS-F1 aft panel are presented in Figure 3-14. The solid portion of the curve represents the range of actual

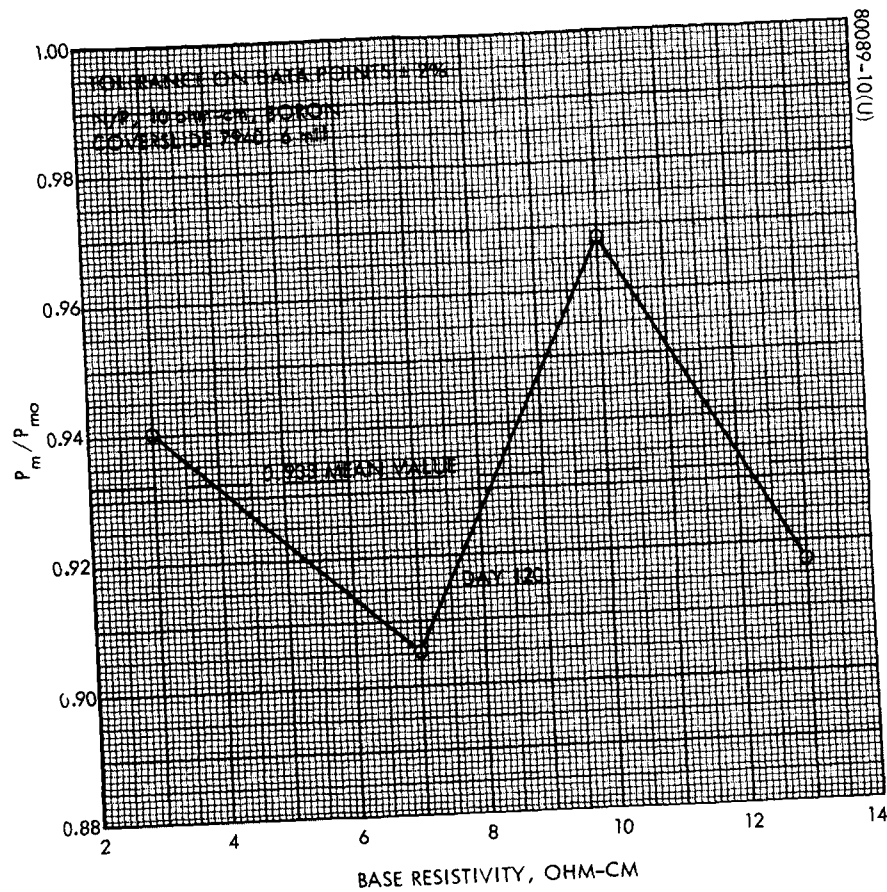


Figure 3-9. Effect of Base Resistivity on Degradation of Maximum Power

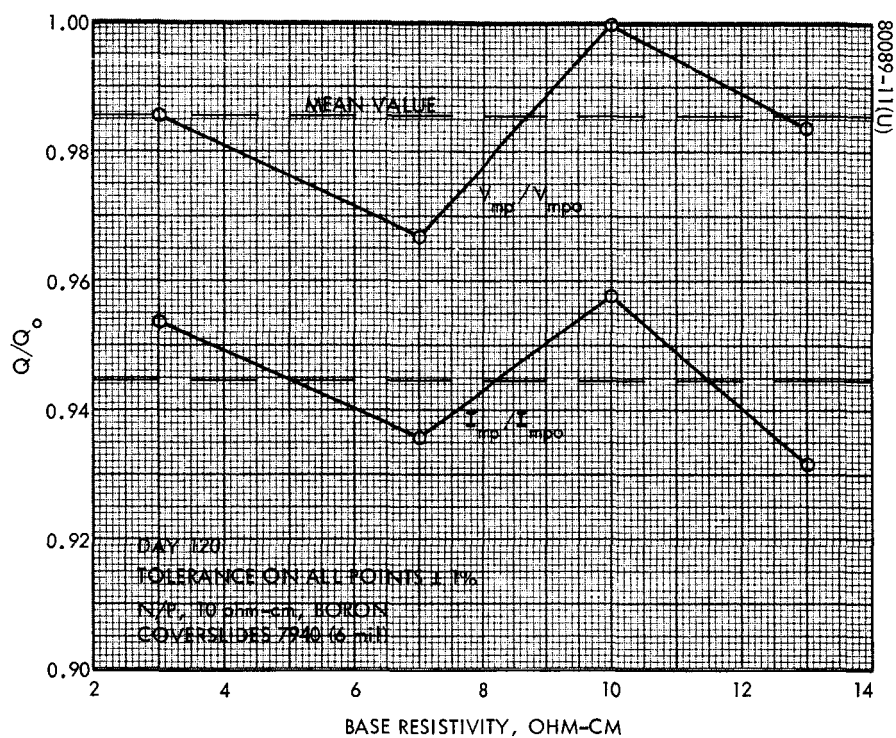


Figure 3-10. Effect of Base Resistivity on Degradation of Maximum Power Current and Voltage

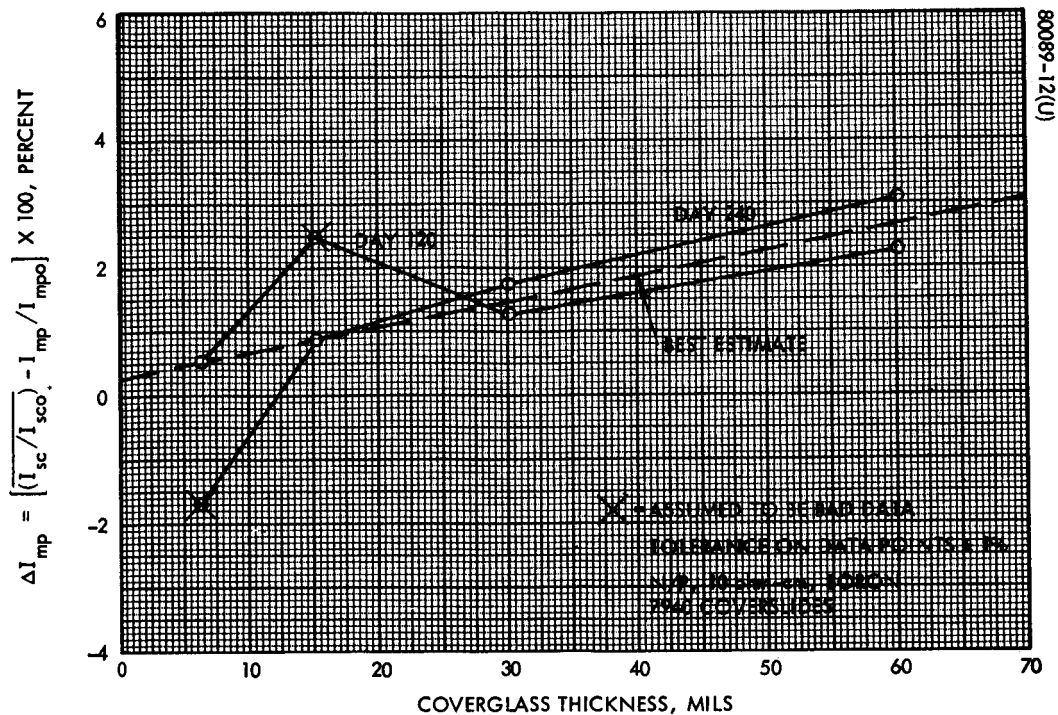


Figure 3-11. Differential Loss in Maximum Power Current as Function of Coverglass Thickness

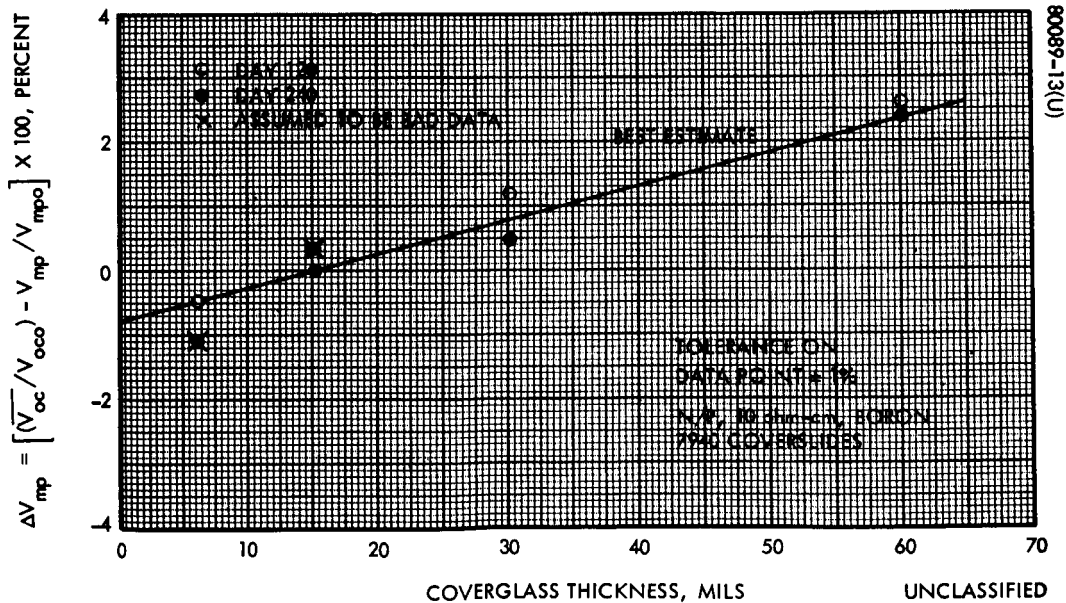


Figure 3-12. Differential Loss in Maximum Power Voltage as Function of Coverglass Thickness

telemetry data with the mathematical extrapolations shown as dotted lines. A complete set of reduced flight V-I data is shown in Figure 3-15. Maximum power voltage, maximum power current, and open-circuit voltage data are presented in Figures 3-16, 3-17 and 3-18 respectively. Similar data for the ATS-F1 forward panel is presented in Figures 3-19 through 3-23.

Intelsat II Array Performance

As previously noted, the Intelsat II spacecraft do not have sufficient instrumentation to directly assess array performance. The bus voltage is the only telemetered data. For the current analysis, command information was utilized to define the load profile corresponding to a set of bus voltage levels. The corresponding load currents were then estimated from ground measurements. Average battery charge currents, which are additive to the spacecraft load, were calculated analytically. The mean array temperature was also calculated analytically.

The resulting V-I points were corrected for solar intensity, angle of incidence, and temperature in the manner outlined in Appendix C. The solar cell model and the associated optimization subroutine (see Appendix C) were then used to generate optimal V-I curves that most nearly matched the flight data. The resulting data for the F2, F3, and F4 spacecraft are presented in Figures 3-24, 3-25, and 3-26, respectively. From these data, it was possible to obtain comparative information as shown in Figure 3-27 for current degradation at 26 volts, which is near the maximum power point. Through extrapolation and some additional data, the degradation in current at 24 volts was derived for the F3 panel as shown in Figure 3-28.

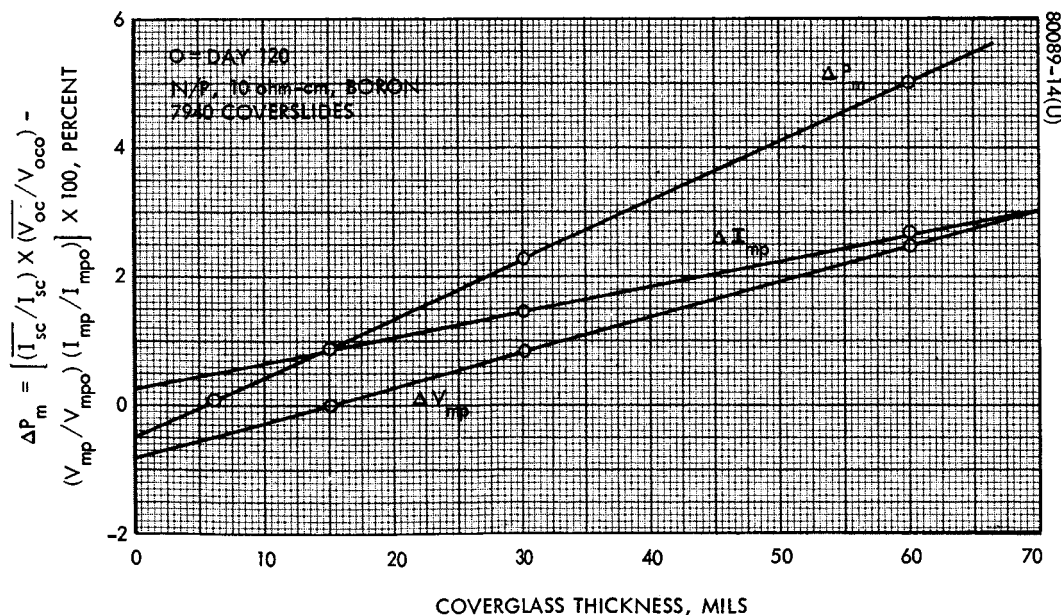


Figure 3-13. Differential Loss in Maximum Power as Function of Coverglass Thickness

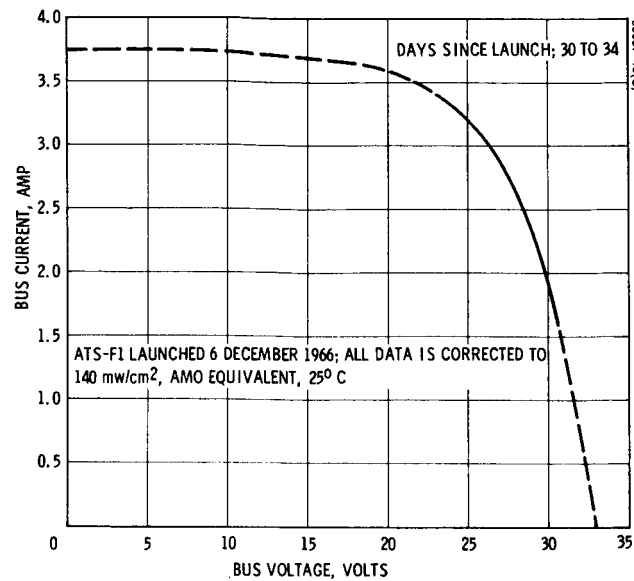


Figure 3-14. ATS-F1 Aft Solar Panel Typical Model Results

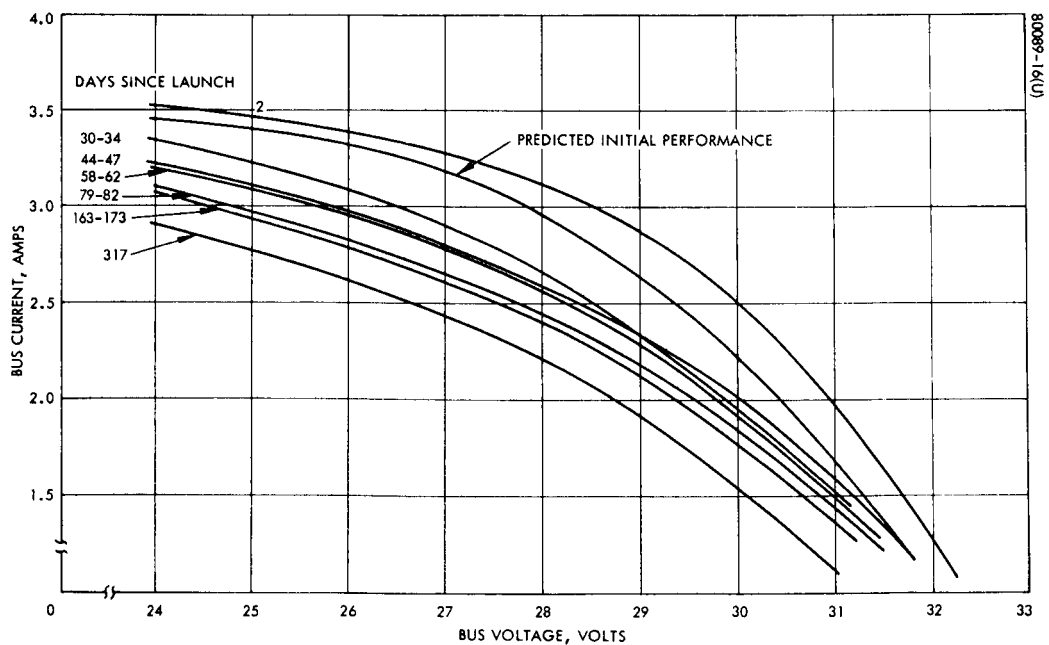


Figure 3-15. ATS-F1 Aft Solar Panel Performance

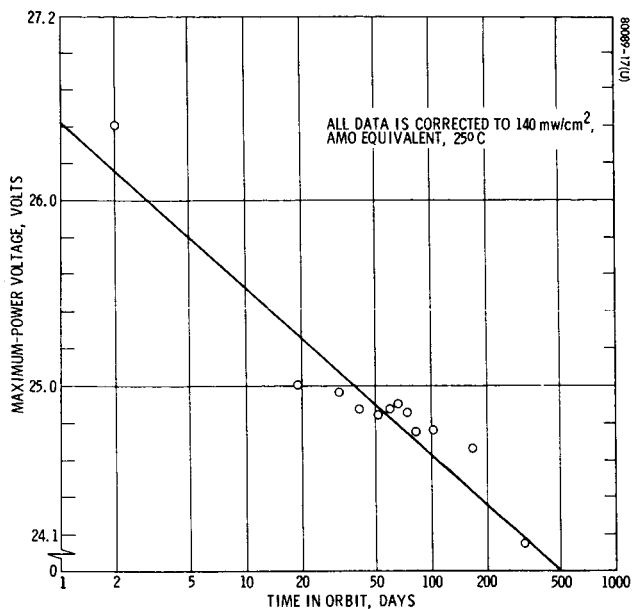


Figure 3-16. ATS-F1 Aft Solar Panel Maximum Power Voltage Performance

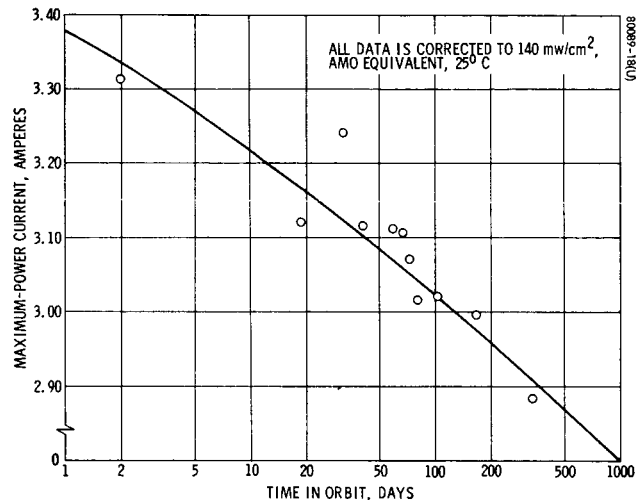


Figure 3-17. ATS-F1 Aft Solar Panel Maximum Power Current Performance

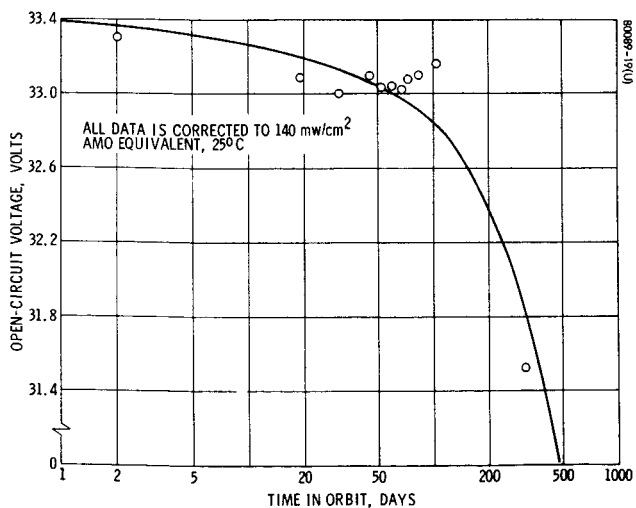


Figure 3-18. ATS-F1 Aft Solar Panel Open-Circuit Voltage Performance

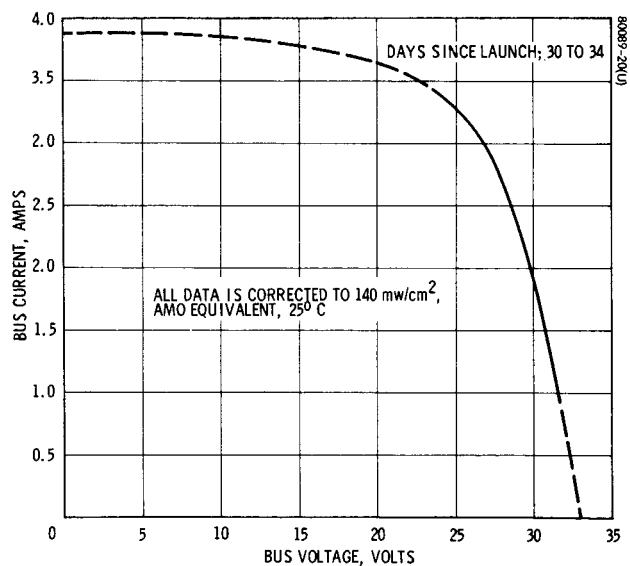


Figure 3-19. ATS-F1 Forward Solar Panel Typical Model Results

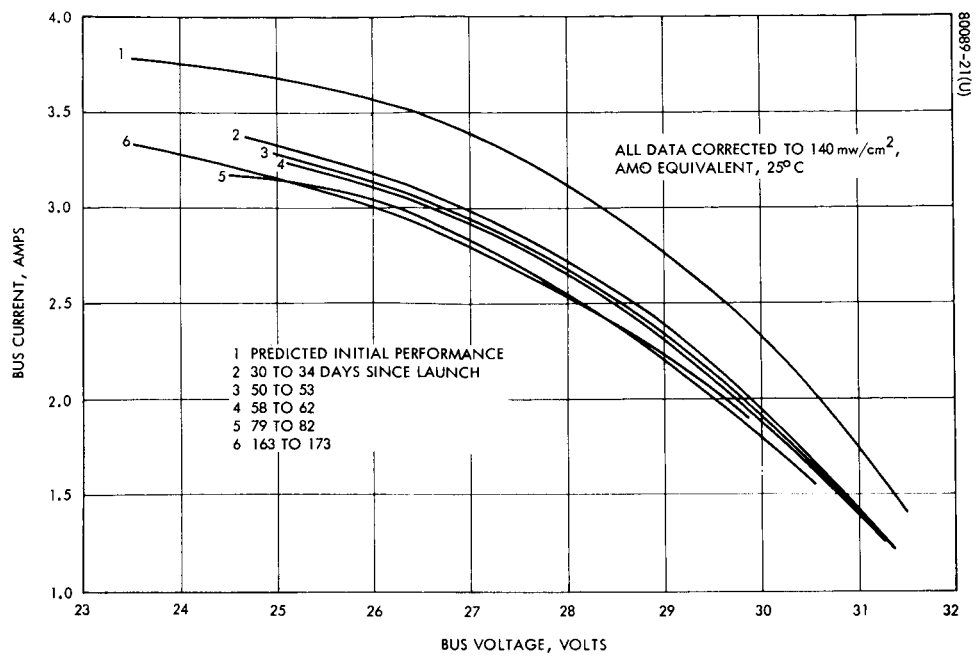


Figure 3-20. ATS-F1 Forward Solar Panel Performance

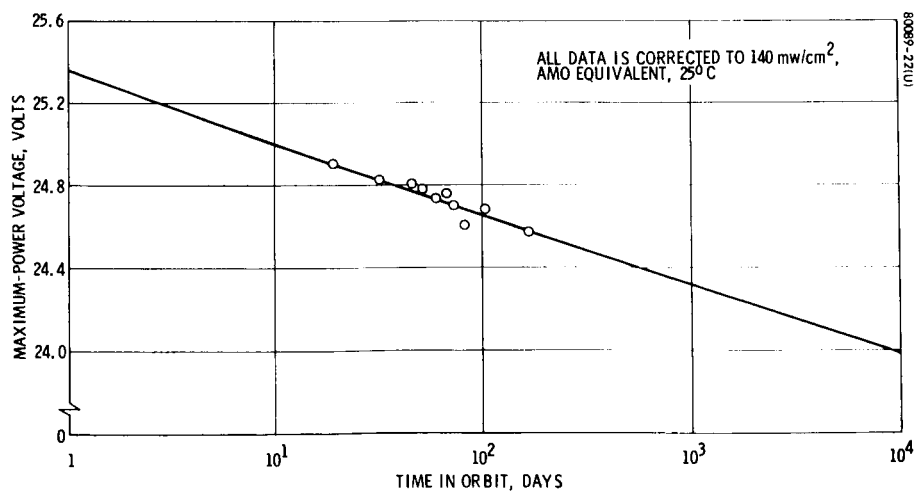


Figure 3-21. ATS-F1 Forward Solar Panel Maximum Power Voltage Performance

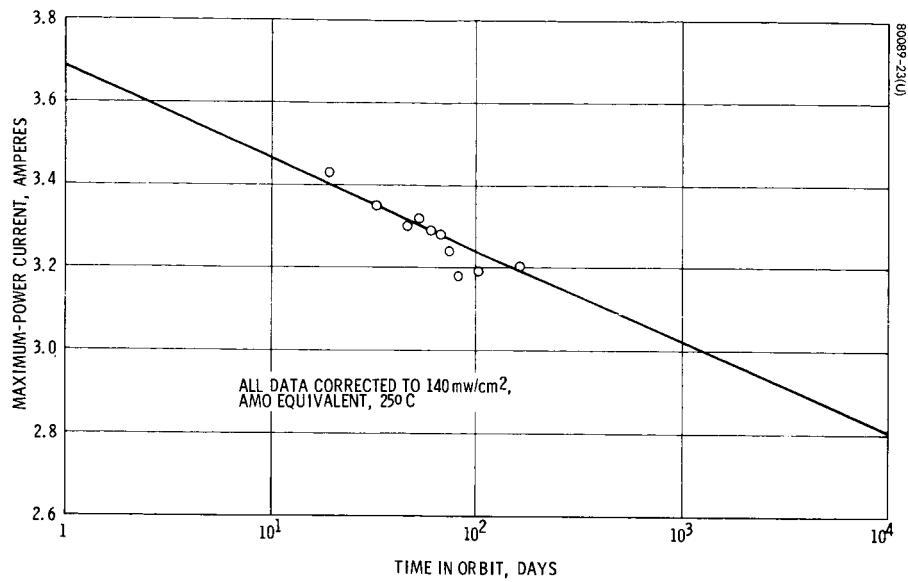


Figure 3-22. ATS-F1 Forward Solar Panel Maximum Power Current Performance

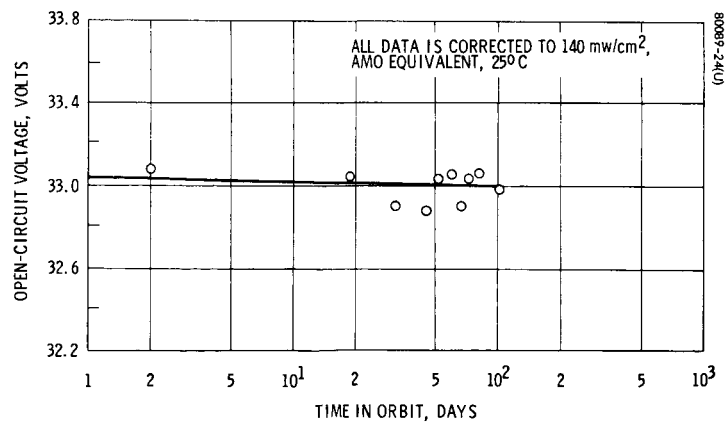


Figure 3-23. ATS-F1 Forward Solar Panel Open-Circuit Voltage Performance

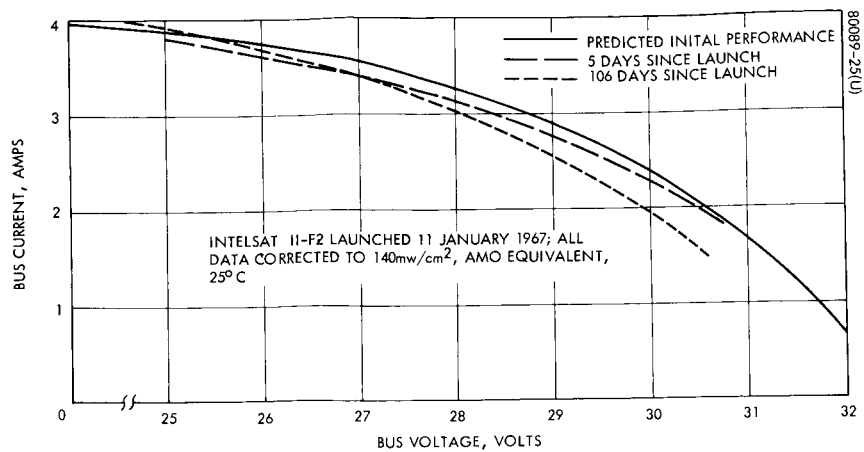


Figure 3-24. Intelsat II - F2 Solar Array Performance

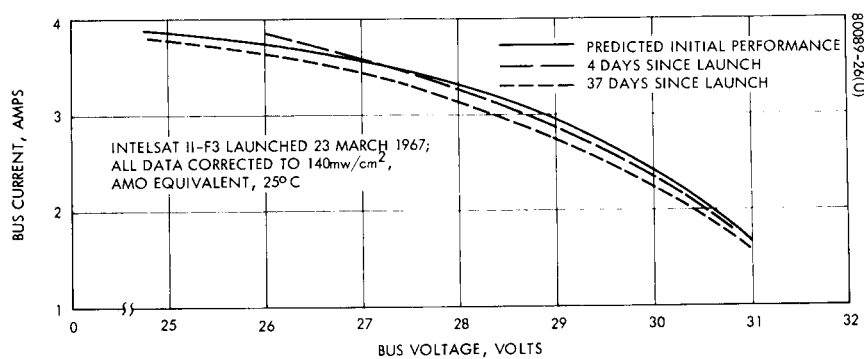


Figure 3-25. Intelsat II - F3 Solar Array Performance

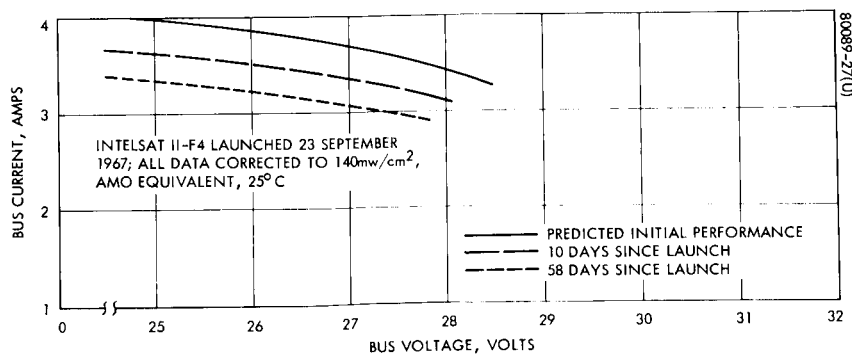


Figure 3-26. Intelsat II - F4 Solar Array Performance

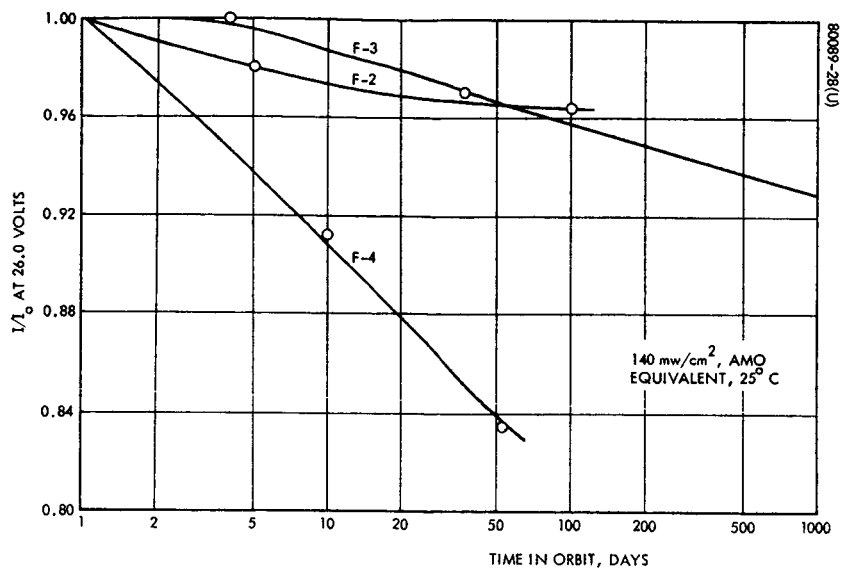


Figure 3-27. Intelsat II Solar Array Performance Comparison

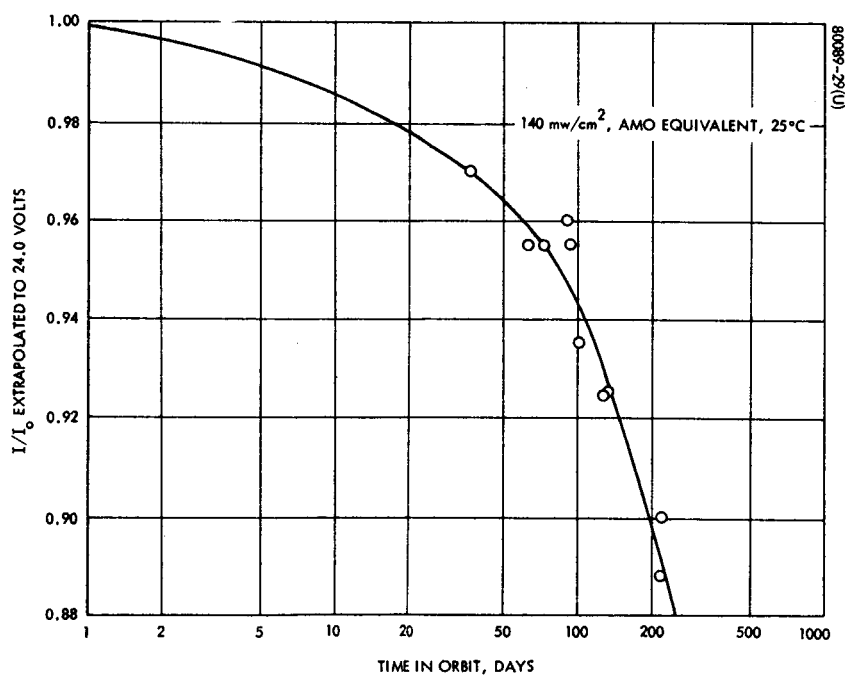


Figure 3-28. Intelsat II - F3 Solar Array Performance

4.0 RADIATION EFFECTS ANALYSIS

From the flight data discussed in Section 3.0, it was apparent that the synchronous orbit radiation environment had vastly differing effects on the various solar arrays and on the ATS-F1 solar cell experiment. The apparent degradation after 1 year in orbit varied from an almost negligible 2 percent for Syncom III and Intelsat I to a totally anomalous 32 percent for the ATS-F1 aft panel. A comparison of the Intelsat II-F4 and the ATS-F1 panels is shown in Figure 4-1 for a fixed voltage near the maximum power point. As shown, the data for two ATS panels on the same spacecraft appeared to have significantly different degradation rates. The solar cell experiment data did not correlate with either prediction or any of the array data. The inconsistency of the flight data strongly suggested one or more uncontrolled, significant variables associated with the solar cells or solar cell modules. A comparative evaluation of the various cell and/or module properties was conducted in an attempt to identify these variables.

4.1 COMPARATIVE EVALUATION OF COMPONENT PROPERTIES

A general comparative list of cell and array data is presented in Table 4-1. As noted in the subject table, Syncom III and Intelsat I were the last Hughes spacecraft to use a shingled cell module. These modules were mechanically and electrically assembled prior to the application of the coverslides, and as a result, essentially no bare cell area was left exposed around the periphery of the coverslides. All subsequent arrays have used a flat-mounted, series-parallel matrix which was electrically and mechanically assembled with cells having premounted coverslides. To prevent interference with the soldering operation, these prefabricated cell-coverslide assemblies did permit small exposed cell areas adjacent to the cell top contact strip. Other tolerance considerations permitted exposed areas adjacent to the other coverglass sides. The specification requirements for all of the prefabricated cell-coverslide assemblies under consideration are illustrated in Figure 4-2. The ATS and Intelsat II-F4 designs permit the largest exposed area. These were also the spacecraft which suffered the most degradation in-orbit. With reference to the solar cell experiment, exposed areas around the periphery of the coverslides were not controlled⁴. However, the coverslides were mounted after the cells were electrically and mechanically assembled and no attempt was made to control or to remove any excess coverslide adhesive⁴.

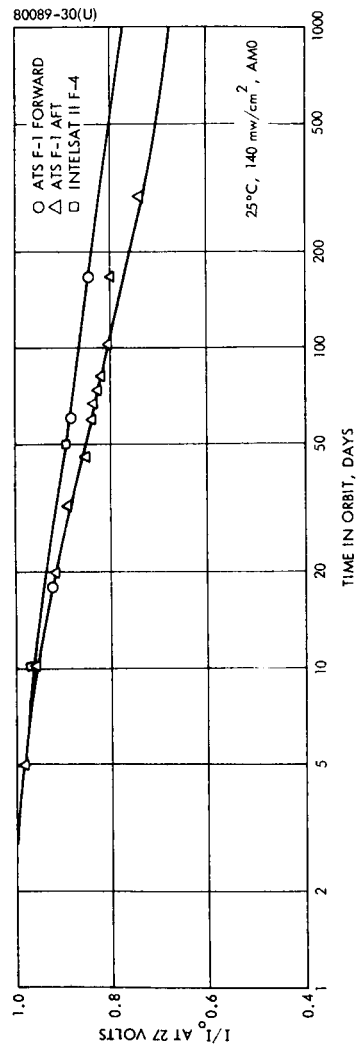


Figure 4-1. Comparison of Solar Panel Performance at Fixed Voltage

TABLE 4-1. SUMMARY OF SOLAR ARRAY CHARACTERISTICS

Spacecraft	Cell Type	Cell Resistivity (ohm-cm)	Minimum Efficiency or Minimum Average Power, 25° C, 140 mw/cm ² , A	Cell Dimensions, cm	Cell Contact	Cell Top Contact Configuration	Module Configuration	Cell Adhesive	Cell Manufacturer	Coverslide Type	Coverslide Thickness, mils	Coverslide Adhesive	Worst Case Exposed Bare Cell Area, (percent)
Syncom II	P/N	10	9.92 percent	1 x 2	Solder dipped electroless Ni	Bar	5-cell rigid series shingle	RTV-731	Heliotek	Corning micro-sheet	6	Furane 15E	~0
Syncom III	N/P	10	11 percent	1 x 2	Solder dipped electroless Ni	Bar	5-cell flexible series shingle	Hughes HP-16-110	Heliotek	Corning 7940 quartz	12	GE LTV-602	~0
Intelsat I	N/P	10	125 mw per shingle	1 x 2	Solder dipped electroless Ni	Bar	5-cell flexible series shingle	Hughes HP-16-110	Heliotek	Corning 7940 quartz	12	GE LTV-602	~0
Intelsat II-F2	N/P	10	28 mw at 0.445 volts	1 x 2	Zone solder Ag-Ti	Corner dart		Hughes HP-16-110	Heliotek	Corning 7940 quartz	12	GE LTV-602	3.2
Intelsat II-F3	N/P	10	28 mw at 0.445 volts	1 x 2	Zone solder Ag-Ti	Corner dart		Hughes HP-16-110	Heliotek	Corning 7940 quartz	12	GE LTV-602	3.2
Intelsat II-F4	N/P	10	56.74 mw at 0.445 volts	2 x 2	Zone solder Ag-Ti	Bar		Hughes HP-16-110	Centralab & Heliotek	Corning 7940 quartz	12	Dow XR-6-3489 GELTV-602	6.4
ATS-F1	N/P	10	26 mw at 0.445 volts	1 x 2	Solder dipped Ag-Ti	Bar		Hughes HP-16-110	Texas Instruments	Corning 7940 quartz	30	Dow XR-6-3489	6.4
ATS-F2	N/P	10	26 mw at 0.445 volts	1 x 2	Solder dipped Ag-Ti	Bar		Hughes HP-16-110	Texas Instruments	Corning 7940 quartz	30	Dow XR-6-3489	6.4

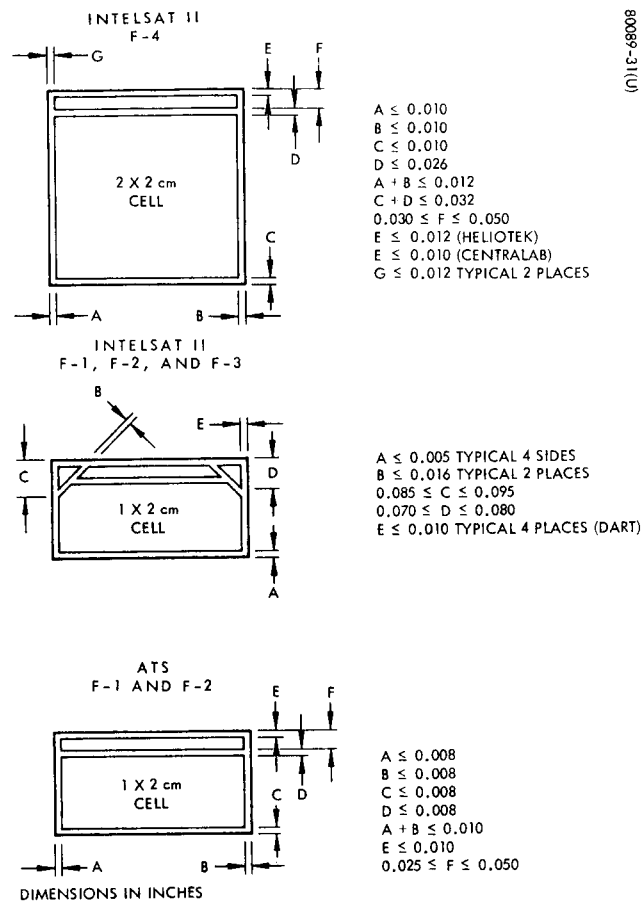


Figure 4-2. Coverslide Specification Tolerances

It may also be significant to note in Table 4-1 that Syncom III and Intelsat I were the last Hughes spacecraft to use electroless nickel cell contacts. Silver-titanium cell contacts have been used on all subsequent arrays as well as the solar cell experiment. The cells used on ATS main arrays and in the solar cell experiment were completely solder-dipped, including the grid contacts. The cells used on the Intelsat II arrays were zone-soldered with bare grid contacts.

With the exception of ATS, all of the solar arrays used 12-mil, 7940 quartz coverslides with standard coatings and filters. The ATS arrays used thicker 30-mil, 7940 shields. Syncom III, Intelsat I, and Intelsat II-F2 and F-3 used GE LTV-602 coverglass adhesive. The ATS arrays and the solar cell experiment used Dow Corning XR-6-3489 and XR-6-3488 coverslide adhesives, respectively. The cells on Intelsat II-F4 were mixed.

Since the Intelsat II-F4 solar panel (which used 12-mil, 7940 coverslides) had apparently degraded at a rate similar to ATS (See Figure 4-1), it seemed improbable that the coverglass thickness was the critical parameter. The only known variable which appeared to correlate with the various flight data was exposed cell area around the periphery of the coverslides. Relative to penetrating radiation damage, such unshielded regions would result in a loss directly proportional to the fraction of the total active cell area that was exposed. These losses would normally be negligible. However, the effect of low-energy protons had not been considered. A well defined model for trapped low-energy protons did not become available until early 1967 (See Appendix A). For a synchronous orbit, as well as for many other regions of the magnetosphere, this environment model predicted very high flux rates for protons having energies below approximately 0.5 mev. Unfortunately, the significance of this environment component was not fully appreciated.

4.2 IDENTIFICATION OF POSSIBLE DAMAGE MECHANISMS

In general, the effect of low-energy proton irradiations of partially shielded cells had not been carefully evaluated. The first reported experiments were conducted in 1966 by Brucker, et al., of RCA (Reference 7). The irradiation tests were performed using 200 kev protons at fluences between 10^{11} and 10^{15} particles/cm². Unfortunately, these test results proved to be misleading, perhaps because maximum power was chosen as the principal performance indicator, instead of performance at a fixed voltage. The consideration of only a single energy was also unfortunate. In any event, the true extent of the hazard was missed.

Subsequent tests by Hughes as part of this ATS study have verified that low-energy proton irradiations, particularly spectrum irradiations, result in losses totally out of proportion to the exposed area. The results of these tests were dramatic in several respects. The loss mechanism is basically a shunting effect, resulting from a marked change in the junction characteristics of the affected regions. As might be expected, areas immediately adjacent to the bus collector were found to be most damage effective. A more complete discussion of the test results is presented in Appendix D.

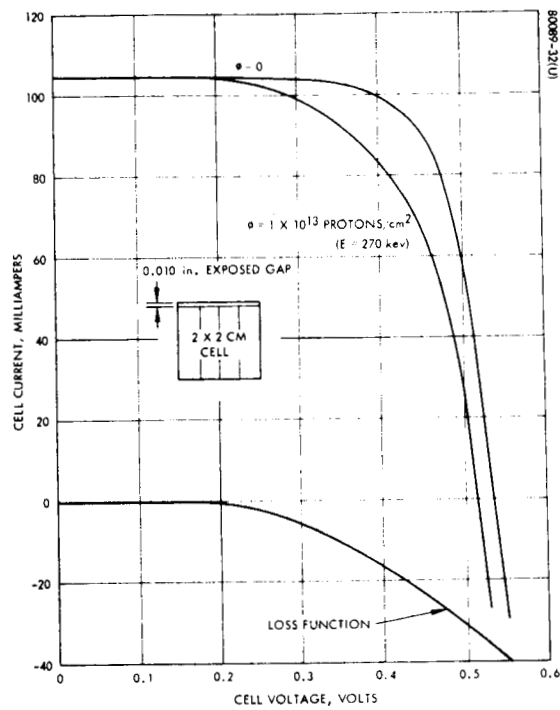


Figure 4-3. Typical V-I Curve of Loss Mechanism

The typical effect of low-energy proton irradiation on the V-I curve of a partially shielded cell is illustrated in Figure 4-3. If one regards the degradation phenomenon as an effective parasitic load, then a loss function can be defined as shown in Figure 4-3, which represents the V-I characteristic of the parasitic load. A loss function of this type is in a sense the "fingerprint" of low-energy proton damage to limited regions of the cell. We will use the term "loss function analysis" hereafter when referring to the technique of treating a degradation phenomenon as a parasitic load or other circuit element that can be modeled as a two-port network completely defined by a V-I characteristic. The general concept of the loss function will prove to be a very valuable analysis tool.

The test program described in Appendix D also revealed that the low-energy proton loss function is virtually independent of illumination intensity. Therefore, the percentage degradation at any given voltage will vary linearly with the effective illumination intensity of the cell (i. e., will vary linearly with the available current). Therefore, a cylindrical array, which inherently has a large effective intensity gradient, is especially sensitive to low-energy proton effects. However, note in Figure 4-3 that the short-circuit current is not affected by this mechanism. Therefore, the short-circuit current losses observed in the solar cell experiment cannot be attributed to this loss phenomenon.

As was noted in Section 3.0, the short-circuit current degradations observed in the solar cell experiment appeared to be independent of coverglass type, thickness, coatings and adhesives; semiconductor dopants; and cell base resistivity. Therefore, the loss mechanism appears to be a surface phenomenon which has essentially an equal effect on all of the coverglass assemblies. Since the Syncom III and Intelsat I arrays were apparently not affected, it is plausible that a contaminate could be the source of the problem.

It is also plausible that the high fluence of low-energy protons could produce color center defects in the first few microns of the coverslide materials that would result in a significant transmission loss. Laboratory irradiation tests of 7940 quartz samples were conducted using 270 keV protons at fluences up to 10^{16} protons/cm². The highest fluence proved to be the worst case and the resulting effect on coverslide transmittance is illustrated in Figure 4-4. When the degraded response curve is integrated with the solar spectrum and solar cell response characteristic, the net loss in short-circuit current is negligible. Transmittance measurements at other angle of incidence revealed no increase in the loss. It is also entirely possible that rapid room temperature annealing may have occurred and the real transmission loss effect may only exist under steady state irradiation. However, if this were true, why were the Syncom III and Intelsat I spacecraft not affected?

If the data for the mechanically supported sapphire shields is ignored, then the coverslide coatings, filters, and adhesives become suspect. Of these three possibilities, the only known difference between the Syncom III and Intelsat I arrays and subsequent arrays is the coverslide adhesive. However, as discussed in Reference 6, all available ground test data indicates that the Dow XR-634-89(88) adhesive is more resistant to radiation darkening than the GE LTV-602. There is also ample evidence to suggest that the blue

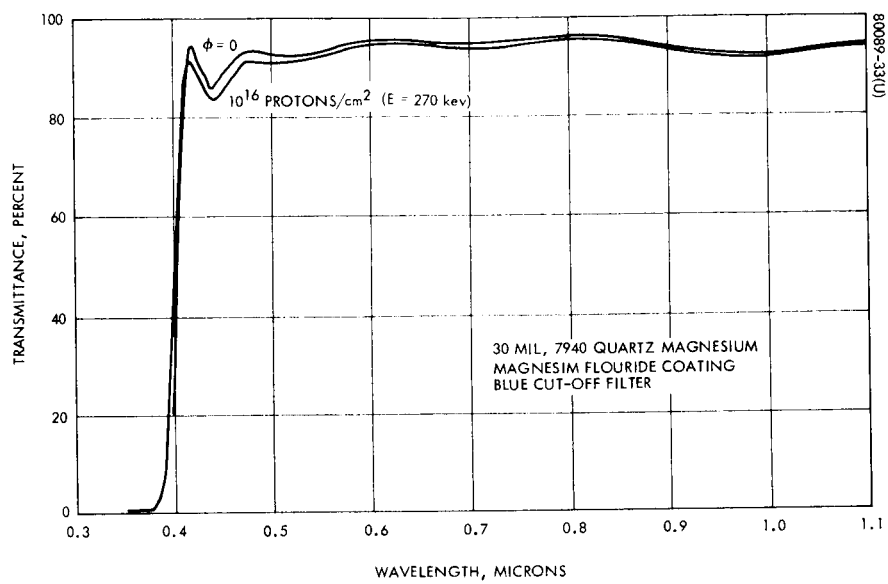


Figure 4-4. Effect of Low Energy Proton Irradiation on Coverslide Transmittance

reflecting filter used on virtually all of the coverslides can be significantly damaged by both UV and particulate radiation⁶. Maximum degradations observed in laboratory UV tests have been in the range of 2 to 3 percent⁶. This mechanism may well be a component of the observed transmission losses in the coverslide assemblies.

In any event, it is certainly hazardous to blindly interpret the sapphire data as a confirmation of a surface phenomenon as the primary transmission loss mechanism. The aluminum doped cells which have the sapphire shields are extremely blue sensitive. Transmittance changes qualitatively similar to that illustrated in Figure 4-4, which primarily affect the blue wavelengths, would have a far more significant effect on the aluminum cells. However, the short-circuit performance for the aluminum-doped cells with 6- and 30-mil, 7940 coverslides correlated excellently with the average data in Figure 3-3 for the boron doped cells with 7940 coverslides.

The correlation of maximum power degradation with coverglass thickness that was observed in the solar cell experiment (See Figure 3-13) is possibly the result of yet another damage mechanism. The differential loss function for the worst case (60-mil, 7940 coverglass) is illustrated in Figure 4-5. At any given voltage, the loss current represents the additional differential current degradation beyond that which would normally result from the observed average degradations in I_{sc} and V_{oc} . The recovery at high voltages is not considered significant because this region is extremely sensitive to small temperature errors. In terms of a "fingerprint," this loss function is similar to that corresponding to low-energy proton damage to a partially shielded cell (See Appendix D). However, a similar effect could also result from a degradation of the silver-titanium contacts. Shunting effects at high temperatures have been observed for titanium contacts. It is plausible that another energy transfer mechanism, perhaps associated with the electron environment, could cause a similar effect. The apparent strong correlation with coverglass thickness, as evidenced in Figure 3-13, is inconsistent with low-energy proton damage unless the exposed cell area were in some way related to the coverglass thickness. Such a correlation seems improbable.

4.3 Correlation Analyses

As shown in Figure 4-1, the ATS-F1 forward and aft panels appeared to degrade at different rates for at least the first year of operation. The solar cell experiment, which observed an apparent transmission loss phenomenon, was located on the aft panel. If it is assumed that the performance difference between the forward and aft panels is due to a transmission loss mechanism which is proportional to the cosine of the sun angle, then the data correlate with the apparent transmission loss evidenced by the solar cell experiment. These comparative data are shown in Figure 4-6. The derivation of the angle of incidence correction function may be found in Appendix F. Therefore, it is plausible that a contaminate affecting only the ATS-F1 aft solar panel is the source of the observed transmission losses in the solar cell experiment. Obviously, the uncertainty of the data precludes any absolute confirmation of this possibility.

Assuming the above transmission loss and assuming that the remaining degradation was due to low-energy proton damage, the V-I data for days 2 and 317, respectively, in Figure 3-15 were corrected to equivalent data for a sun normal planar array (see Figure F-1, Appendix F for transformation curve). A loss function was then calculated as shown in Figure 4-7. The apparent differential proton loss after 317 days in orbit was approximately 12 percent at 27 volts, which, based on the spectrum irradiation data of Appendix D, corresponds to an exposed gap of approximately 2 mils adjacent to the cell bus bar. Actual laboratory measurements of exposed areas for the ATS cells indicated a nominal bar gap of approximately 2 mils (see Appendix D for definitions). Other exposed areas were found to be negligible. Due to the uncertainty in the environment and the small sample size underlying the experimental data, such a precise correlation is not per se significant. However, the shape of the loss function shown in Figure 4-7 is considered significant as a characteristic of low-energy proton effects.

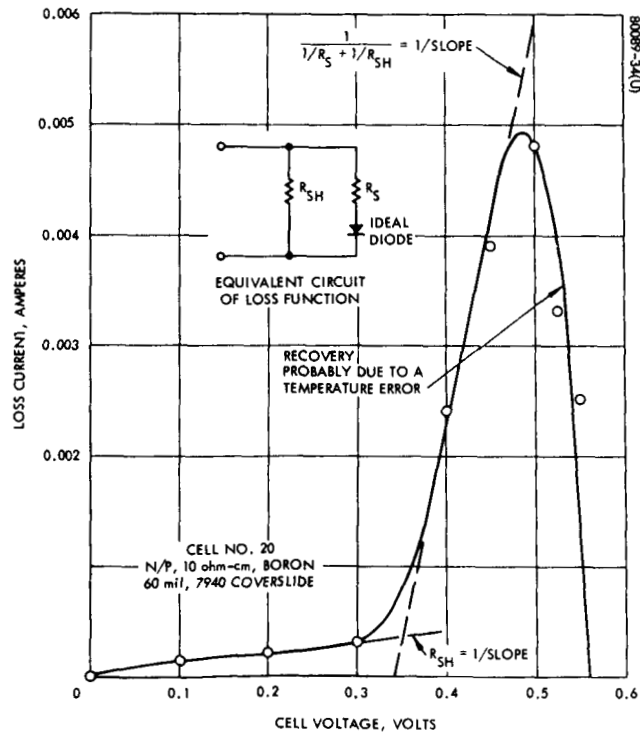


Figure 4-5. Differential Loss Function

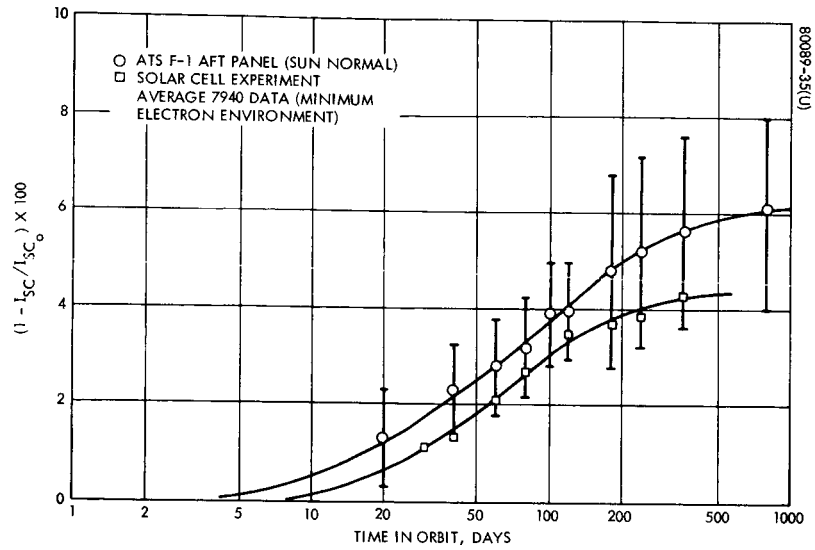


Figure 4-6. Comparative Transmission Loss Analysis

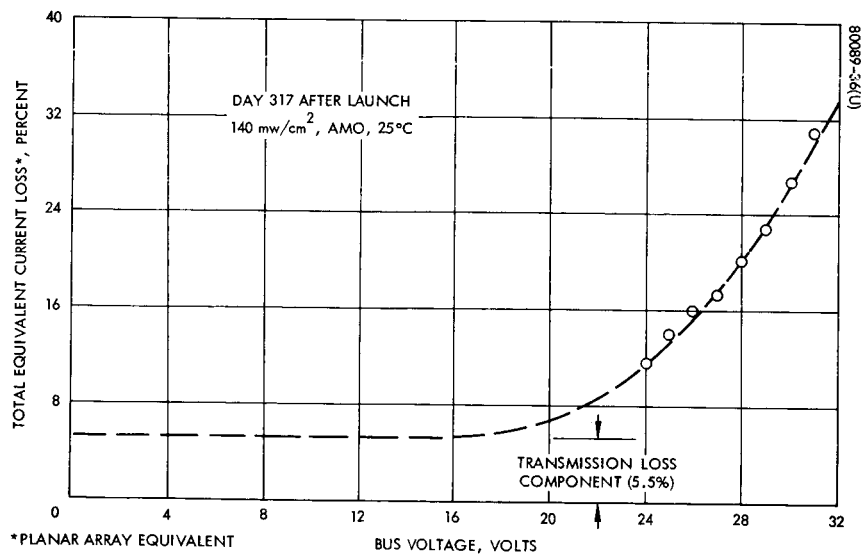


Figure 4-7. ATS-F1 Aft Array Loss Function

5.0 CONCLUSIONS AND RECOMMENDATIONS

5.1 CONCLUSIONS

Based on the results of this study, it is tentatively concluded that the observed solar cell and solar array performance degradations are the result of one or more of the following three primary damage mechanisms:

- 1) Low energy proton damage to exposed cell areas around the periphery of the cell coverslides
- 2) Coverglass assembly transmission losses which appear to be the result of a surface phenomenon, possibly a contaminate
- 3) Conventional radiation damage resulting from the trapped electron radiation environment

In addition, the solar cell experiment data evidenced a fourth damage mechanism which is correlated with coverglass thickness and which is possibly a shunt loss associated with the deterioration of the silver-titanium contacts. Shunt losses due to titanium contacts are known to occur at high temperatures, and it is plausible that a similar effect could result from other energy transfer mechanisms, possibly as a result of electron irradiation.

A summary of the relative magnitudes of the degradation components after 1 year in orbit for both the solar cell experiment and the respective solar arrays is presented in Table 5-1. The data shown are for a typical operating voltage in the maximum power region.

The apparent low energy proton degradations were found to correlate with known exposed cell areas and the corresponding degradations that would result from the model environment. The experimental test results indicate that virtually no exposed area can be tolerated. A modified epoxy shield has been qualified to protect bare cell areas (see Appendix E). A minimum coat thickness of 3 mils should be assured to provide adequate protection from the trapped environment defined in Appendix A.

TABLE 5-1. SUMMARY OF DEGRADATION COMPONENTS AFTER 1 YEAR IN ORBIT
Percent current degradation at voltage near maximum power

Degradation Mechanism	Spacecraft Array or Experiment									Comments
	Syncom III	Intelsat I	Intelsat II-F2	Intelsat II-F3	Intelsat II-F4	ATS-F1 FWD	ATS-F1 AFT	ATS-F1 Experiment	Solar Cell	
Low Energy Proton Damage to Exposed Cell Areas	~ 0.0	~ 0.0	~ 2.0	~ 10.0	~ 14.0	~ 15.5	~ 16.5	~ 0.0		
Coverslide Assembly Transmission Losses	~ 0.0	~ 0.0	~ 0.0	~ 0.0	~ 0.0	~ 0.0	~ 7.0	~ 4.5		Probable Contamination Problem
Conventional Radiation Effects from Trapped Electrons	≤ 4.0	≤ 4.0	≤ 4.0	≤ 4.0	≤ 4.0	~ 2.0	~ 2.0	~ 2.0		
Silver-Titanium Contact Degradation	0.0	0.0	~ 0.0	~ 0.0	~ 0.0	~ 1.5	~ 1.5	< 2.5		Function of Shield Thickness
Total Degradation	≤ 4.0	≤ 4.0	~ 6.0	~ 14.0	~ 18.0	~ 19.0	~ 27.0	~ 9.0		

The transmission loss phenomenon observed in the solar cell experiment apparently also affected the ATS-F1 aft panel but not the forward panel. The solar cell experiment was physically mounted on the aft panel and these surface areas were exposed to the gas jet exhausts associated with the spacecraft spinup operation. This is a unique feature of the ATS spacecraft in general and the aft panel in particular. It is plausible that the products of combustion of the valve squib mixed with the gas jet, and contaminated these surfaces. The transmission characteristics of the contaminate probably degraded with time and exposure to both trapped proton and solar ultraviolet radiations. Ground testing will be required to confirm this effect.

5.2 RECOMMENDATIONS

In general, a continuation of the ATS flight data reduction effort is recommended to permit evaluation of the radiation effects over a longer time period and thereby greatly facilitate the resolution of the degradation components. The ATS-F2 flight data should be reduced, especially as a check on the array contamination hypothesis based on the squib-actuated, spinup jets.

The optimal modeling technique used to reduce the solar cell experiment data met all expectations. It is recommended that the complete set of available solar cell experiment data be processed using this program and that the resulting data be evaluated using the "loss function" technique. The cross-correlation permitted by loss function analyses will no doubt provide additional valuable insight into the damage mechanisms and effects.

A complementary ground test program should be conducted in conjunction with the additional flight data analyses to investigate possible array contamination sources and possible degradation mechanisms associated with irradiation effects on silver-titanium contacts. Additional low-energy proton tests should be conducted, supported by comprehensive theoretical analyses. All of the above discussed efforts should culminate in the definition of a radiation effects experiment for ATS-E to provide in-orbit confirmation of the analysis and/or ground test results.

6.0 REFERENCES

1. Raymond C. Waddel, Early Results from the Solar Cell Radiation Experiment on ATS-1, NASA-GSFC Document X-711-67-176, April 1967.
2. Raymond C. Waddel, ATS-1 Solar Cell Radiation Damage Experiment, First 120 Days, NASA-GSFC Document X-710-67-412.
3. Supplement A to Reference 2), November 1967.
4. Private Communications, R. C. Waddel.
5. W. D. Brown, G. W. Hodgman and A. T. Spreen, "Computer Simulation of Solar Array Performance," Conference Record of the Sixth Photovoltaic Specialists Conference, Vol. III, March 1967.
6. W. C. Cooley and M. J. Barrett, Handbook of Space Environmental Effects on Solar Cell Power Systems, Exotech Report TR-025, January 1968.
7. G. J. Brucker et al., "Low-Energy Proton Damage in Partially Shielded Solar Cells," Proceedings of the IEEE, May 1966.

APPENDIX A. SYNCHRONOUS ORBIT RADIATION ENVIRONMENT

INTRODUCTION

A spacecraft in synchronous orbit about the earth is exposed to a composite radiation environment which includes trapped particulate radiation; solar flare protons; and neutrons, X-rays and ultraviolet radiation of solar origin. These radiations will severely degrade the performance of a solar cell array unless appropriate shielding is provided. The current Hughes design models for these environment components are presented in the following subsections.

TRAPPED ENVIRONMENT

The geomagnetic field traps high energy electrons and protons forming doughnut shaped radiation belts, with the axis of revolution aligned with the magnetic axis of earth. For a synchronous orbit, the trapped particles encountered by a spacecraft are primarily electrons and low energy protons.

Trapped Electrons

AE3 Environment

The magnetosphere is distorted in the synchronous region through interaction with the solar wind, resulting in large variations in the electron flux levels within time periods of a few weeks. However, the time-averaged flux, which is the significant factor influencing solar array degradation, remains relatively constant except for gradual changes with the 11-year solar activity cycle. The most recent analysis by J. I. Vette of Goddard Space Flight Center indicates that the time-averaged electron flux is enhanced during solar minimum by a factor of approximately 2 (Reference 1). This is an unexpected trend, since previous qualitative arguments by numerous investigators predicted an opposite effect.

Based on information from radiation detectors on board several satellites (Explorers 6, 12, and 14, Imp A, OGO A, and ERS-17), Dr. Vette has proposed the AE3 environment for electrons at synchronous altitudes (Reference 2). This integral electron environment, averaged over local time, is shown in Table A-1.

TABLE A-1. INTEGRAL ELECTRON ENVIRONMENT (REFERENCE 2)
(Synchronous Equatorial Orbit, Averaged Over Local Time)

Electron Energy E, MEV	Time Averaged Omnidirectional Electron Flux Greater than Energy E, electrons/cm ² /sec
0.01	6.51E+07
0.02	5.80E+07
0.03	5.33E+07
0.04	4.97E+07
0.05	4.65E+07
0.10	3.50E+07
0.20	2.10E+07
0.30	1.29E+07
0.40	7.94E+06
0.50	4.93E+06
0.60	3.07E+06
0.70	1.91E+06
0.80	1.15E+06
0.90	7.45E+05
1.00	4.66E+05
1.10	2.91E+05
1.20	1.82E+05
1.30	1.14E+05
1.40	7.14E+04
1.50	4.47E+04
1.60	2.80E+04
1.70	1.75E+04
1.80	1.10E+04
1.90	6.89E+03
2.00	4.32E+03
2.50	4.18E+02
3.00	4.06E+01
3.50	3.95E+00
4.00	3.84E-01
5.00	3.64E-03

ATS Electron Spectrometer Data

Dr. Vette's AE3 electron environment was developed from spectrometer data from several satellites, in highly eccentric orbits, passing through the synchronous region. The electron spectrometer experiment designed by Aerospace Corporation (Reference 3) for the ATS-F1 spacecraft is providing the first continuous data for the synchronous environment. From the Aerospace detector, electron fluences have been obtained for energies of

0.1, 0.3, 0.7 and 1.4 million electron volts (mev). A plot of minimum and maximum flux rates was supplied by Dr. Paulikas (Reference 4) of Aerospace Corporation (see Figure 2-1). Superimposed on Figure A-1 are Dr. Vette's nominal AE-3 electron environment and the combined Explorer XII and XIV spectra. Considering the factor of 2 uncertainty in Vette's time-averaged environment, the curves are in good agreement.

Paulikas, et al. (Reference 5) have reported diurnal variations in the electron fluxes during normal periods (data during storms and poststorm recovery periods have been excluded). Such diurnal variations in the trapped environment are the result, primarily, of the depression of the magnetosphere by the steady-state solar wind.

Vette, et al. (Reference 2) noted a variation of flux levels, during quiet flare periods, with the 27-day solar rotation. These observations have been tentatively confirmed by the ATS-F1 spectrometer data (Reference 5). For the AE-3 environment, the effects of both diurnal and 27-day variations have been averaged into the nominal model (Reference 2).

Trapped Protons

AP5 Environment

In previous studies it has been assumed that if the solar cells have minimal coverslide protection the low energy trapped protons would have a negligible effect on solar cell array performance. This is true provided the coverslide completely covers those regions of the solar cell which are affected by radiation. When there are gaps, however, the effect of low energy protons must be considered.

A low energy proton environment (AP5) has been recently defined by Dr. J. H. King of Aerospace Corporation (Reference 6). For a synchronous equatorial orbit ($L = 6.6$, $B/B_0 = 1.0$), the integral proton spectrum is defined as

$$\phi = F e^{(E_1 - E) / E_0}$$

where

$\phi \equiv$ protons/cm²/sec of omnidirectional particles with energy greater than E(mev)

$F \equiv$ protons/cm²/sec of omnidirectional particles with energy greater than 0.4 mev = 3.29×10^5

$E_1 \equiv$ normalization energy = 0.4 mev

$E_0 \equiv$ spectral parameter = 0.11 mev

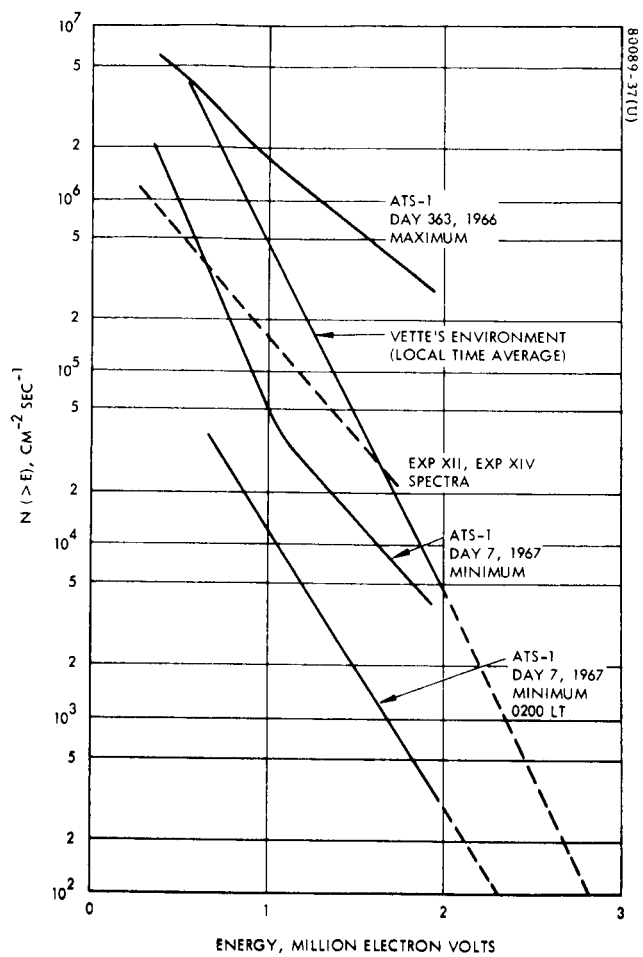


Figure A-1. Extremes in Electron Fluxes

Dr. King's omnidirectional environment (protons/cm²/sec) has been converted to a unidirectional integral spectrum (protons/cm²/day). The unidirectional environment is shown in Figure A-2. At synchronous altitude, the AP5 environment does not consider energies below 0.1 mev due to a lack of data.

From the integral spectrum, a differential proton spectrum for synchronous orbit has been derived. The fluxes for the differential spectrum (see Figure A-3) represent an equivalent unidirectional fluence of protons/cm²/day over an energy range of 0.1 mev. For example, the differential flux of 1.3×10 inches protons/cm²/day indicated in Figure A-3 for 0.15 mev represents the number of protons with energies in the range of 0.1 to 0.2 mev.

It should be noted that at synchronous altitude, the constant solar wind causes diurnal variations in the magnetic field. This effect is similar to that previously discussed for trapped electrons. Unlike the AE3 environment, there was not sufficient data on low-energy protons to estimate a time-averaged value.

Flare Influence. The AP5 environment was obtained from limited spectrometer data from several satellites passing through the magnetosphere. Due to lack of data, time-averaging was not possible. A considerable variation in data was noted during periods of high solar activity (Reference 6). A solar flare emits a magneto-hydrodynamic shock wave and a plasma cloud which depress the earth's magnetic field, thereby altering the effective L value at a given point in the magnetosphere. As the L value is altered, the flux of trapped protons and electrons is also altered. Temporal variations of about a factor of 2 occur in the lower altitudes ($L \leq 4.5$). The growth and decay factors were noted to be both energy and position dependent. For larger L values, fluctuation amplitudes become larger (Reference 6). For $L > 6$, differences in flux rates of about two orders of magnitude were noted over a 2-year period. The larger flux rates were selected as the basis for the AP5 model.

NONTRAPPED ENVIRONMENT

In addition to the trapped protons and electrons, the synchronous orbit radiation environment includes protons, neutrons, X-rays and ultraviolet (UV) radiations, all of which are primarily of solar origin.

Neutrons, X-Rays and Ultraviolet

In addition to a charged particle radiation environment there are specific radiations that are not affected by electric and/or magnetic fields which include:

- Neutrons
- X-rays and bremsstrahlung ($1 < \lambda < 100 \text{ \AA}$)

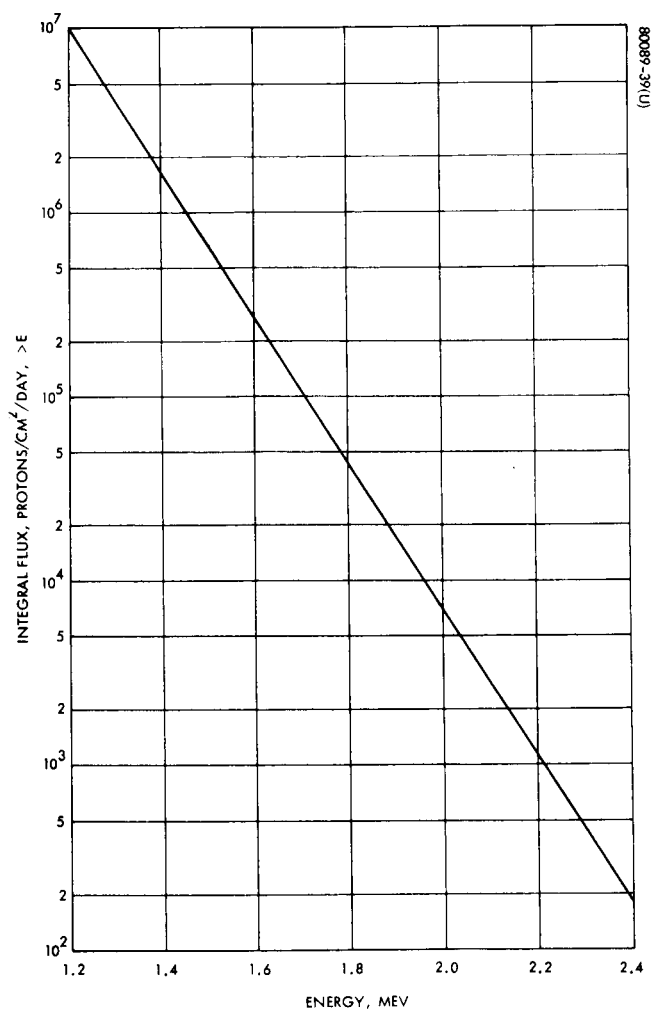
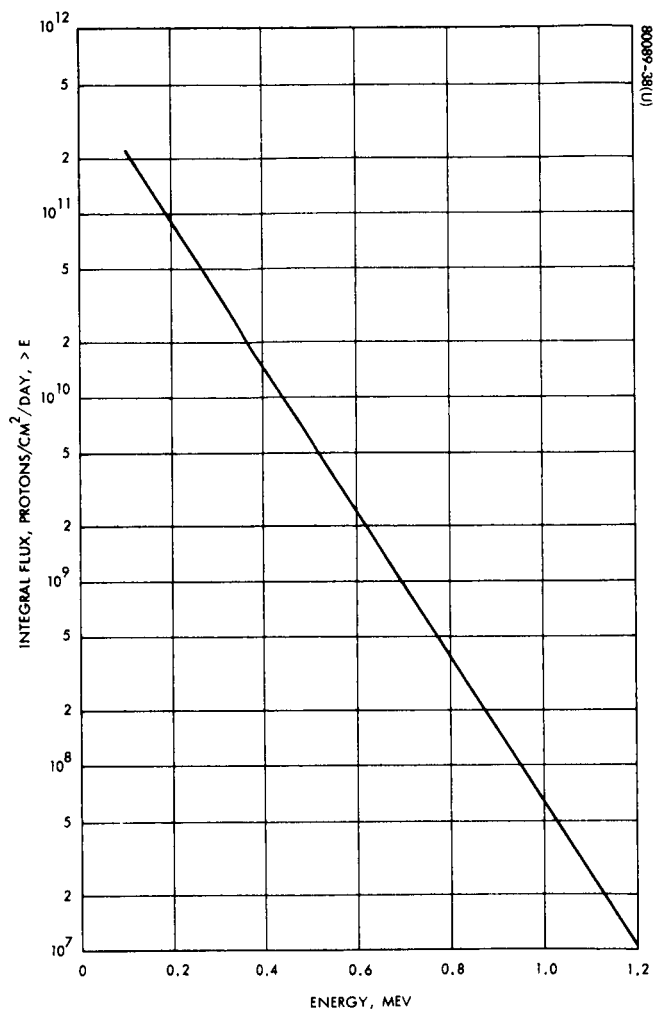


Figure A-2. Equivalent Unidirectional
Integral Proton Spectrum Synchronous
Equatorial Orbit

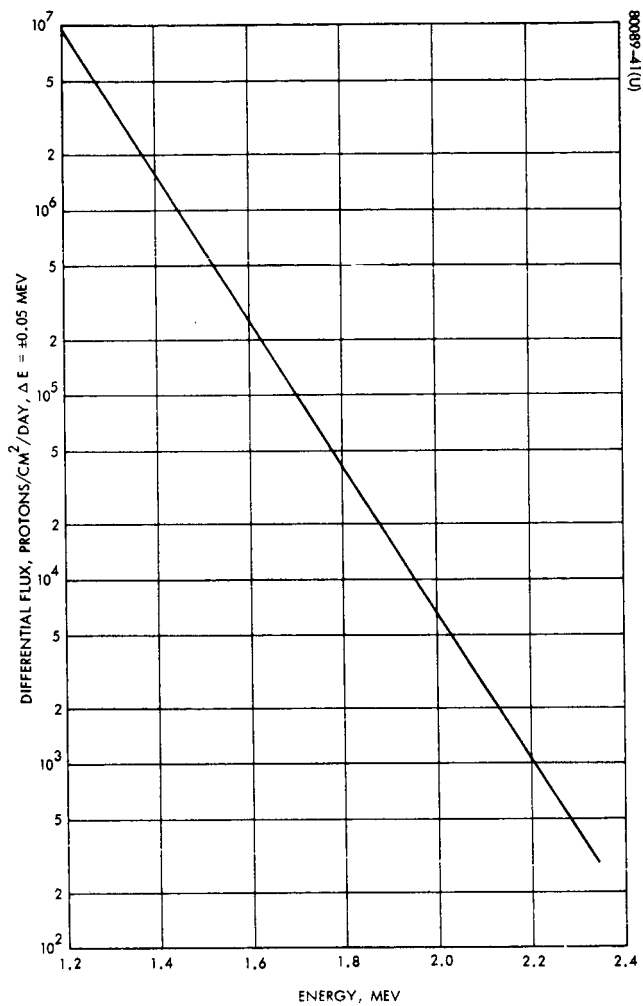
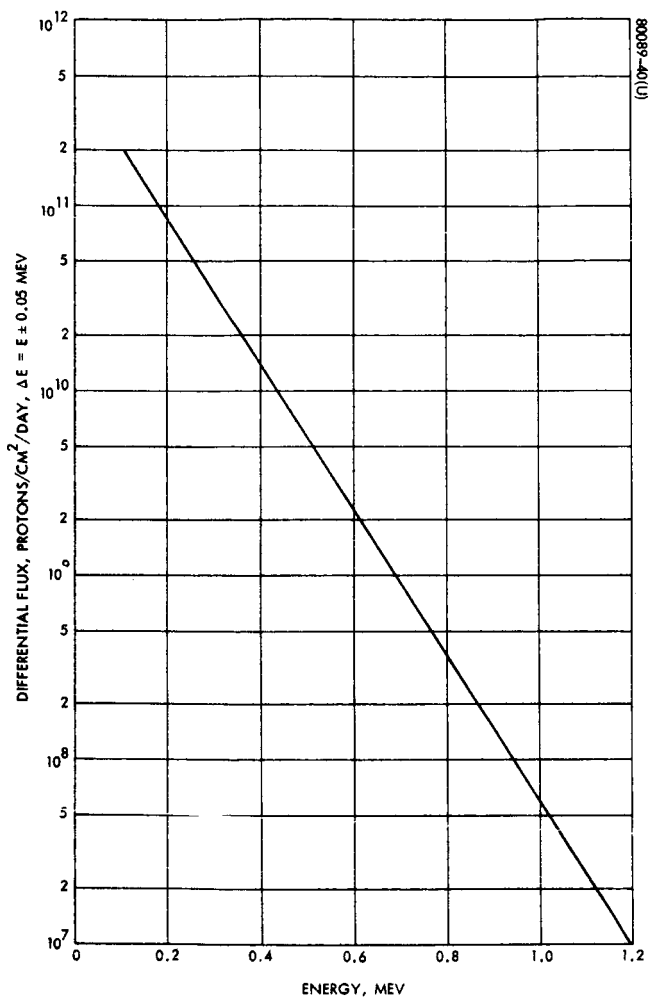


Figure A-3. Equivalent Unidirectional
Differential Proton Spectrum
Synchronous Equatorial Orbit

Ultraviolet ($\lambda < 3000 \text{ \AA}$)

Gamma rays ($\lambda < 1 \text{ \AA}$)

These forms of radiation are only attenuated by the number density of atoms or particles in the material penetrated. As applied to synchronous satellite orbits and associated transfer orbits, the number density of particles is insufficient to appreciably attenuate these neutral radiations.

The only charged particle influence on the neutral radiation is the formation of neutrons by knock-on collision of solar flare and cosmic ray energetic particles with atmospheric particles over the magnetic poles (see References 7 through 16). Cosmic rays are a continuous and constant value and therefore provide a general neutron albedo. Solar flare energetic particles vary greatly with each solar event and can as much as double the neutron count for a short period of time. During the 120-day period, July 1967 through November 1967, about 40 solar flare events occurred. Only five of these produced any significant effects at the magnetic poles. The results shown in Table A-2, reflect only these five solar flare events. The duration of a flare in terms of charged particle bombardment is assumed to be an average of 24 hours. Of all the neutrons generated in the atmosphere about 10 percent escape into space as illustrated by the difference in low and synchronous altitude values.

The X-ray, gamma ray, and ultraviolet radiation are primarily of direct solar origin all the way to the ionosphere. Some bremsstrahlung is formed in telluric space with acceleration of electrons. However this is about 10 to 10^2 times less than the direct solar radiation levels.

The effect of solar flares is to increase the electromagnetic radiation during the rise time of the H α visible phase. However the X-ray and ultraviolet are the greatest producers of ionization in the region of the ionosphere and any increase in intensity will increase electron density in the ionosphere. The amount of the solar radiation increase is illustrated in Table A-2 showing the quiet sun values as compared to the active sun values. Generally there is no increase in the near ultraviolet but there may be an increase of about 10 times in the far ultraviolet (below Ly α ; 1216 \AA). It is quite apparent from Table A-3 that the ultraviolet is the greatest source of energy but most of this provides a skin dose. In fact, the soft X-rays ($50 < \lambda < 100 \text{ \AA}$) are a surface effect and produce only a skin dose. Table A-4 shows the total energy on solar cells.

From the above discussion, it is concluded that the total contribution of the neutrons, X-rays and ultraviolet is small compared to the radiation levels contributed by the natural charged particles.

Solar Protons

The charged particle emissions associated with solar flare events are comprised primarily of protons with an energy spectrum ranging from a few million electron volts (mev) to a few billion electron volts (bev). These

TABLE A-2. NEUTRON ENVIRONMENT AT SYNCHRONOUS ALTITUDE

<u>Neutrons</u>		
Solar	$8.6 \times 10^2 \text{ n cm}^{-2} (\text{day})^{-1}$	
	$E_n > 100 \text{ mev}$	
Albedo	$8.6 \times 10^4 \text{ n cm}^{-2} (\text{day})^{-1}$	low altitudes
	$1.72 \times 10^4 \text{ n cm}^{-2} (\text{day})^{-1*}$ (during flare)	
	$1.72 \times 10^4 \text{ n cm}^{-2} (\text{day})^{-1}$ (during flare)	at synchronous altitudes
	$8.6 \times 10^3 \text{ n cm}^{-2} (\text{day})^{-1}$	

*Forty flares occurred over the 120 days. Of these about five were considered strong flares sufficient to produce changes in output at specific wavelengths.

emissions are sporadic in nature and vary greatly in duration and total proton flux. For design purposes, it is assumed that the total flux intercepted by a spacecraft in earth orbit can be correlated with the relative phase of the mission period in the 90-year solar cycle, but is independent of relative phase in any particular 11-year cycle. There appears to be some correlation of flare events with the 11-year solar cycles but the data are inconclusive. It is expected that the peak of the current 90-year cycle will occur in 1969-70 and that solar activity during this period will be 25 to 30 percent higher than the peak of the last 11-year cycle in 1958-59 (Reference 17 and 18). Specifically, it is assumed that the total flux intercepted by a spacecraft during the 1965 to 1976 period will be 25 percent larger than for a comparable mission period during epoch 1954 to 1965.

In addition to solar flare events, G. A. Paulikas, et al. (Reference 5) have reported from ATS-F1 spectrometer data, a recurrent stream of protons not clearly associated with any pronounced flare activity. This discovery is based on results from the time period 7 January - 1 March 1967 (two solar rotations). It was noted that for 60 percent of the time between 2 February and 1 March there was a proton flux above detector background (apparently of solar origin). Extrapolating this data, Paulikas suggests that during solar maximum, interplanetary space is seldom free of protons of solar origin.

TABLE A-3. ELECTROMAGNETIC ENVIRONMENT AT
SYNCHRONOUS ALTITUDE

X-ray	$1 < \lambda < 100 \text{ \AA}$
Quiet sun	$10^{-5} \text{ to } 10^5 \text{ ergs cm}^{-2} (\text{day})^{-1}$ $10^3 \text{ to } 10^{14} \text{ photons cm}^{-2} (\text{day})^{-1}$
Active sun	$10^{-1} \text{ to } 10^6 \text{ ergs cm}^{-2}$ $10^7 \text{ to } 10^{15} \text{ photon cm}^{-2} \text{ per event}$
γ -ray	$\lambda < 1 \text{ \AA}$
Quiet sun	$< 10^{-2} \text{ ergs cm}^{-2} (\text{day})^{-1}$ $10^6 \text{ photons cm}^{-2} (\text{day})^{-1}$
Active sun	$< 10 \text{ erg cm}^{-2}$ $10^9 \text{ photons cm}^{-2} \text{ per event}$
Ultraviolet	$500 < \lambda < 3000 \text{ \AA}$
	$2.2 \times 10^8 \text{ to } 1.3 \times 10^9 \text{ ergs cm}^{-2} (\text{day})^{-1}$ $2.2 \times 10^{17} \text{ to } 1.3 \times 10^{20} \text{ photons cm}^{-2} (\text{day})^{-1}$
Bremsstrahlung	(Atmospheric X-rays)
	$< 10^{-3} \text{ ergs cm}^{-2} (\text{day})^{-1}$ $10^5 \text{ photons cm}^{-2} (\text{day})^{-1}$

Shielding Effects of the Magnetosphere

Charged particles approaching earth are deflected by the geomagnetic field, and therefore the depth of penetration into the magnetosphere is a function of particle energy and direction of approach. For any given point in the magnetosphere, an approach cone (or solid angle) exists such that only

TABLE A-5. CHARACTERISTIC RIGIDITY P_0
FOR 29 SOLAR EVENTS

Date	*Integrated Intensity, protons/cm ²		*Characteristic Rigidity P_0 , millivolts
	>30 mev	>100 mev	
23 February 1956	1.0×10^9	3.5×10^8	195
31 August 1956	2.5×10^7	6.0×10^6	144
20 January 1957	2.0×10^8	7.0×10^6	61
29 August 1957	1.2×10^8	3.0×10^7	56
20 October 1957	5.0×10^7	1.0×10^7	127
23 March 1958	2.5×10^8	1.0×10^7	64
7 July 1958	2.5×10^8	9.0×10^6	62
16 August 1958	4.0×10^7	1.6×10^6	64
22 August 1958	7.0×10^7	1.8×10^7	56
26 August 1958	1.1×10^8	2.0×10^6	51
22 September 1958	6.0×10^6	1.0×10^5	50
10 May 1959	9.6×10^8	8.5×10^7	84
10 July 1959	1.0×10^9	1.4×10^8	104
14 July 1959	1.3×10^9	1.0×10^8	80
16 July 1959	9.1×10^8	1.3×10^8	105
1 April 1960	5.0×10^6	8.5×10^5	116
28 April 1960	5.0×10^6	7.0×10^5	104
4 May 1960	6.0×10^6	1.2×10^6	127
13 May 1960	4.0×10^6	4.5×10^5	94
3 September 1960	3.5×10^7	7.0×10^6	127
26 September 1960	2.0×10^6	1.2×10^5	73
12 November 1960	1.3×10^9	2.5×10^8	124
15 November 1960	7.2×10^8	1.2×10^8	114
20 November 1960	4.5×10^7	8.0×10^6	118
11 July 1961	3.0×10^6	2.4×10^5	81
12 July 1961	4.0×10^7	1.0×10^6	56
18 July 1961	3.0×10^8	4.0×10^7	102
20 July 1961	5.0×10^6	9.0×10^5	120
28 September 1961	6.0×10^6	1.1×10^6	121

*Data from Reference 21.

TABLE A-6. CALENDAR OF SOLAR PROTON EVENTS
FROM 1956 TO 1961

Date	Integrated Intensity, protons/cm ²		Source Reference No.
	>30 mev	>100 mev	
23 February 1956	1.0×10^9	3.5×10^8	22
10 March 1956	1.1×10^8		23
31 August 1956	2.5×10^7	6.0×10^6	22
13 November 1956	1.1×10^8		23
20 January 1957	2.0×10^8	7.0×10^6	22
3 April 1957	5.6×10^7		23
6 April 1957	3.8×10^7		23
22 June 1957	1.7×10^8		23
3 July 1957	2.0×10^7		22
9 August 1957	1.5×10^6		22
29 August 1957	1.2×10^8	3.0×10^6	22
31 August 1957	5.3×10^7		23
2 September 1957	1.4×10^7		23
21 September 1957	1.5×10^6		22
20 October 1957	5.0×10^7	1.2×10^7	22
4 November 1957	9.0×10^6		22
9 February 1958	1.0×10^7		22
23 March 1958	2.5×10^8	1.0×10^7	22
25 March 1958	7.8×10^8		23
4 May 1960	6.0×10^6	1.2×10^6	22
6 May 1960	4.0×10^6		22
13 May 1960	4.0×10^6	4.5×10^5	22
1 June 1960	4.0×10^5		22
12 August 1960	6.0×10^5		22
3 September 1960	3.5×10^7	7.0×10^6	22
26 September 1960	2.0×10^6	1.2×10^5	22
12 November 1960	1.3×10^9	2.5×10^8	22

Table A-6. (continued)

Date	Integrated Intensity, protons/cm ²		Source Reference No.
	>30 mev	>100 mev	
10 April 1958	5.0×10^6		22
7 July 1958	2.5×10^8	9.0×10^6	22
16 August 1958	4.0×10^7	1.6×10^6	22
22 August 1958	7.0×10^7	1.8×10^6	22
26 August 1958	1.1×10^8	2.0×10^6	22
22 September 1958	6.0×10^6	1.0×10^5	22
13 February 1959	2.8×10^7		23
10 May 1959	9.6×10^8	8.5×10^7	22
13 June 1959	8.5×10^7		22
10 July 1959	1.0×10^9	1.4×10^8	22
14 July 1959	1.3×10^9	1.0×10^8	22
16 July 1959	9.1×10^8	1.3×10^8	22
18 August 1959	1.8×10^6		22
11 January 1960	4.0×10^5		22
29 March 1960	2.7×10^7		23
1 April 1960	5.0×10^6	8.5×10^5	22
5 April 1960	1.1×10^6		22
28 April 1960	5.0×10^6	7.0×10^5	22
29 April 1960	7.0×10^6		22
15 November 1960	7.2×10^8	1.2×10^8	22
20 November 1960	4.5×10^7	8.0×10^6	22
11 July 1961	3.0×10^6	2.4×10^5	22
12 July 1961	4.0×10^7	1.0×10^6	22
18 July 1961	3.0×10^8	4.0×10^7	22
20 July 1960	5.0×10^6	9.0×10^5	22
10 September 1961	3.7×10^7		23
28 September 1961	6.0×10^6	1.1×10^6	22

TABLE A-4. TOTAL ENERGY ON SOLAR CELLS

Synchronous Orbit (120 days)	Quiet	With Flares
Neutrons (n-cm ⁻²)	1.04×10^6	1.13×10^6
X-ray (ergs-cm ⁻²)	1.2×10^7	1.7×10^7
Y-ray (ergs-cm ⁻²)	Negligible	Negligible
Bremsstrahlung	Negligible	Negligible
Ultraviolet (ergs-cm ⁻²)	1.2×10^{11}	1.2×10^{11}

particles having a minimum critical energy and the proper spatial orientation to pass through the cone will penetrate. Solar flare protons are assumed to be omnidirectional. Therefore, the ratio of the approach cone solid angle to the total spherical angle represents the fraction of incident omnidirectional particles of a given energy that will reach the given point.

Using the Störmer approach cone theory (Reference 19) (a dipole approximation to the magnetic field), a minimum cutoff energy of 24 mev is predicted. (A Störmer cutoff energy of 24 mev corresponds to an approach cone solid angle of 0 steradians.) However, Vela and ATS-F1 data (Reference 5) indicate that in the synchronous region the magnetosphere is a "Very leaky shield" with a cutoff energy much lower than that predicted by Störmer theory.

The latest ATS-F1 spectrometer results (Reference 20) indicate that the magnetospheric cutoff energy in synchronous orbit may be below 5 mev for at least part of the time. Paulikas (Reference 5) reports a diurnal variation in the protons in the 6 to 20 mev range. This result is probably due to the distortion of the magnetosphere by the solar wind. The low energy protons may be gaining access by diffusion through the magnetically neutral tail of the distorted magnetosphere. Exposure to these relatively low energy proton fluxes (5 to 10 mev) during the upcoming peak of the solar cycle may constitute a very real hazard to solar array performance in synchronous orbit. This potential problem has not yet been fully evaluated.

Statistical Model for Protons with Energies Greater than 30 MEV

Flare events during the 1956 to 1961 period have been recorded and analyzed by W.R. Webber (Reference 21) and D.K. Bailey (Reference 22). The results were conveniently organized by Modisette, et al. (Reference 23),

and are shown in Tables A-5 and A-6. For energies greater than approximately 20 mev, the energy spectrum is taken to be of the form:

$$F(>E) = A \exp (-P(E)/P_0) \quad (1)$$

where A is the event size parameter, P(E) the magnetic rigidity, and F(>E) the flux having rigidity greater than P. The spectral parameter is P_0 . The spectral parameters for 29 events are shown in Table A-5. An analysis of these data revealed that with the exception of the 23 February 1956 event, the P_0 values fit a rectangular distribution with a mean of 97 mv and extreme values of 50 and 144 mv (Reference 23). The significance of the P_0 variation is illustrated in Figure A-4 for an average flare of 1.85×10^8 protons ($E > 30$ mev).

The flare event data, shown in Table A-6, were further analyzed by Modisette, et al. (Reference 23), to determine the probability that a free space flux of greater than N protons/cm² ($E > 30$ mev) would be intercepted during mission periods ranging from 2 to 104 weeks. The approach adopted was to consider each day in the period 1956 to 1961 as a launch date, and then use Table A-6 to determine the total number of protons to be encountered. Most of the shorter missions did not encounter any protons. For missions that did encounter protons, the statistical distribution of the number of protons encountered was determined. To prevent redundancy, the missions were grouped such that the number of missions in each group equaled the number of days in the mission. For short missions, the distributions were found to be normal with respect to the logarithm of the number of protons. For longer missions, the data were insufficient to determine the distribution with assurance. A normal distribution was assumed, however, as being consistent with the results of shorter missions.

The results of the above statistical analysis are shown in Figure A-5 for three probability levels: 0.1, 0.01, and 0.001. Modisette only considered mission periods less than 104 weeks, but the shape of the resulting curves permits extrapolation to longer periods with a minimal probable error.

Statistical Model for Protons with Energies Greater than 5 MEV

As was previously discussed, recent data indicate that the magnetosphere cutoff energy for the synchronous region is probably below 5 mev.

A solar proton spectrum for soft events (an extreme case) has been presented by Bailey (see Figure A-6) (Reference 22). From Bailey's curve the relative flux for two energies can be obtained. Thus, the flux can be adjusted as a function of energy.

Using Modisette's data and assuming a 2σ design point, a proton fluence of approximately 2×10^{10} protons/cm² is obtained for a 1-year mission (free space) for proton energies greater than 30 mev. Bailey's

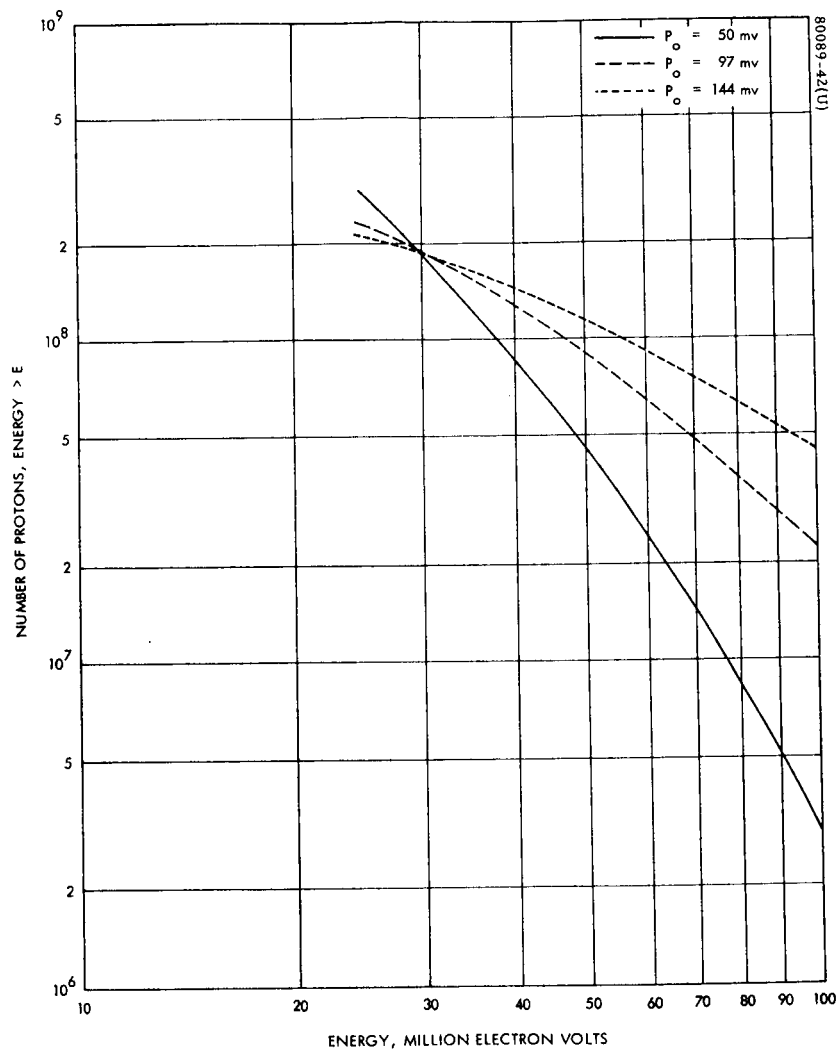


Figure A-4. Average Energy Spectrum - Solar Flare Protons

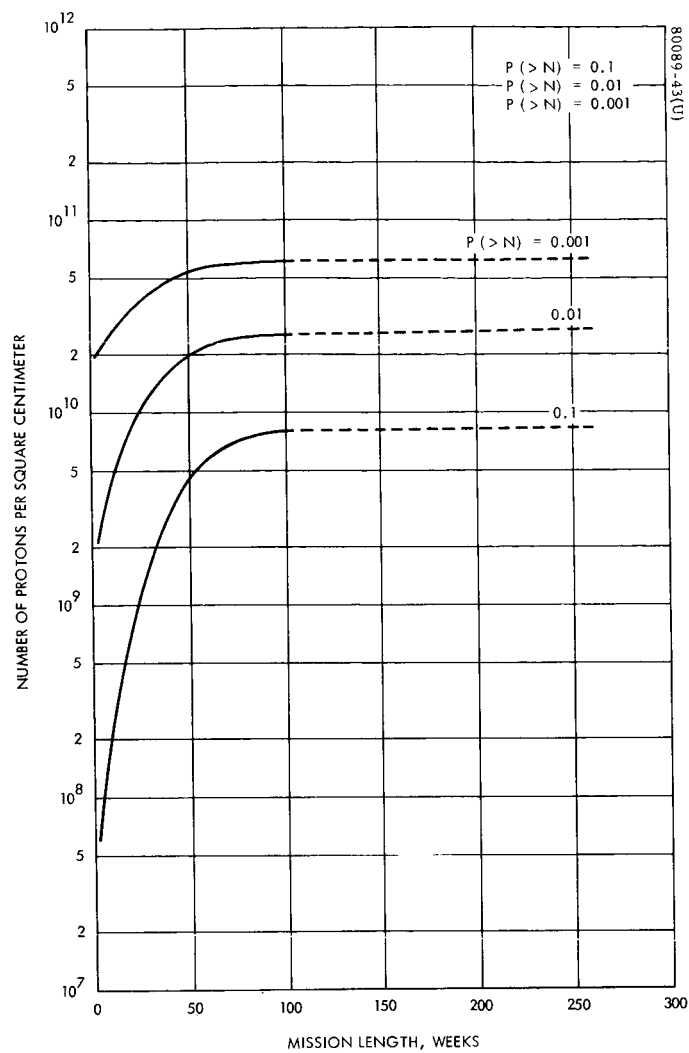


Figure A-5. Variation of Number of Solar Protons per cm^2 (E730 mev) with Mission Length at Three Probability Levels

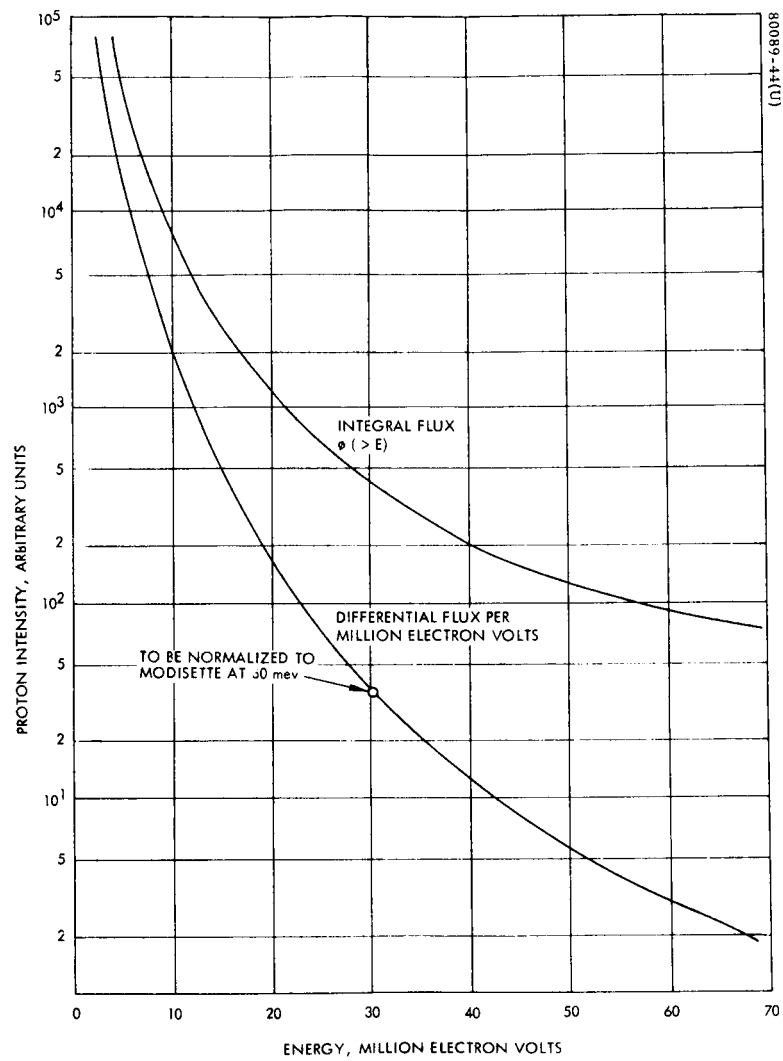


Figure A-6. Solar Proton Spectrum Model for Soft Events (Extreme Case)

integral flux curve (Figure A-6) shows an increase of about two orders of magnitude from 30 mev to 5 mev. Thus the yearly fluence for protons greater than 5 mev would be about 2×10^{12} protons/cm².

Prediction of a worst-case proton spectrum is, at best, an inaccurate guess. The most recent recommendation by Aerospace (Reference 24) was to extrapolate the 12 November 1960 proton event on a log-log scale as a worst-case assumption. This has been done in Figure A-7 based on data supplied by Masley (Reference 24), which does not exactly agree with that supplied by Modisette. It should be noted that the 12 November 1960 flare was very soft.

REFERENCES

1. J. I. Vette, "Synchronous Orbit Composite Electron Environment," Aerospace Corporation, 15 October 1966.
2. J. I. Vette, et al., "Models of the Trapped Radiation Environment, Volume III: Electrons at Synchronous Altitudes," NASA SP-3024, Vol. 3, 1967.
3. Paulikas, G. A., et al., "First Quarterly Report for ATS-1 Omnidirectional Spectrometer," Technical Data Report for the Applications Technology Satellite (ATS) Program, Goddard Spaceflight Center, Greenbelt, Maryland, 1967.
4. Paulikas, Dr. G. A., Aerospace Corporation, 16 November 1967.
5. Paulikas, G. A., et al., "Third Quarterly Report for ATS-1 Omnidirectional Spectrometer (15 May 1967 - 15 August 1967)," prepared for Goddard Spaceflight Center, 6 October 1967.
6. King, Dr. Joseph H., "Models of the Trapped Radiation Environment, Volume IV: Low Energy Protons," NASA SP-3024, Vol. IV, 1967.
7. Hess, Wilmot N., Introduction to Space Sciences. Gordon and Breach Science Publication. New York 1965, p. 174.
8. Chupp, E. L., Hess, W. N., Curry, C., "The Neutron Flux in Space After the 15 November 1960 Polar Cap Neutron Event," JGR, 1 August 1967, Vol. 72, No. 15, pp. 3804-3816.
9. Webber, W. R., Ormes, J. F., "An Upper Limit on the Quiet Time Solar Neutron Flux at Energies > 60 Mev," JGR, 1 July 1967, Vol. 72, No. 13, pp. 3387-3394.
10. Freden, Stanley C. and White, R. Stephen, "Trapped Proton and Cosmic-Ray Albedo Neutron Fluxes," JGR, January 1962, Vol. 67 No. 1, pp. 25-29.

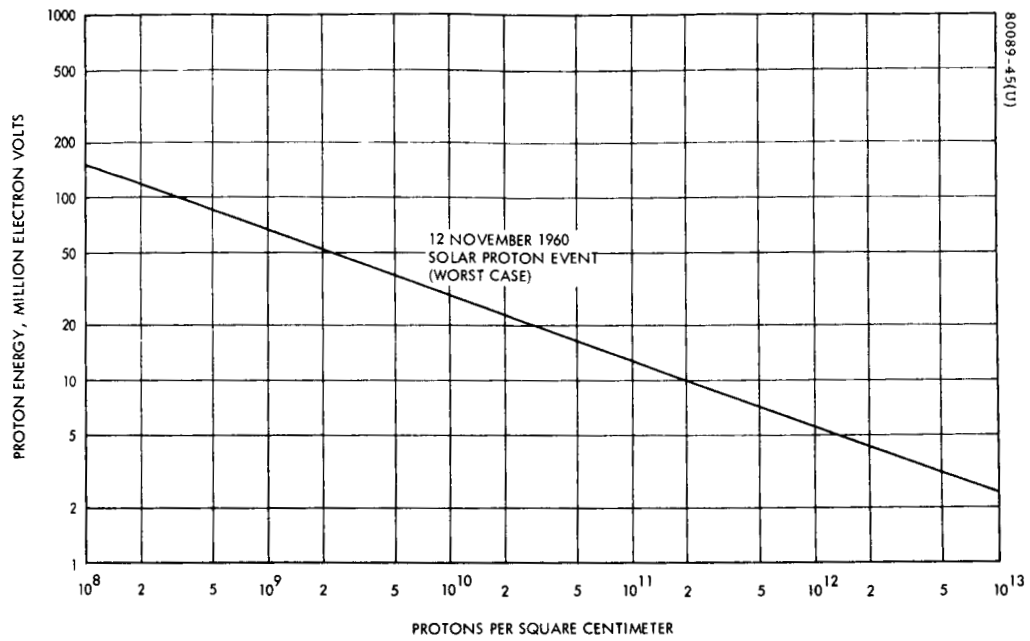


Figure A-7. Worst Case Solar Flare Spectrum Model

11. Hess, W. N., Canfield, E. H., Lingenfelter, R. E., "Cosmic-Ray Neutron Demography," JGR, March 1961, Vol. 66, No. 3, pp. 665-677.
12. Ratcliffe, J. A., Physics of the Upper Atmosphere, Academic Press 1960, pp. 203-208.
13. Le Galley, Donald P., Space Science, John Wiley & Sons, New York, 1963, p. 593.
14. Tousey, Richard, "The Solar Spectrum in Space," Astronautics, July 1961, Vol. 6, No. 7, p. 32.
15. Valley, Shea L., Handbook of Geophysics and Space Environments, AFCRL, McGraw-Hill, New York, 1965, pp. 16-16 to 16-17.
16. Brandt, John C., Hodge, Paul W., Solar System Astrophysics, McGraw-Hill, New York, 1964, p. 184.
17. E. Angle, private communication, Hughes Aircraft Company, El Segundo, California, July 1966.
18. H. Friedman, and R. Kreplin, Comments at COSPAR Meeting, Vienna, Austria, May 1966.
19. R. A. Alpher, "Theoretical Geomagnetic Effects in Cosmic Radiation," J. of Geophysical Research, Vol. 55, No. 4, December 1960.
20. Paulikas, G. A., Aerospace Corporation, private communication, December 1967.
21. W. R. Webber, "An Evaluation of the Radiation Hazard Due to Solar Particle Events," DZ-90469, The Boeing Company, 1963.
22. D. K. Bailey, "The Detection and Study of Solar Cosmic Rays by Radio Techniques," J. Phys. Soc., Japan, Vol. 17, Suppl A1, Part I, January 1962, pp. 106-112.
23. J. L. Modisette, et al., "Model Solar Proton Environments for Manned Spacecraft Design," NASA TN-D-2746, April 1965.
24. Masley, A. J., Aerospace Corporation, private communication, November 1967.

APPENDIX B. ATS TRANSFER ORBIT RADIATION ENVIRONMENT

INTRODUCTION

The trapped proton radiation environment for the ATS (and Intelsat) satellite transfer orbits has been evaluated and compared with the synchronous environment. The trapped electron environment was not considered significant for this study.

ORBITS

Initial orbital elements for the nominal ATS transfer orbit are as follows:

Inclination = 31.0774 degrees

Argument of perigee = 179.6794 degrees

Longitude of ascending node at time of injection
= 158.0634 degrees

Time of perigee (after injection) = 175.05 seconds

Semimajor axis = nautical miles 13432.031

Eccentricity = 0.7363751

The nominal and actual transfer orbits for Intelsat II-F2, 3, and 4 as well as ATS-F1 and F2 are very close to the orbit defined above. The primary difference between the transfer maneuvers of these satellites is the total time period in the transfer orbit. Intelsat II-F2 and F4 were in the transfer orbit for 6.5 orbits and F3 for 5.5 orbits while ATS-F1 and F2 were in the transfer orbit for 1.5 orbits.

RADIATION ENVIRONMENT

The composite transfer orbit radiation environment includes trapped electrons, trapped protons, and some neutral radiations. Trapped electrons were not considered significant for this study.

TRAPPED PROTONS

Integral and differential proton flux-energy spectra for one transfer orbit are shown in Figures B-1 and B-2 respectively. Comparative data in terms of an equivalent number of days in synchronous orbit are presented in Figures B-3 and B-4. The synchronous orbit data are based on King's AP5 map.

NEUTRONS, X-RAYS, AND ULTRAVIOLET

As in synchronous orbit (see Appendix A), the composite transfer orbit environment includes some neutral radiations. However, as shown in Table B-1, these components are negligible relative to charged particle radiation.

TABLE B-1. TOTAL ENERGY ON SOLAR CELLS

Transfer Orbit (5.5 hours)	Quiet	With Flares
Neutrons (n-cm ⁻²)	3.58×10^4	7.2×10^4
X-ray (ergs-cm ⁻²)	2.3×10^4	2.3×10^5 (max)
γ-ray (ergs-cm ⁻²)	Negligible	Negligible
Bremsstrahlung	Negligible	Negligible
Ultraviolet (ergs-cm ⁻²)	2.3×10^3	2.3×10^3

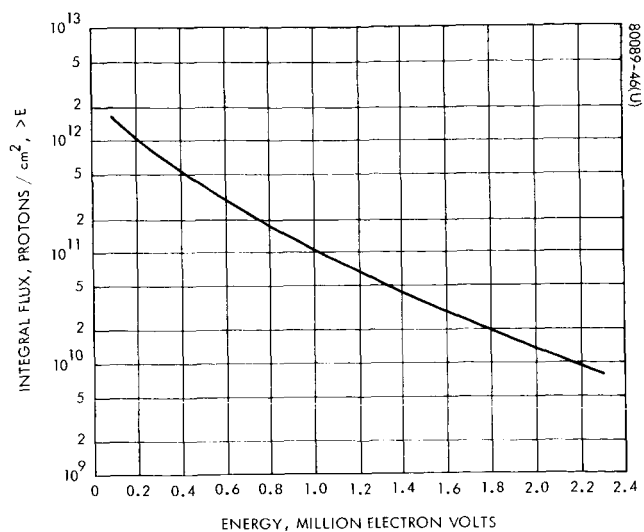


Figure B-1. Equivalent Unidirectional Integral Proton Spectrum - One Transfer Orbit

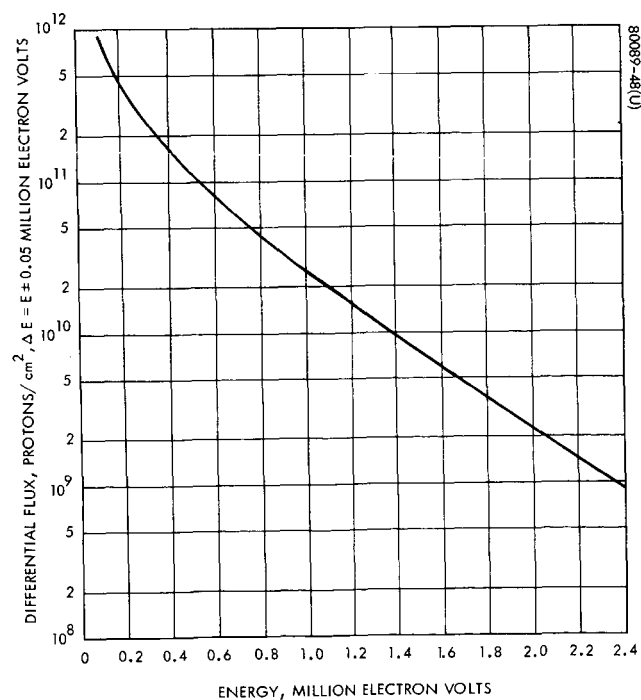


Figure B-2. Equivalent Unidirectional Differential Proton Spectrum - One Transfer Orbit

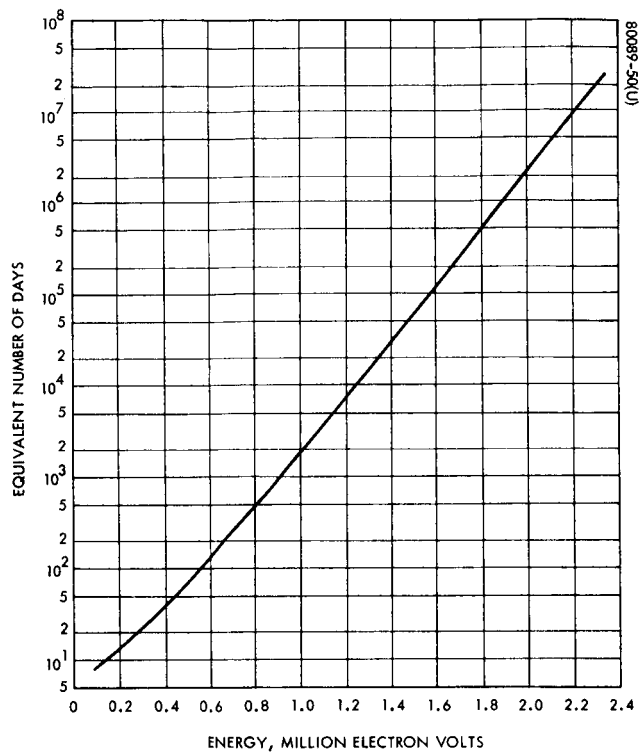


Figure B-3. Equivalent Number of Days in Synchronous Orbit Versus Energy (One Transfer Orbit - Integral Proton Spectrum)

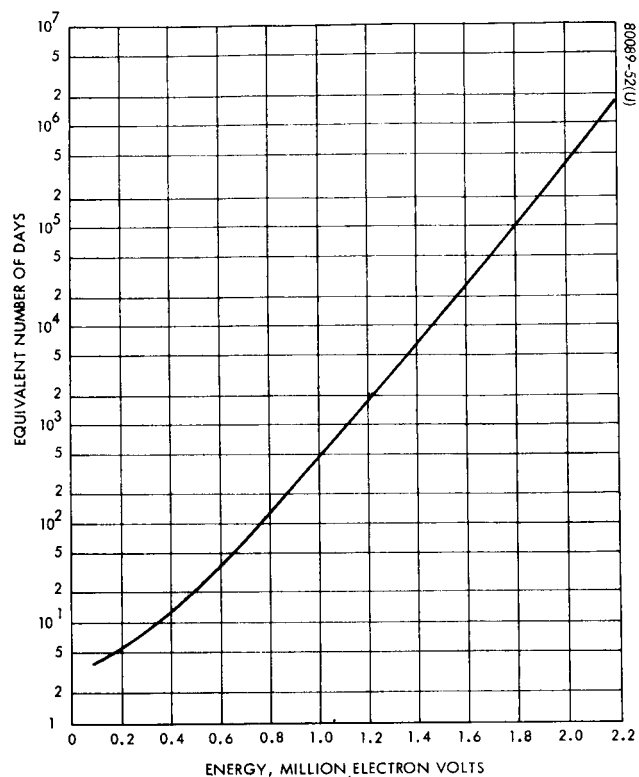


Figure B-4. Equivalent Number of Days in Synchronous Orbit Versus Energy (One Transfer Orbit - Differential Proton Spectrum)

APPENDIX C. DATA REDUCTION TECHNIQUES

INTRODUCTION

In general, in-orbit array performance data is in the form of individual V-I data pairs with the associated sun angle and mean array temperature data. In the case of ATS-F1, all of these parameters are measured by on-board sensors. The Syncom and Intelsat telemetry data included only bus voltage and sun angle; the other parameters were calculated using ground test data and thermal models.

The array performance parameter of most significance is the V-I curve spanning a bus voltage range from 0 to open-circuit. However, during typical operation in space, the array operating voltage is usually held to within a relatively narrow operating region spanning the array maximum power point. These data over a limited voltage (or current) range must then be in some way extrapolated to deduce the complete array V-I curve.

The complete data reduction task is essentially a four step process:

- 1) Conversion of telemetry data to engineering units
- 2) Statistical evaluation of raw data
- 3) Correction of individual V-I pairs for intensity and temperature
- 4) Modeling or "curve fitting" the point data for extrapolation purposes and to further reduce random error

Steps 1 and 2 are intimately associated with the respective telemetry subsystems and will not be considered in this report. Steps 3 and 4 are discussed in the following subsections of this Appendix.

DATA CORRECTION TO STANDARD CONDITIONS

Mean values of the flight data quantities discussed in the above introduction were grouped over a narrow time span chosen to maximize the bus voltage range. Specifically, changes in degradation were assumed to be negligible over time spans of less than 3 days.

A computer program was used to correct each V-I pair to standard conditions of 25°C, 140mw/cm², AMO. Due to the nonlinearities resulting from the inherent intensity gradients associated with cylindrical arrays, it is difficult to define a theoretically rigorous procedure for point data translations. However, experience has shown that a linear translation does yield accurate results over virtually the entire V-I curve.

CORRECTION TO STANDARD TEMPERATURE

Both array current and voltage are influenced by temperature. For temperature changes in the range 25°C ± 20°C, these changes are linear functions of temperature, independent of illumination intensity.

Current corrections to a standard temperature of 25°C were made in accordance with Equation (1)

$$I = I_1 + (29.0 \times 10^{-6}) \times (25 - P_1) \times E \quad (1)$$

where

I = corrected aft panel current

I_1 = uncorrected current

$P_1 = (5/9) (T_1 - 32)$ = panel temperature in °C

T_1 = panel temperature in °F

E = effective cells in parallel

29.0×10^{-6} = current temperature correction coefficient for
1 x 2 cm cells (amps/°C/cell)

Voltage temperature corrections were made in accordance with Equation (2)

$$V_{C2} = V_{C1} - 2.1 \times 10^{-3} \times M \times (C_2 - C_1) \quad (2)$$

where

V_{C1} = voltage at temperature C_1

V_{C2} = voltage at temperature C_2

m = number of cells in series, and

$- 2.1 \times 10^{-3}$ = temperature coefficient (volts/°C)

CORRECTION TO STANDARD INTENSITY

For the small intensity corrections required for the flight data under consideration, it may be assumed that only the array current at any given voltage is affected. Each current point can be corrected to standard intensity conditions through the use of simple multiplicative correction ratios.

The solar intensity at a given point in time is found from

$$I = 139.7 + 4.7 \times \cos(\text{day}) \text{ mw/cm}^2$$

where the day is based on a 360-day year, and treated as degrees. It is assumed that perihelion occurs on December 31 (day 360 or day 0). Standard intensity (day 90 or day 270) is assumed to be 139.7 mw/cm². To correct to standard intensity (139.7 mw/cm²), the intensity factor is determined by the ratio 139.7/I. Intensity is assumed to affect current, but not voltage (a reasonable assumption for small changes in intensity). To correct the current for intensity, the current is multiplied by the intensity factor.

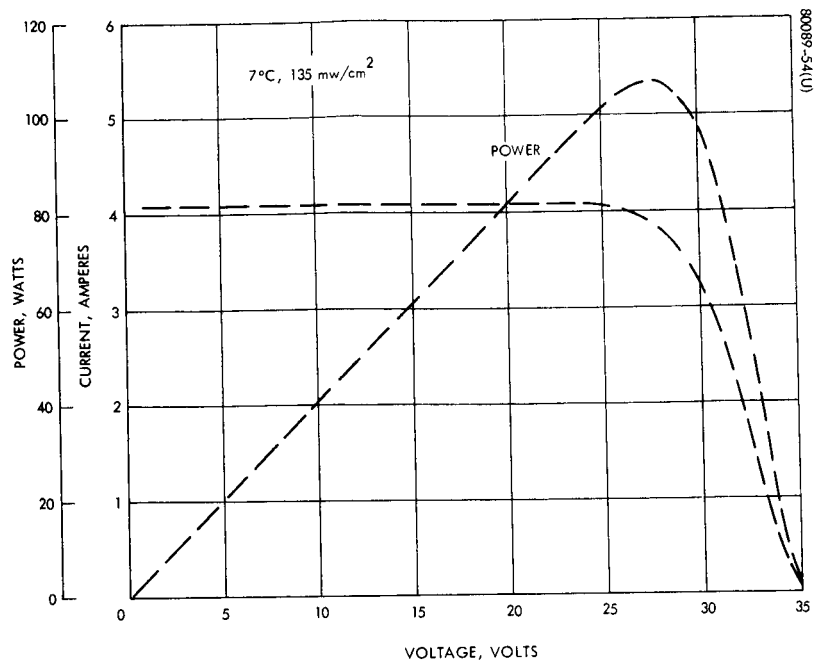
In addition to solar intensity, the current (again, voltage corrections are assumed negligible) must be corrected for sun angle. The telemetered sun angle (phi angle) is the angle between the spacecraft spin axis and the sun line. Subtracting the phi angle from 90 degrees gives the sun angle as the angle between the sun line and the normal to the panels. The solar intensity on the panels varies as the cosine of the angle between the normal and the sun line. To correct to standard sun normal conditions, the angle of incidence factor is determined from the ratio 1/cos (sun angle off normal). Like the intensity factor, the current is corrected by multiplying by the angle of incidence factor.

Both solar intensity and angle of incidence corrections are made under standard temperature (25°C) conditions.

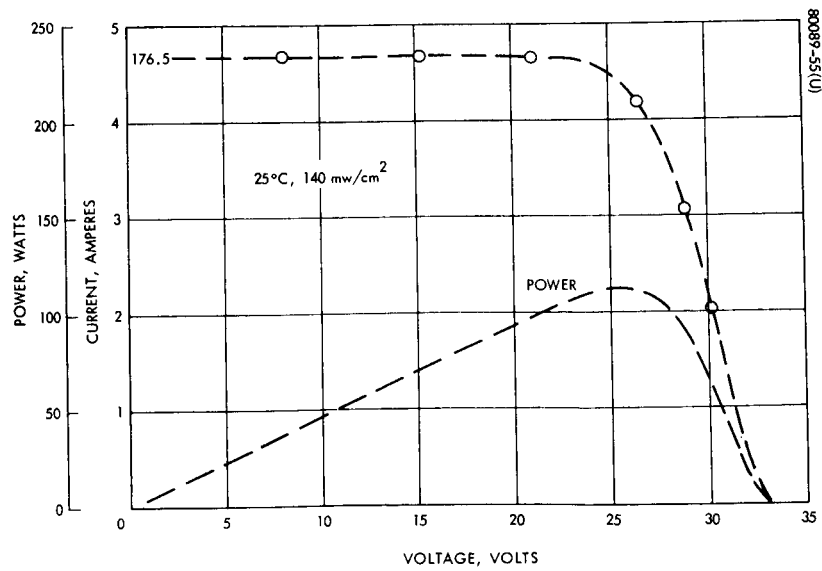
VERIFICATION ANALYSIS

To verify the accuracy of the temperature and intensity corrections discussed above, the Hughes cylindrical array simulation computer program was used to generate a V-I curve for a typical cylindrical array under both standard conditions (25°C, 140 mw/cm²) and summer solstice conditions (7°C, 135 mw/cm²). The theory underlying this computer simulation is rigorous in all essential respects and totally independent of the simple correction technique being evaluated.

The summer solstice curve shown in Figure C-1a was used as the test case. Current points spanning the array voltage range were corrected to standard conditions with the results shown as circled points superimposed on the V-I curve of Figure C-1b. Excellent correlation was obtained.



a) Summer Solstice Conditions



b) Under Standard Conditions

Figure C-1. Typical V-I Curve

SOLAR CELL V-I MODEL

As was previously noted, flight V-I data typically span a narrow voltage range. To extrapolate these data to a complete V-I curve, it is necessary to employ a mathematical model. The cell or array model developed by Hughes for performance simulation studies was utilized in this application with excellent results. The model is totally controlled by the four-cell parameters I_{sc} , V_{oc} , I_{mp} , and V_{mp} . An optimization subroutine, described in the following subsection was used to determine the parameter values. A detailed description of this modeling technique is presented in a separate Hughes report. The temperature correction used to reduce the ATS-F1 solar cell experiment data was based on the translation of these optimized model parameters which vary in a linear fashion.

OPTIMIZATION TECHNIQUE FOR GENERALIZED MATHEMATICAL MODELS

The subject optimization program uses the method of steepest descent to minimize the square root of the sum of the squares of the errors between model predictions and data current for a given voltage. A simplified explanation of the optimization technique is as follows:

Experimentally derived V-I pairs, corresponding to the V-I curve of a solar array, are supplied to the program along with estimates of the model parameters, I_{sc} , V_{oc} , I_{mp} , and V_{mp} . Using these initial estimates of the model parameters, the model is evaluated for current at each input voltage point. The square root of the sum of the errors squared (called the cost function) between model predictions and input currents is calculated.

The gradient of the cost function with respect to the model parameters is numerically calculated and evaluated at the initial estimates of the model parameters. Since the gradient vector points in the direction of the greatest rate of change of the cost function surface, a less than or equal cost can be found in a direction opposite to the gradient. Therefore, by means of an iteration procedure, a lowest value of cost is found along the surface in the negative gradient direction in a neighborhood about the initial estimate point. This procedure results in a second set of estimates for the model parameters and, based on these estimates, another gradient is calculated and a second lower cost is found. This method is continued until the absolute value of the difference between two successive cost values is less than or equal to some epsilon greater than zero. At this point a local minimum has been found and corresponding optimum values of I_{sc} , V_{oc} , I_{mp} , and V_{mp} are given.

A study was conducted to evaluate the accuracy of the optimization procedure in obtaining values of I_{sc} , V_{oc} , I_{mp} , and V_{mp} , given V-I data points only in the "knee" region of the curve. Data points from V-I curves of a cylindrical panel, obtained from Table Mountain tests, were supplied to the optimization program. These data points covered a range about the

knee of the curve that was similar to the average range of the ATS-F1 flight data. Since the actual values of I_{SC} and V_{OC} for these Table Mountain curves were known, a comparison between the resulting optimized values and the true values could be made.

This comparison resulted in a maximum error in current of about 2.5 percent and in voltage of less than 0.5 percent. These percentage errors were considered acceptable relative to the magnitude of the expected environmental degradation.

APPENDIX D. LOW ENERGY PROTON IRRADIATION TESTS OF SOLAR CELL ASSEMBLIES

THEORETICAL CONSIDERATIONS

Qualitatively, a solar cell can be regarded as a parallel assembly of differential cell sections normal to the grid (top contact) collection system. This concept is presented in Figure D-1, where, for illustrative purposes, the cell is sectioned into three parts. The grid contact configuration has an associated resistance, R_c . The sheet resistance of the thin N-layer is represented by R_s and the bulk resistance of the relatively thick P-layer by R_b . The photovoltaic conversion process is modeled in a conventional manner as a constant current source, S , shunted by a forward biased diode. The shunt resistance bypassing the junction region is represented by R_H . Ignoring the shunt resistances (normally very large) and lumping all series resistance resistances into an equivalent term, R , a differential section of the cell can be represented by Equation (1).

$$I = S - I_o \left\{ \exp \left[q \frac{(V + IR)}{AKT} \right] - 1 \right\} \quad (1)$$

where

I = load current

V = load voltage

q = Electronic charge

K = Boltzmann's constant

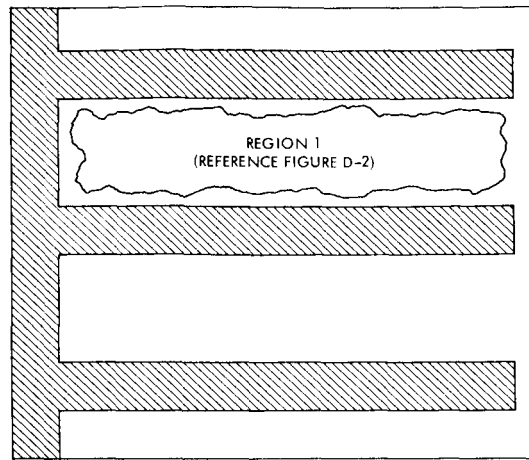
T = temperature

R = equivalent series resistance

I_o = diode reverse saturation current

A = a complex parameter having a value in the range 1 to 2.

Equation (1) is based on classic diffusion theory for semiconductor junctions.



80802-68008
(U)95-68008

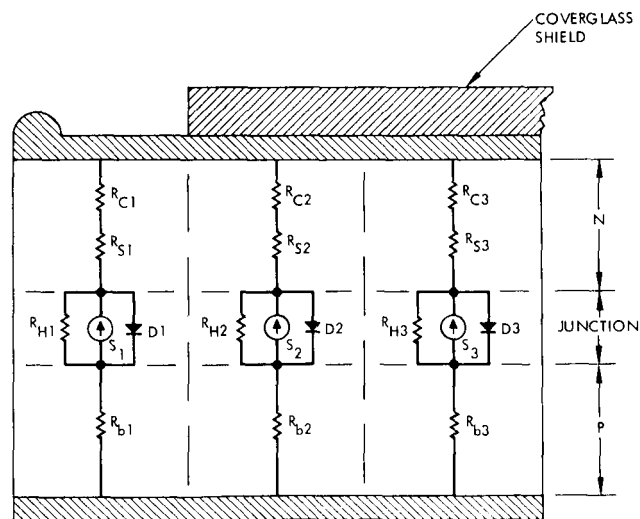


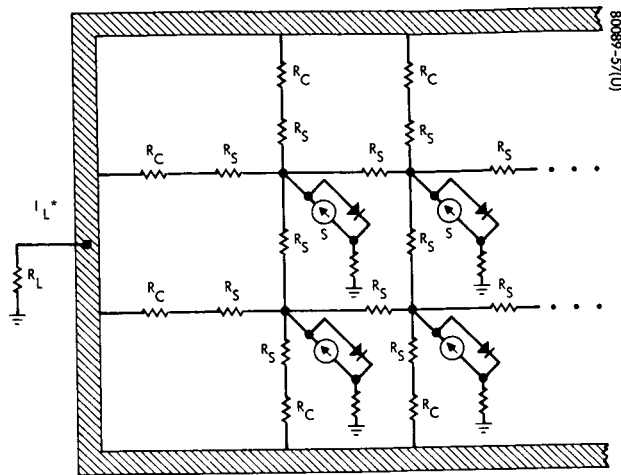
Figure D-1. Simplified Solar Cell Schematic

With reference to Figure D-1, suppose the differential cell section adjacent to the bus bar were irradiated with low-energy protons which would be absorbed in the immediate junction area. The first order effect of such irradiation would be a reduction in minority carrier lifetime. In Equation (1), the photovoltaic current, S , would be reduced and the reverse saturation current, I_0 would increase. Since the differential exposed area of concern normally represents only a small fraction of the total cell active area, the loss in generated current would not be significant. However, a significant increase in I_0 would dramatically alter the junction characteristic. The effective open-circuit voltage of this damaged section would be reduced and for cell terminal voltages greater than this value, the subject cell section would act as a shunt load. The magnitude of the shunt loss current will be greatly influenced by the effective series resistance of the damaged area. Since the sheet resistance of the N-layer is the predominate contributing element, the effective series resistance of any given differential area will be a direct function of proximity to the bus bar and grid lines. Areas adjacent to the bus bar should be the most damage effective.

As shown in Figures D-1 and D-2, the region of a cell bounded by the bus bar and two grid lines can be regarded as a network of resistors, diodes, and current generators. A localized damaged area will act as a current "sink" affecting some collection area in its vicinity. The total current lost through the sink cannot be greater than the total current generated over the region significantly influenced by the damaged area. In effect, the series resistance elements control the effective collection area that is influenced. Damaged areas adjacent to the bus bar or grid lines have, in effect, a much larger effective collection area. For these regions, which have extremely low series resistance components, the loss current will be independent of the effective illumination intensity of the cell (i.e., independent of the current generation rate per unit cell area). Therefore, the percentage loss at any given voltage will vary inversely with total available current.

A simple model can be used to illustrate the effect of low energy proton damage to a small gap adjacent to the cell bus bar. First, it is assumed the area involved is approximately 1 percent of the total cell area. Before irradiation, this bare area will have most of the qualitative characteristics of a solar cell. However, being immediately adjacent to the bus bar, we can assume the effective series resistance element is zero. Consider the curves of Figure D-3.

Curve 1 is a conventional V-I curve for a 2 x 2 cm cell having a series resistance of approximately 0.4 ohm. If this series resistance term is mathematically removed, the new V-I relation will be curve 2. With reference to Equation (1) ($R = 0$), the V-I curve of the diode term (i.e., $I_0 \left\{ \exp \left(\frac{qV}{AKT} \right) - 1 \right\}$) can be simply determined from Figure D-3 by performing the subtraction $S - I(V, \text{Curve 2})$. The resulting V-I relation is curve 3. Since $R = 0$, changes in the effective active area will simply scale the ordinate.



*FOR N/P CELLS I_L IS NEGATIVE

Figure D-2. Solar Cell Region Model

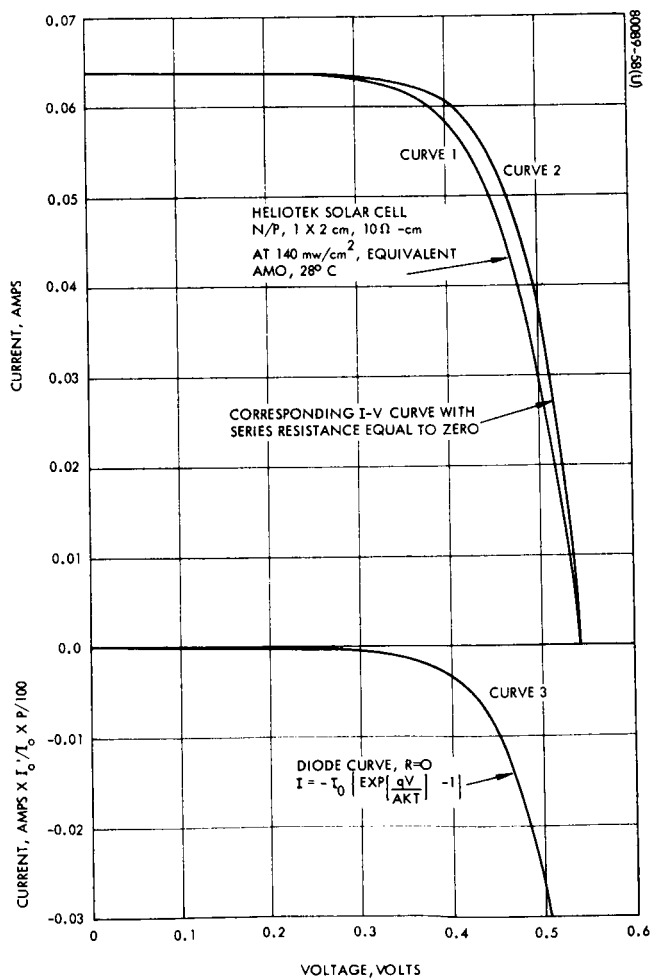


Figure D-3. Equivalent Damage Model
for Low Energy Proton Effects

Let p = percentage exposed area relative to the total active cell area. Let $p = 1$ for the example under consideration. It is further assumed that sufficient radiation damage has occurred to essentially reduce the short-circuit current of the damaged area to zero but that the reverse saturation current has not been changed; i. e., $I_0' = I_0$. The load represented by the exposed area is then precisely curve 3 of Figure D-3 with $P = 1$ and $I_0'/I_0 = 1$. The "load" current at a cell voltage of 0.45 volt would be only 0.1 milliamperes, which would represent a negligible loss. Now suppose low energy proton irradiation were to cause a two order of magnitude increase in I_0 ; i. e., $I_0' = 100 I_0$. The load current at 0.445 volt now becomes 10 milliamperes, which represents an 18-percent loss. Large effective increases in I_0 , on the order 10^2 , are typical of low energy proton effects. The precise damage mechanisms are complex and poorly understood.

TEST SAMPLE DESCRIPTION

Ten ohm-cm, N/P silicon-solar cells of the following manufacturers were used for the low energy proton tests: (Heliotek (1 by 2 cm) and (2 by 2 cm), Centralab (2 by 2 cm) and Texas Instrument (1 by 2 cm). The terminology chart shown in Figure D-4 shows the possible exposed areas (gaps) which Heliotek (2 by 2 cm), Centralab (2 by 2 cm) and Texas Instrument, (1 by 2 cm) cells may have. The "bar gap" is the exposed part of the cell between the bus bar and the coverslide. The B' gap is the exposed part of the cell between the bus bar and the edge of the cell. The end and side gaps are the exposed parts of the cell between the coverglass and the cell edges. The Heliotek (1 by 2 cm) solar cells differ from Figure D-4 in that the bus bar is replaced with a corner dart configuration. The bar gap for the Heliotek (1 by 2 cm) is defined as the exposed part of the cell between the corner dart and the coverslide. All other definitions for Heliotek (1 by 2 cm) are the same as Figure D-4.

The solar cells were stacked in a shingled configuration for the proton irradiation tests, as shown in Figure D-5. That is, the solar cells were stacked in a stair-step manner so that the cell on top would serve to shield the part of the cell below that was not to be irradiated. Using this type of cell assembly, up to 10 solar cells with gap widths of 0, 2, 5, 10, 15, etc., mils could be irradiated with the same proton beam. The solar cell assemblies were held together by small strips of double-faced masking tape, thereby making it easy to assemble and disassemble the stacks.

TEST PROCEDURE

A model AN-2000 2-million-volt Van de Graaff particle accelerator at the Aerospace Corporation was used to irradiate the solar cells. This accelerator will produce protons in the energy range of 150 kev to 2.5 mev. The beam diameter of the target area was approximately 1.5 inches. Five Faraday cups were used to measure the beam currents and the uniformity of

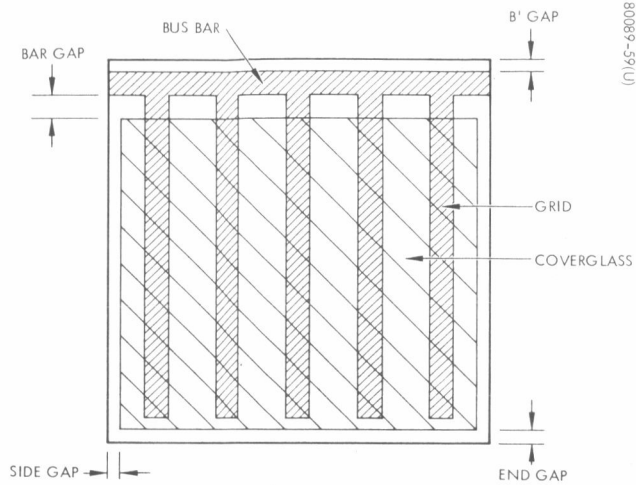


Figure D-4. Terminology Chart

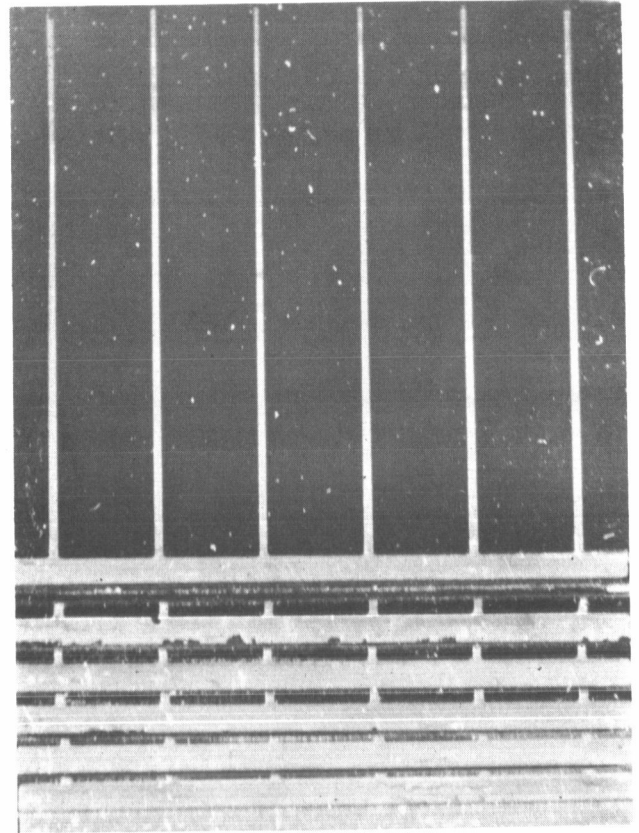


Figure D-5. Typical Shingled Assembly of Solar Cells Ready for Proton Irradiation

(Photo A20336)

the proton beam was accurately known to 1.1 inch diameter. The proton beam was not magnetically analyzed, therefore, the percentages of monatomic and polyatomic components were not known.

Cell voltage-current characteristics were measured before and after each bombardment, using a tungsten light source.* The light source intensity was maintained at 100 milliwatts per square centimeter at air mass one by means of a calibrated balloon cell. An intensity of 100 milliwatts per square centimeter at air mass one is effectively 115.6 milliwatts per square centimeter at air mass zero. The cells were mounted on a water-cooled brass block; the temperature of the block was maintained near 25°C.

Table D-1 shows the exposure period and the corresponding beam current utilized for a given proton fluence. The proton irradiation test procedure can best be illustrated by the following example.

- 1) The voltage-current characteristics of the solar cells to be irradiated were measured (e. g., Heliotek, 2 by 2 cells).
- 2) The solar cells were stacked so as to expose the appropriate gaps with the top cell bare; i. e., entirely exposed to the proton beam.
- 3) The cell stack was then irradiated with 270 kev protons at a fluence of 10^{13} protons/cm² (50-second beam exposure with a beam current of 0.2 microampere).
- 4) The cell stack was disassembled and the individual cell voltage-current characteristics were measured.
- 5) The cells were reassembled and irradiated with 270 kev protons at a fluence of 10^{14} protons/cm² (250-second beam exposure at a beam current of 0.4 microampere).
- 6) The cell stack was disassembled and the individual cell voltage-current characteristics were again measured.
- 7) The cells were again reassembled and irradiated with 270 kev protons at a fluence of 10^{16} protons/cm² (500 seconds beam exposure at a beam current of 2.0 microampere).
- 8) The cell stack was again disassembled and the final cell voltage-current characteristics were measured.

Unirradiated control cells were measured between each test to verify the light source calibration. This irradiation procedure was followed for all the cell types. Fluences for a given proton energy were changed by controlling both the exposure time and the beam current.

*Color temperature of approximately 2800 °K.

TABLE D-1. PROTON FLUENCE WITH CORRESPONDING EXPOSURE PERIODS AND BEAM CURRENTS

Fluence, protons/cm^2	Time, seconds	Beam Current, microamperes
10^{12}	5	0.2
10^{13}	10	1.0
10^{13}	50	0.2
10^{14}	100	1.0
10^{14}	250	0.4
10^{16}	500	2.0

TEST RESULTS

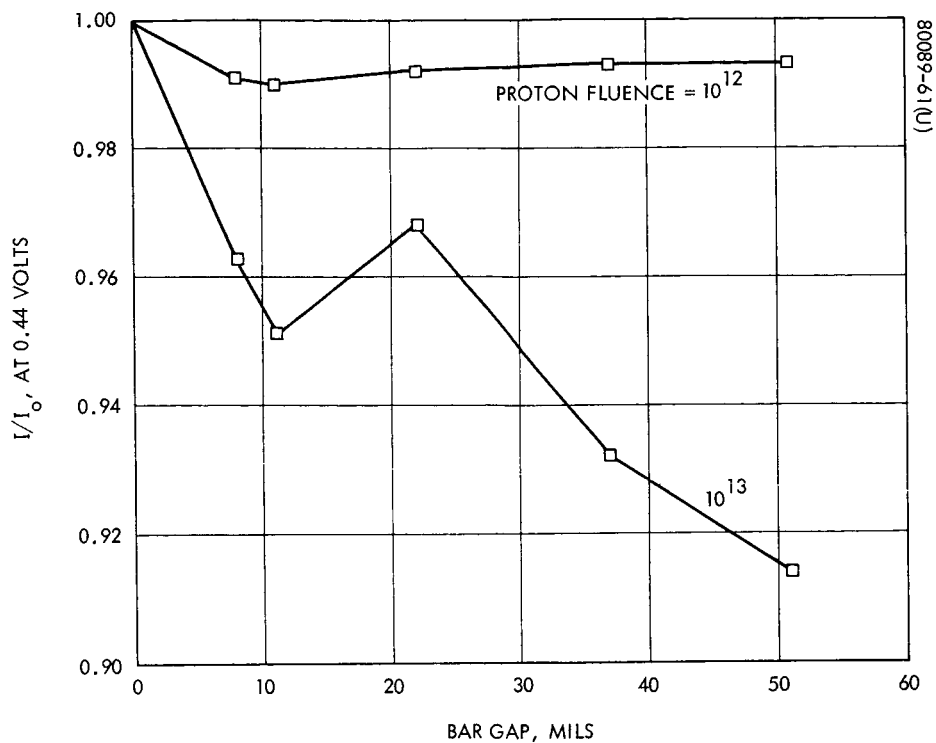
The results of the low-energy proton irradiation tests are presented in Figures D-6 through D-14. These solar cells were irradiated with protons of energies 150 kev, 270 kev, and 1 mev and fluences of 10^{12} , 10^{13} , 10^{14} , and 10^{16} protons/cm². Spectrum irradiations were also conducted. This spectrum was chosen to simulate the energies and fluences which a satellite would experience in synchronous orbit (see Table D-2).

Some of the solar cells (Texas Instruments, 1 by 2 cm; Heliotek, 2 by 2 cm) had B' gaps. The B' gap is defined as the exposed part of the solar cell between the bus bar and the edge of the cell. For best correlation of the data for these cells with cells having no B' gap, it was found that the exposed B' gap was about one-fourth as effective as a bar gap of the same width. All data displayed in Figures D-6 through D-14 have been corrected for this B' exposure. Table D-3 shows the effect of only a B' exposure. In general, each data point represents a sample size of 1. A gap tolerance of approximately ± 0.001 inch should be assumed.

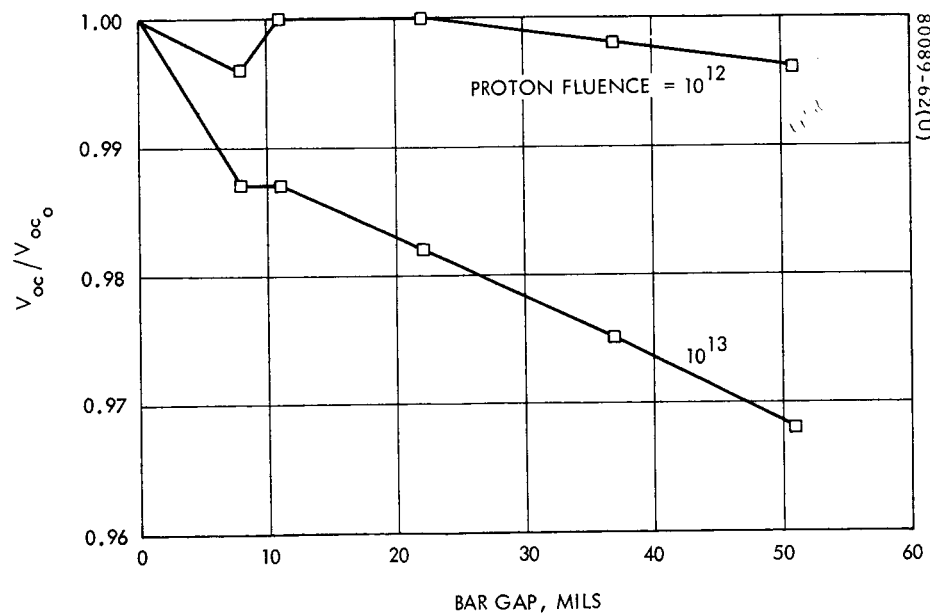
Bar Gap Exposure

Figure D-6 presents normalized current at 0.44 volt and open-circuit voltage versus bar gap for Heliotek (2 by 2 cm) solar cells irradiated with 150 kev protons. Figure D-6 shows that some degradation occurs at even a low fluence of 10^{12} protons/cm². At 10^{13} protons/cm² the cells have degraded significantly. Fluences lower than 10^{12} protons/cm² were not considered because the beam currents required for the lower fluences were unstable and hard to measure.

Figure D-7 presents data for normalized current (at 0.44 volt) and open-circuit voltage as a function of bar gap for Heliotek (2 by 2 cm) and Centralab (2 by 2 cm) solar cells irradiated with 270 kev protons. As indicated, fluences of 10^{13} and 10^{14} protons/cm² are the most damaging.

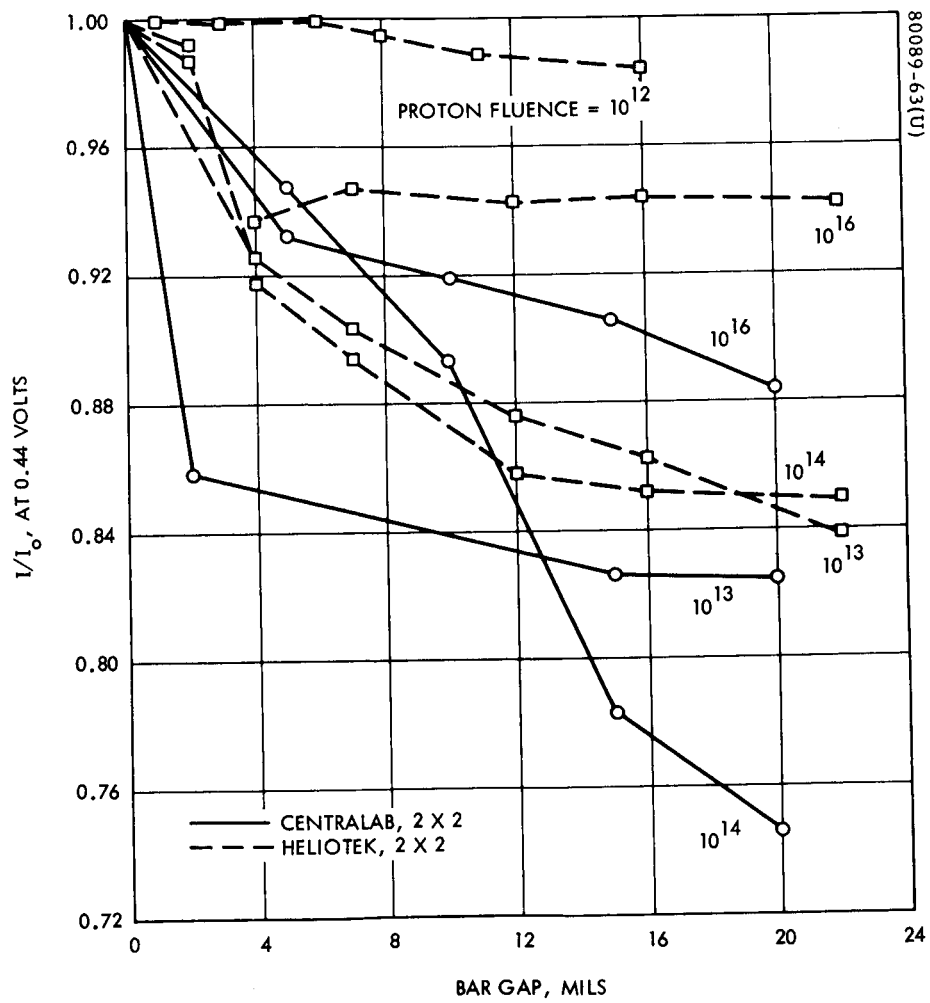


a) Normalized Current at 0.44 volt



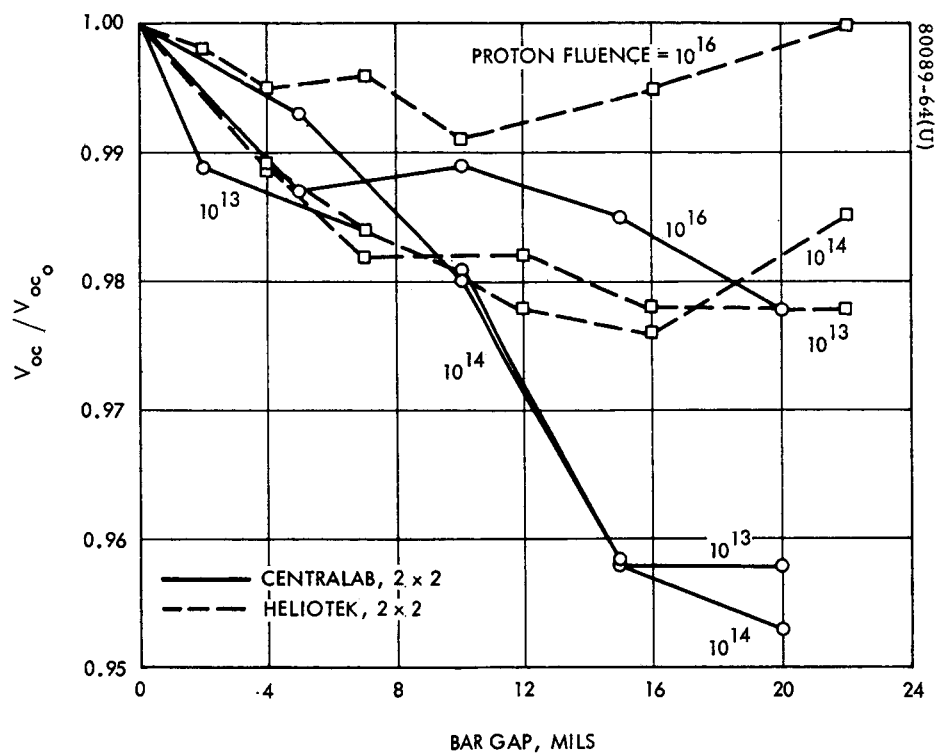
b) Normalized Open-Circuit Voltage

Figure D-6. Normalized Current and Open-Circuit Voltage for Heliotek Solar Cells Irradiated with 150 keV Protons



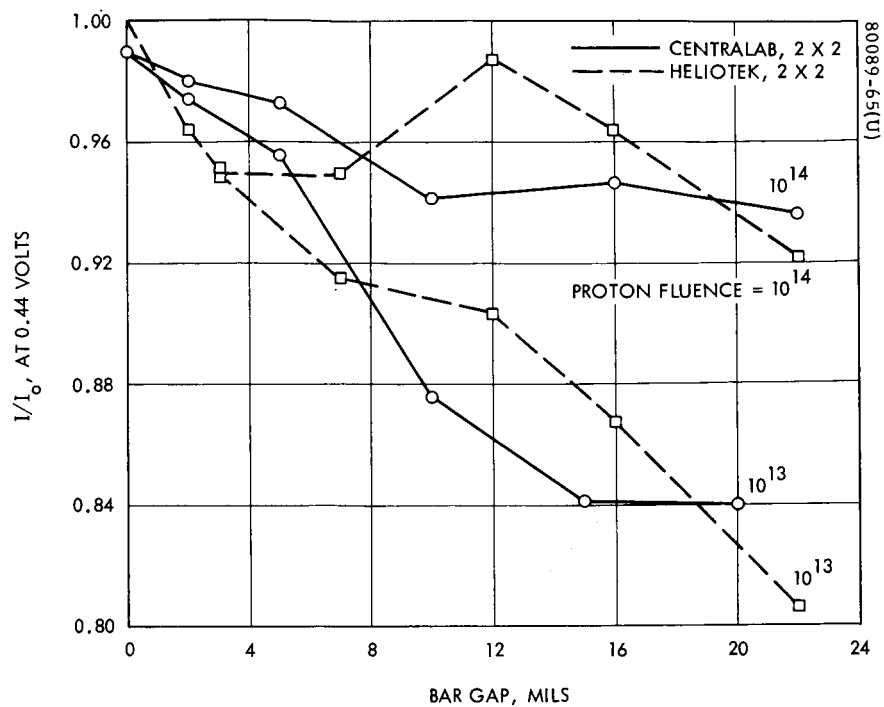
a) Normalized Current at 0.44 volt

Figure D-7. Normalized Current and Open-Circuit Voltage for Centralab and Heliotek Cells Irradiated with 270 kev Protons

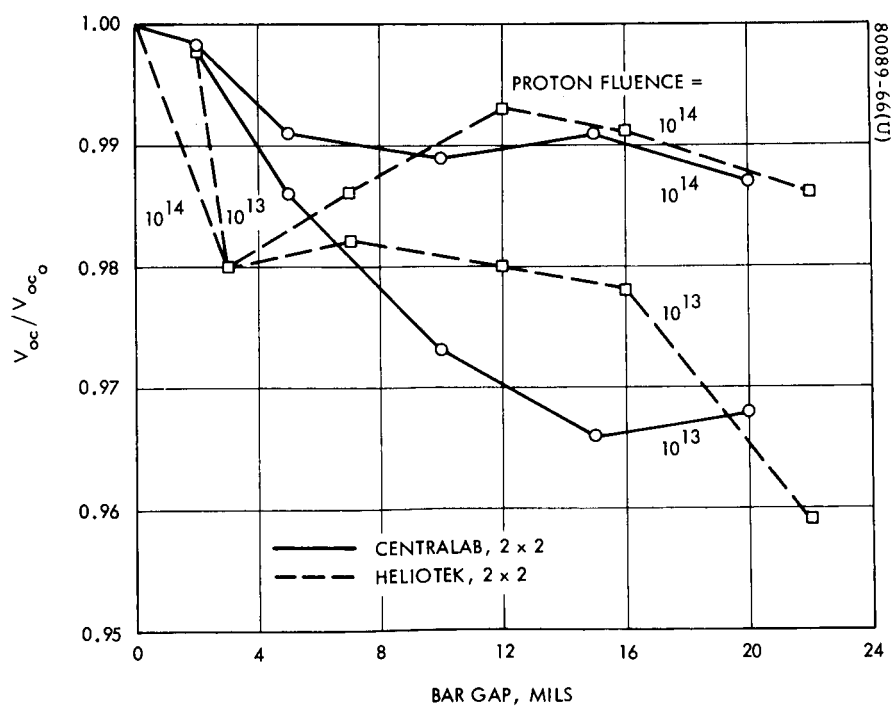


b) Normalized Open-Circuit Voltage

Figure D-7. Normalized Current and Open-Circuit Voltage for Centralab and Heliotek Cells Irradiated with 270 kev Protons (continued)

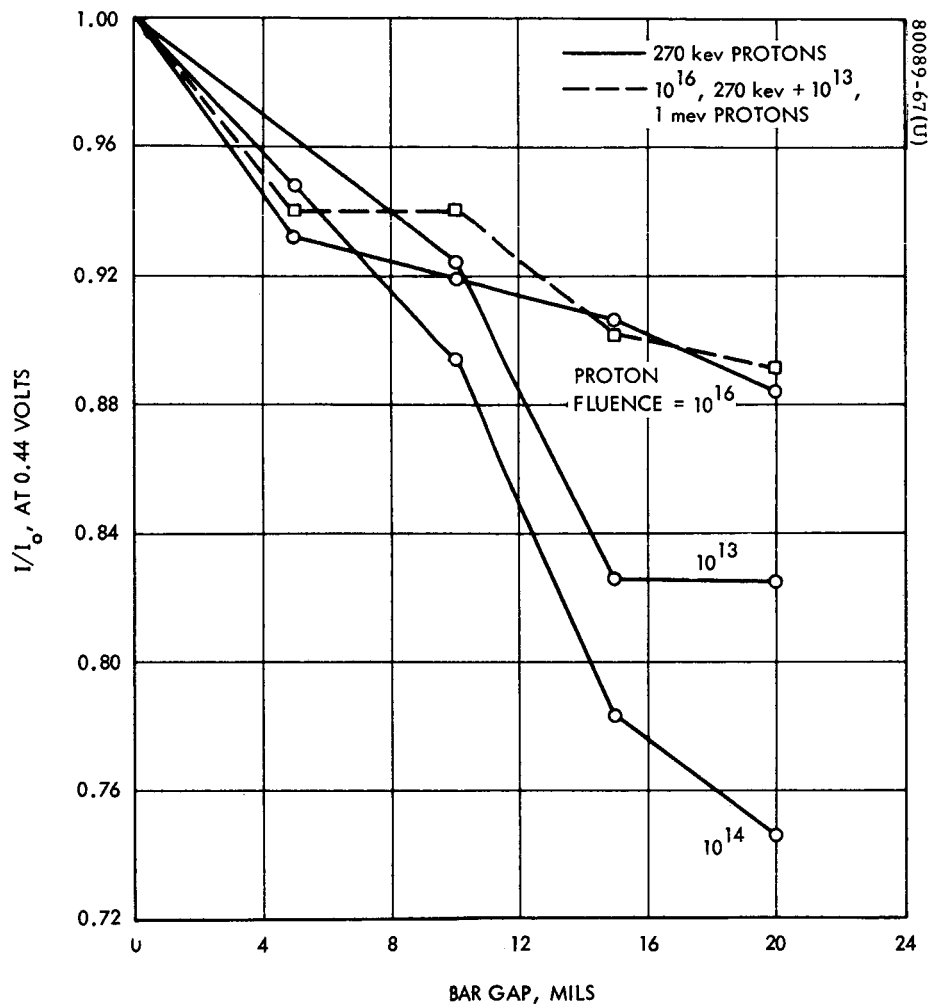


a) Normalized Current at 0.44 volt



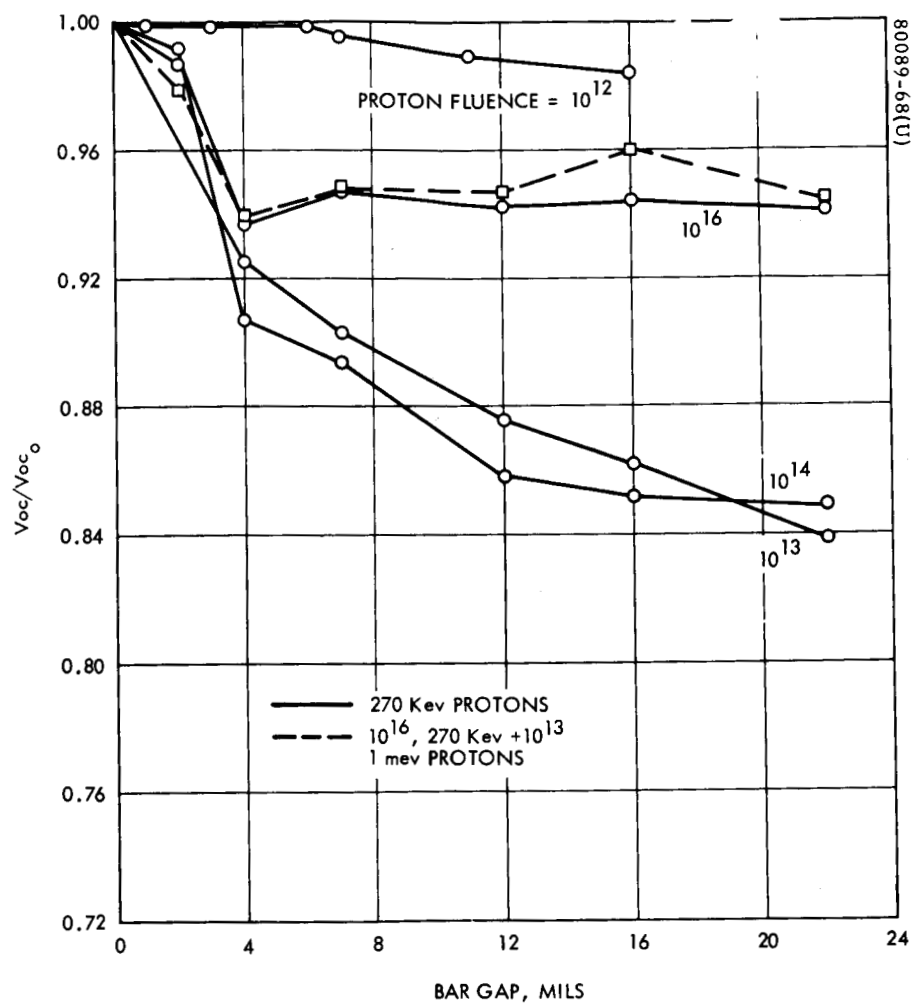
b) Normalized Open-Circuit Voltage

Figure D-8. Normalized Current and Open-Circuit Voltage for Centralab and Heliotek Cells Irradiated with 1 Mev Protons



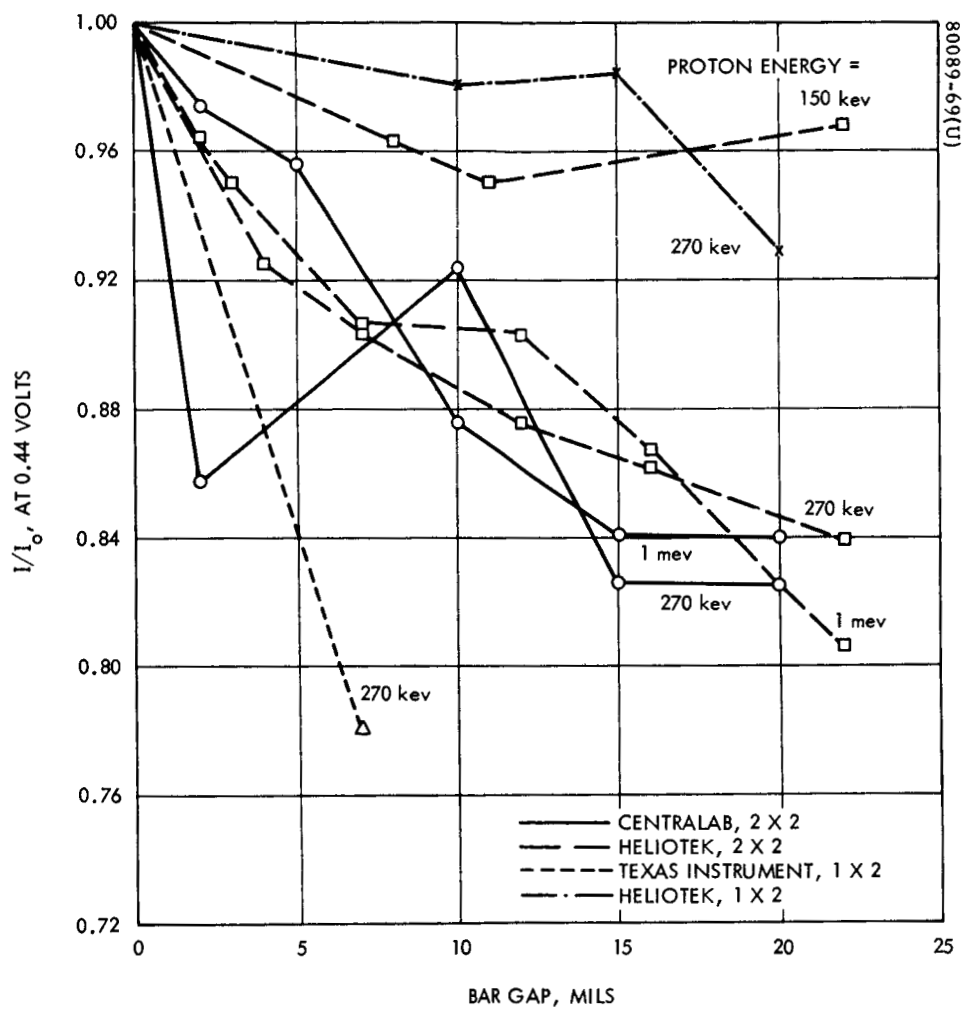
a) Normalized Current at 0.44 volt

Figure D-9. Normalized Current and Open-Circuit Voltage for Cells Irradiated with 270 keV and 1 MeV Protons



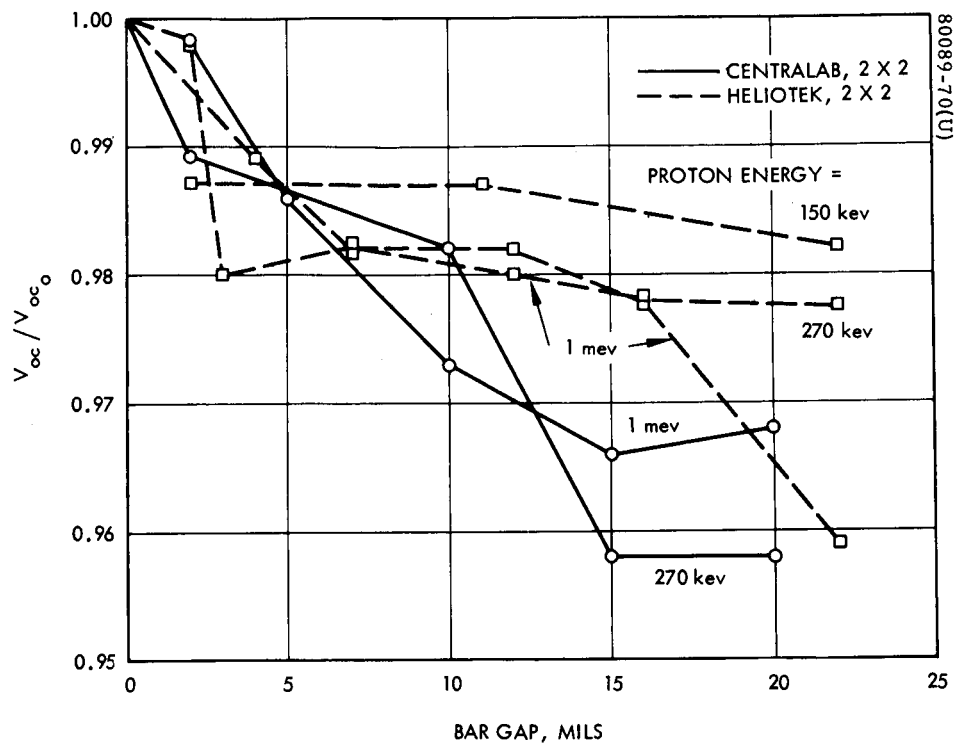
b) Normalized Open-Circuit Voltage

Figure D-9. Normalized Current and Open-Circuit Voltage for Cells Irradiated with 270 kev and 1 mev Protons (continued)



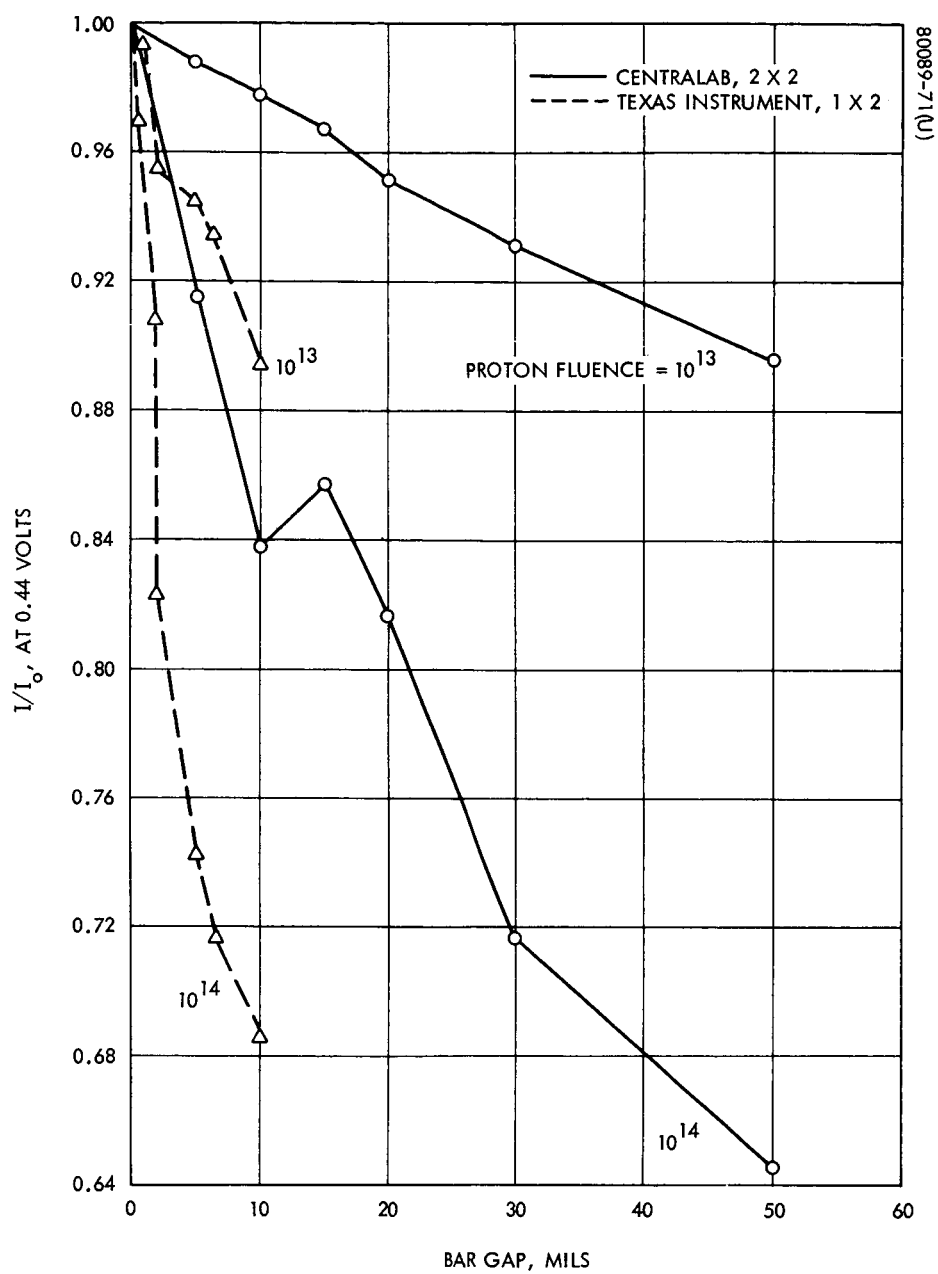
a) Normalized Current at 0.44 volt

Figure D-10. Normalized Current and Open-Circuit Voltage for Cells Irradiated with 10^{13} Protons/cm²



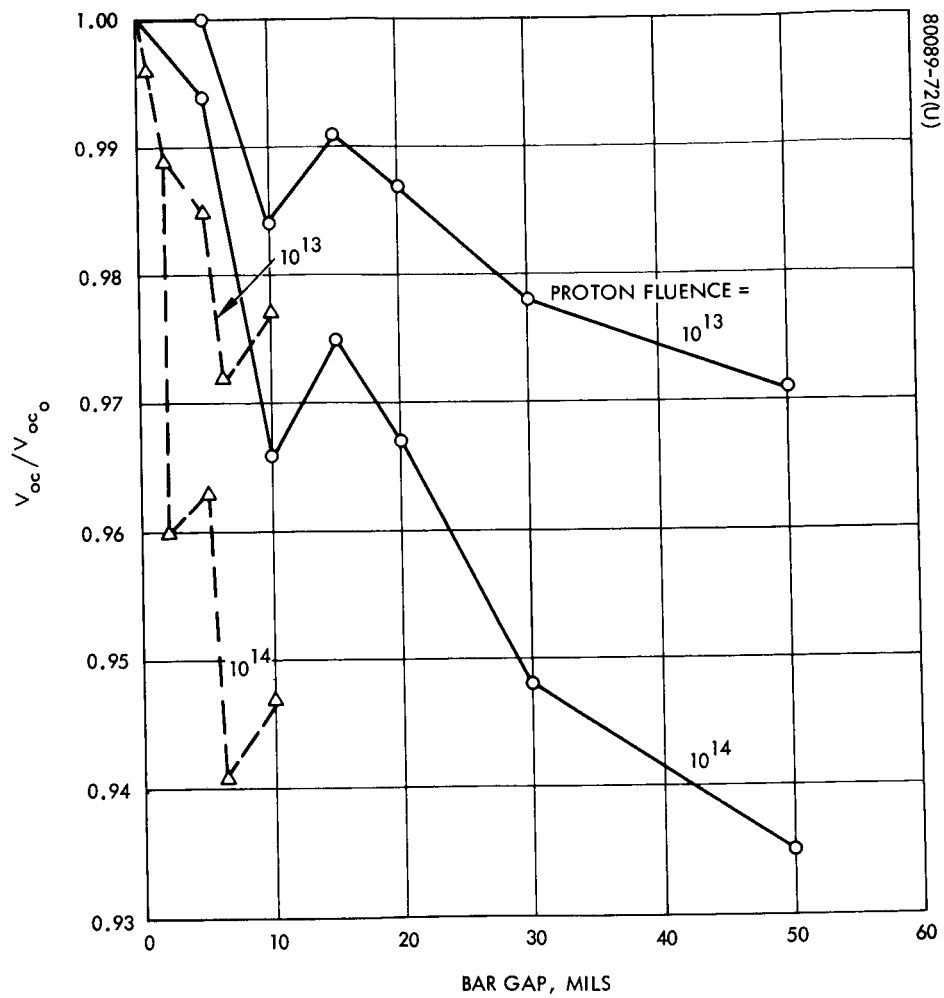
b) Normalized Open-Circuit Voltage

Figure D-10. Normalized Current and Open-Circuit Voltage for Cells Irradiated with 10^{13} Protons/cm²
 (continued)



a) Normalized Current at 0.44 volt

Figure D-11. Normalized Current and Open-Circuit Voltage for Cells Irradiated with Proton Spectrum



b) Normalized Open-Circuit Voltage

Figure D-11. Normalized Current and Open-Circuit Voltage for Cells Irradiated with Proton Spectrum (continued)

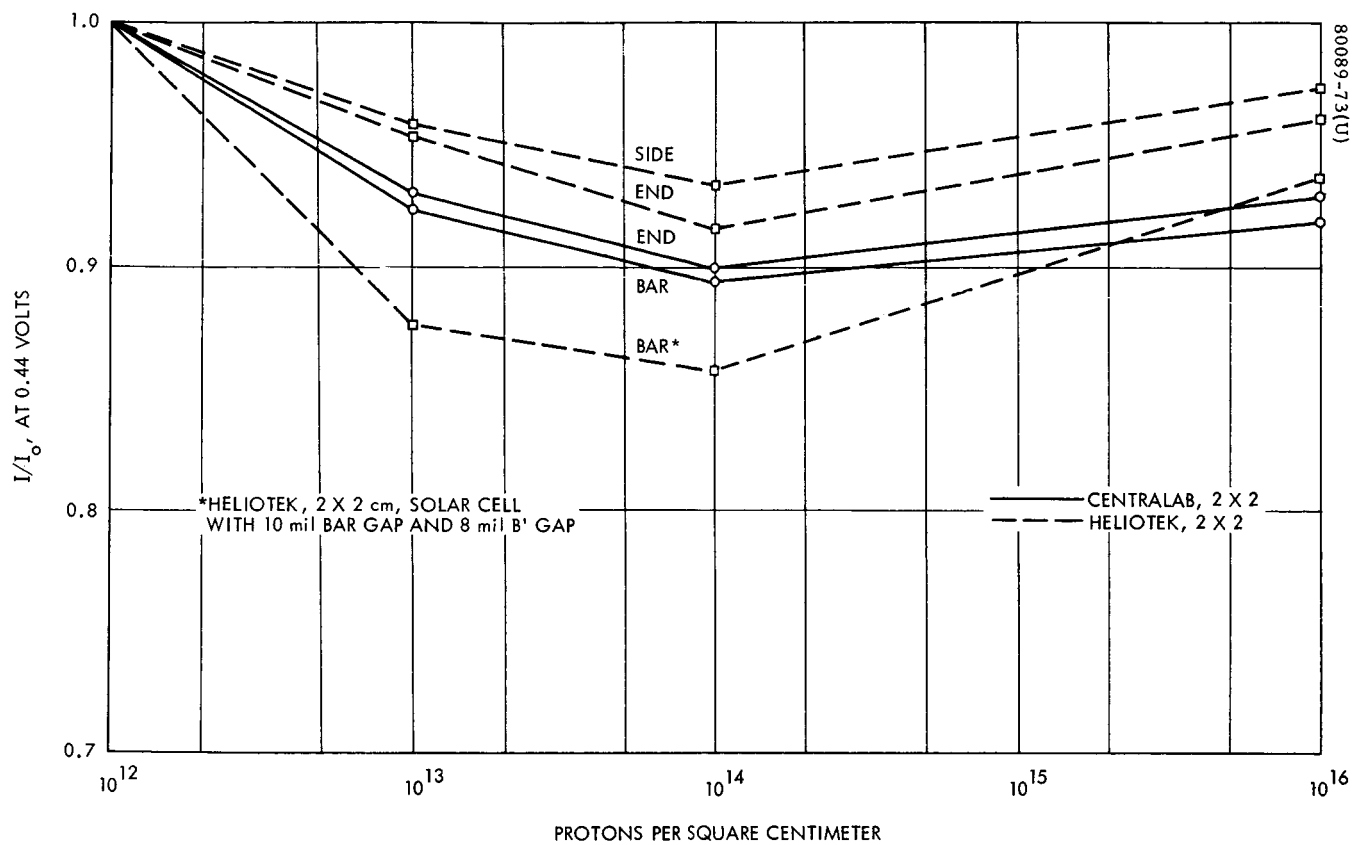


Figure D-12. Normalized Current at 0.44 volt as Function of 270 kev Proton Fluence

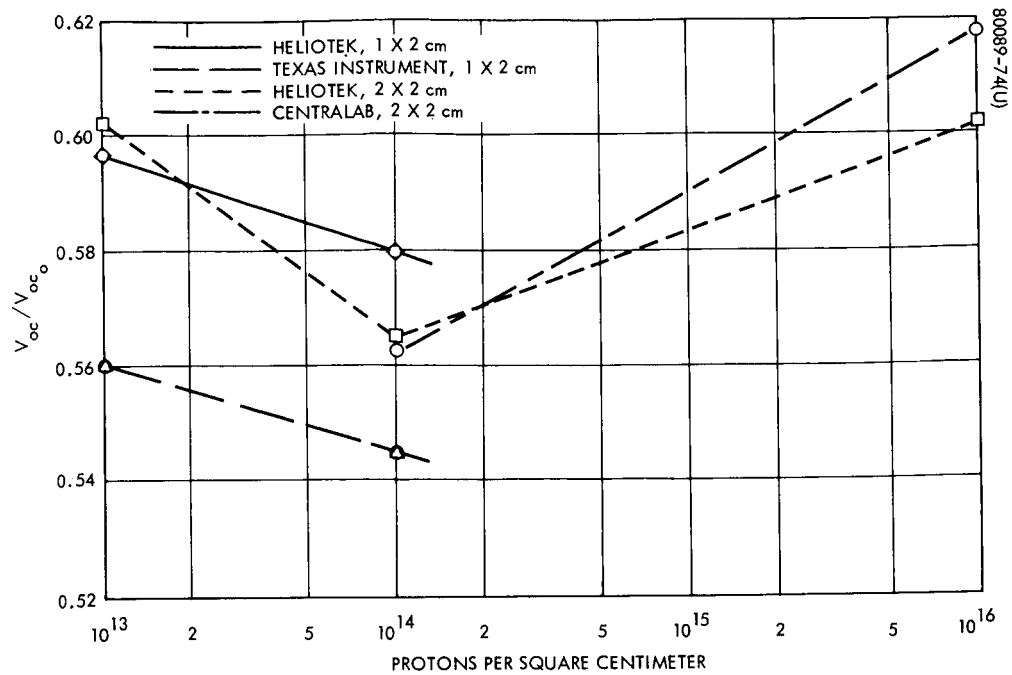


Figure D-13. Normalized Open-Circuit Voltage as Function of 270 keV Proton Fluence for Bare Cells

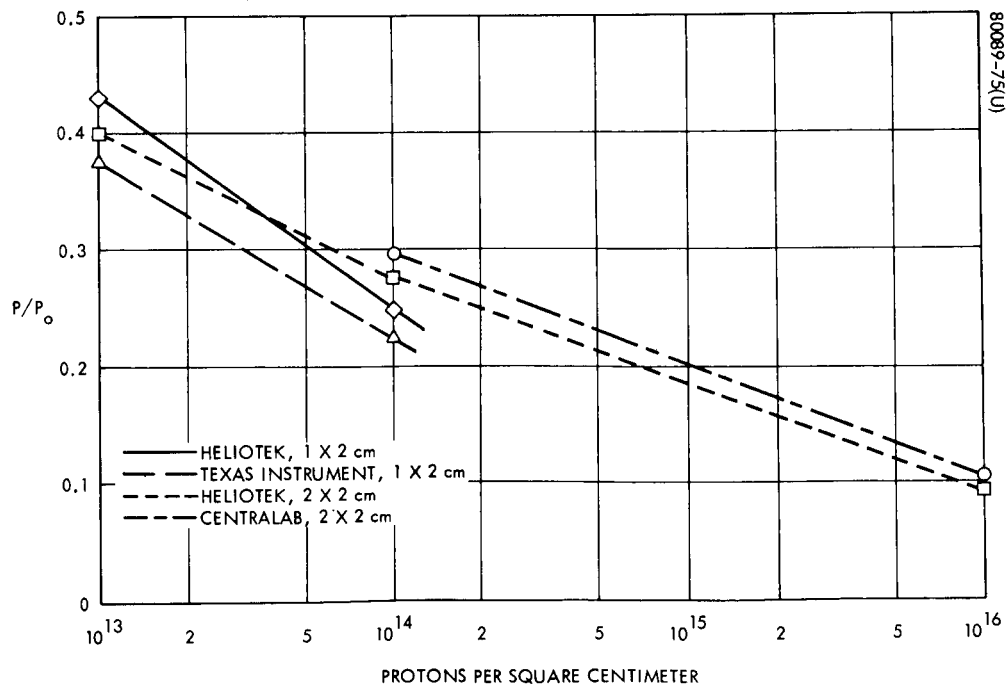


Figure D-14. Normalized Maximum Power as Function of 270 keV Proton Fluence for Bare Cells

There is an apparent recovery at 10^{16} protons/cm². It is interesting to note that bar gaps as small as 2 mils are enough to cause significant degradation.

In Figure D-8, normalized current (at 0.44 volt) and open-circuit voltage are shown as a function of bar gap for Heliotek (2 by 2 cm) and Centralab (2 by 2 cm) solar cells irradiated with 1 mev protons. For this proton energy, an apparent recovery is noted at a fluence of 10^{14} protons/cm². Also it should again be noted that 2 mil bar gaps are sufficient to cause significant degradation.

In Figure D-9, normalized current (at 0.44 volt) and open-circuit voltage are presented as a function of bar gap for Centralab (2 by 2 cm) and Heliotek (2 by 2 cm) solar cells irradiated with 280 kev protons at fluences of 10^{13} , 10^{14} , and 10^{16} protons/cm², and finally with 1 mev protons, in the stated order. As before, an apparent cell recovery was noted at a fluence of 10^{16} protons/cm². Also, irradiating the cells with 1 mev proton at 10^{13} protons/cm², causes a slight cell recovery after a fluence of 10^{16} protons/cm² at 270 kev. These data indicate that one proton energy will tend to recover the cell, while another proton energy will cause degradation.

In Figure D-10, normalized current (at 0.44 volt) and open-circuit voltage are shown as a function of bar gap of all four cell types irradiated with a fluence of 10^{13} protons/cm². For proton energies of 270 kev and 1 mev, the 2 by 2 cm solar cells indicate approximately the same amount of degradation.

In Figure D-11, normalized current (at 0.44 volt) and open-circuit voltages are presented as a function of bar gap for Centralab (2 by 2 cm) and Texas Instruments (1 by 2 cm) solar cells irradiated with a proton spectrum. The 10^{13} proton spectrum approximates the protons energies and their relative fluence for 75 days in synchronous orbit, including the transfer orbit component. Although this simulated spectrum is not continuous, it gives a trend of what might occur in synchronous orbit for a 2-year mission. No recovery is indicated in these figures because the fluences for the particular proton energies were not sufficiently high. It should also be noted that very small bar gaps are sufficient to cause large degradation.

Side and End Gap Exposure

In Figure D-12, normalized current at 0.44 volt versus 270 kev proton fluence is displayed for Heliotek (2 by 2 cm) and Centralab (2 by 2 cm) solar cells with 10-mil bar, side, and end gaps exposed. It is interesting to note that exposed side and end gaps degrade almost as much as the bar gap. Again, an apparent recovery is seen at proton fluences of 10^{16} protons/cm².

Bare Cell Exposure

In Figure D-13, normalized open-circuit voltage and maximum power are shown as a function of 270-keV proton fluence for bare solar cells. The degradation magnitude for these 270-keV proton fluences agrees with data from other experimenters. The apparent open-circuit voltage recovery was noted for bar cells for fluences $> 10^{14}$ protons/cm². However, no maximum power recovery has ever been observed (References 1 and 2).

Edge of Cell Exposure

Solar cells were also irradiated with 270 keV protons at 10^{14} protons/cm² with only the edge exposed to the proton beam (proton beam parallel with the surface of the cell). No degradation in these cells was noted.

Loss Function Considerations

Loss function curves were calculated for Centralab (2 by 2 cm) solar cells as a function of illumination intensity. Solar cells with 20-mil bar gaps were irradiated with a 10^{14} proton spectrum. The loss functions were calculated as a function of intensity in the following manner: the V-I characteristics of a control cell were measured at intensities of 100 mw/cm², 72.0 mw/cm², 50.4 mw/cm² and 25.1 mw/cm². The temperature of the cell was maintained at 25°C for all intensities. The V-I characteristics of the test cell were measured before and after the proton irradiations at 100 mw/cm², but only post-irradiation data were available at intensities of 72.0 mw/cm², 50.4 mw/cm², and 25.1 mw/cm². To stimulate the V-I characteristics of the test cells at the three reduced intensities before the proton irradiation, the following technique was used:

The current of the control cell was measured at the following percentages of V_{oc} at 100 mw/cm²: 98, 95, 90, 85, 80, 75, 50, 25 and 0. The current for the same percentage V_{oc} values was calculated for the other intensities.

The current of the test cell, before proton irradiation, was measured at the percentages of V_{oc} corresponding to 100 mw/cm² intensity. To find the V_{oc} for the reduced intensities of the test cell, the following empirical relationships were used:

72.0 mw/cm²: multiply the V_{oc} at 100 mw/cm² by 0.984

50.4 mw/cm²: multiply the V_{oc} at 100 mw/cm² by 0.971

25.1 mw/cm²: multiply the V_{oc} at 100 mw/cm² by 0.936

The current of the test cell before proton irradiation, for a given percentage of the calculated V_{oc} , was calculated using Equation (D-1).

$$I = \frac{I_{cr} \times I_T}{I_c}, \quad (D-1)$$

where I is the current of the test cell at a percentage of the calculated V_{oc} , I_{cr} is the current at the percentage of V_{oc} of the control-cell for the reduced intensity, I_T is the current at the percentage of the V_{oc} of the test cell at 100 mw/cm² and I_c is the current at the percentage of V_{oc} of the control cell at 100 mw/cm². Using Equation (D-1), the V-I characteristics of the test cells were calculated for the reduced intensities under pre-irradiation conditions.

Having obtained the before and after proton irradiation V-I characteristics, the loss function was generated by subtracting the current at a constant voltage for each intensity. The loss function, as a function of intensity, for the Centralab (2 by 2) test cell, irradiated with a 10¹⁴ proton spectrum with a 20-mil exposed bar gap, is shown in Figure D-15. This figure also shows that the loss function is essentially independent of the intensity.

The loss function as a function of bar gaps (in mils) was generated for the Texas Instruments (1 by 2) solar cells irradiated with 10¹³ and 10¹⁴ proton spectrums (Figure D-16). The cells were maintained at an intensity of 100 mw/cm² and a temperature of 25 °C. As shown in Figure D-16, bar gaps as small as 2 mils display a loss function. The effect of B' gaps is illustrated in the same figure.

TABLE D-2. SIMULATED PROTON SPECTRUM

<u>Spectrum 10¹³</u>	approximately 75 days in synchronous considering transfer orbit
150 kev - 10 ¹³	
300 kev 3 x 10 ¹²	
500 kev 10 ¹²	
750 kev 10 ¹²	
1 mev 10 ¹²	
<u>Spectrum 10¹⁴</u>	approximately 730 days in synchronous orbit
150 kev 10 ¹⁴	
300 kev 3 x 10 ¹³	
500 kev 10 ¹³	
750 kev 10 ¹³	
1 mev 10 ¹³	

TABLE D-3. EFFECT OF THE B' EXPOSURE

Cell Type	Cell Number	Bargap	B ¹	V _{oc} /V _{oco}	I/I _o *	Energy	Flux
Texas Instruments (1 by 2 cm)	93	0	8 mil	0.989	0.946	Spectrum	10 ¹³
				0.989	0.906	Spectrum	10 ¹⁴
Heliotek (2 by 2 cm)	141	0	5 mil	0.998	0.999	270 kev	10 ¹²
				0.996	0.967	270 kev	10 ¹³
Heliotek (2 by 2 cm)	144	0	10 mil	1.000	0.969	270 kev	10 ¹²
				0.994	0.938	270 kev	10 ¹³
Heliotek	128	0	11 mil	0.998	0.964	1 mev	10 ¹³

*Normalized current at 0.44 volt.

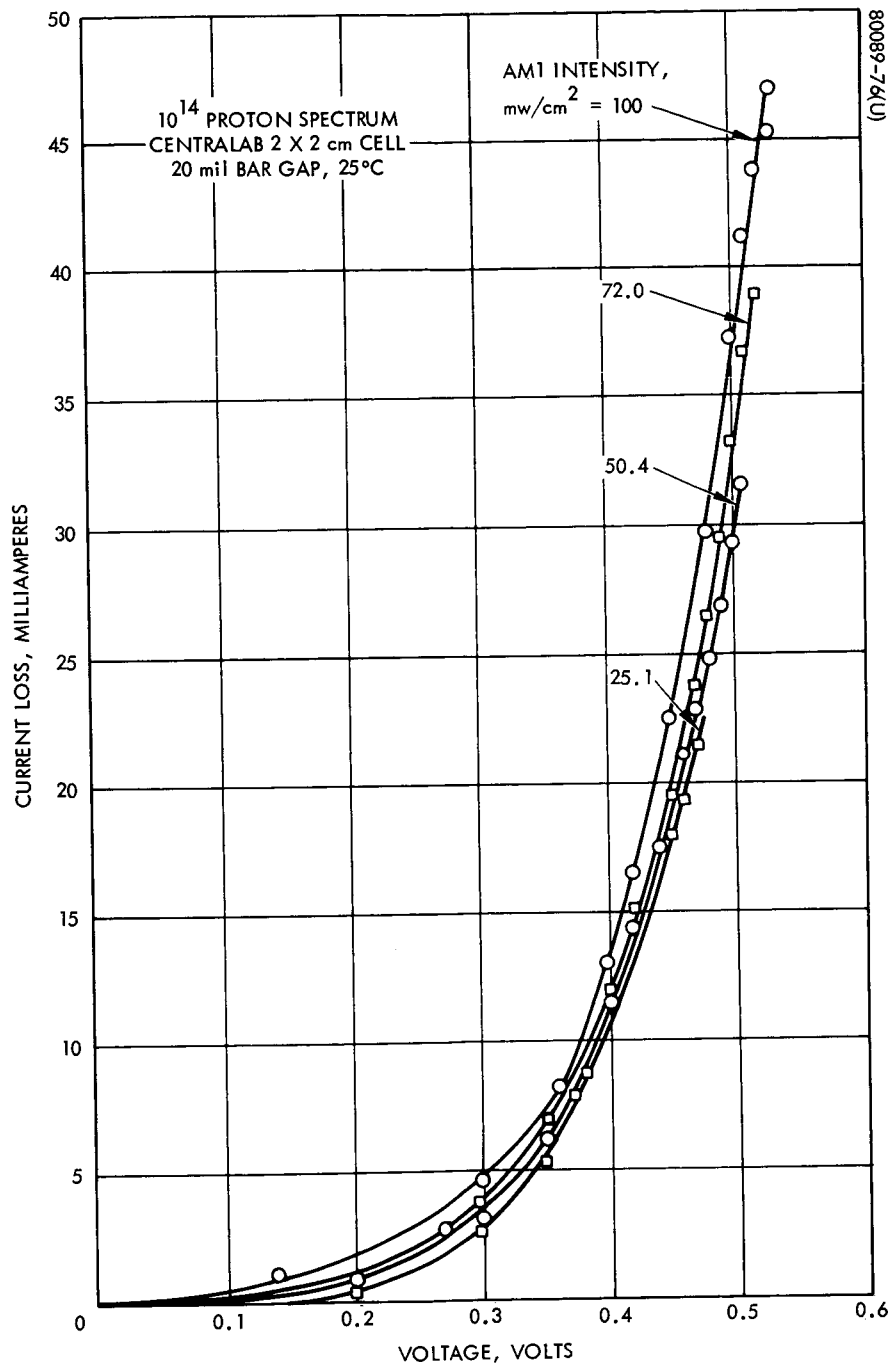
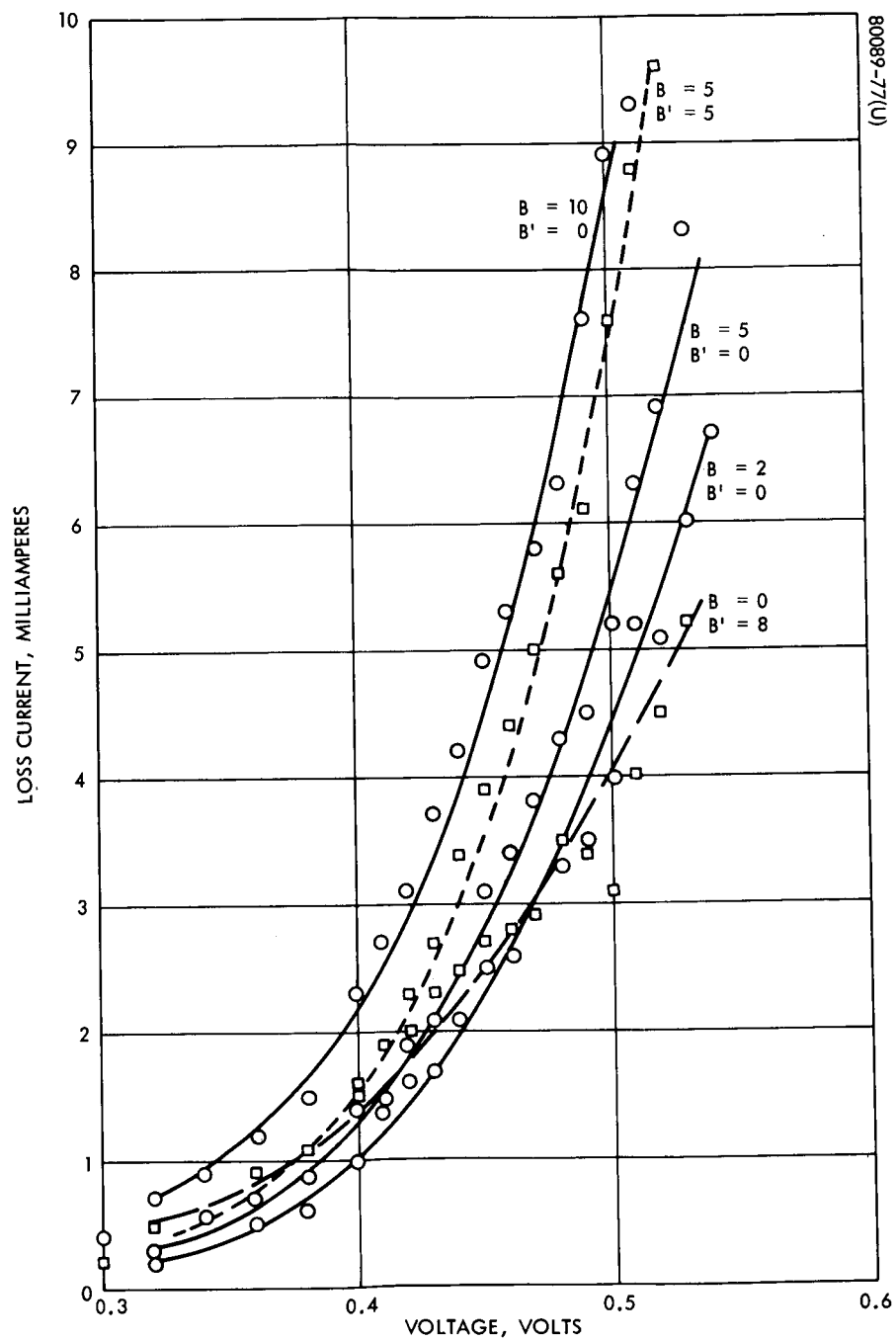
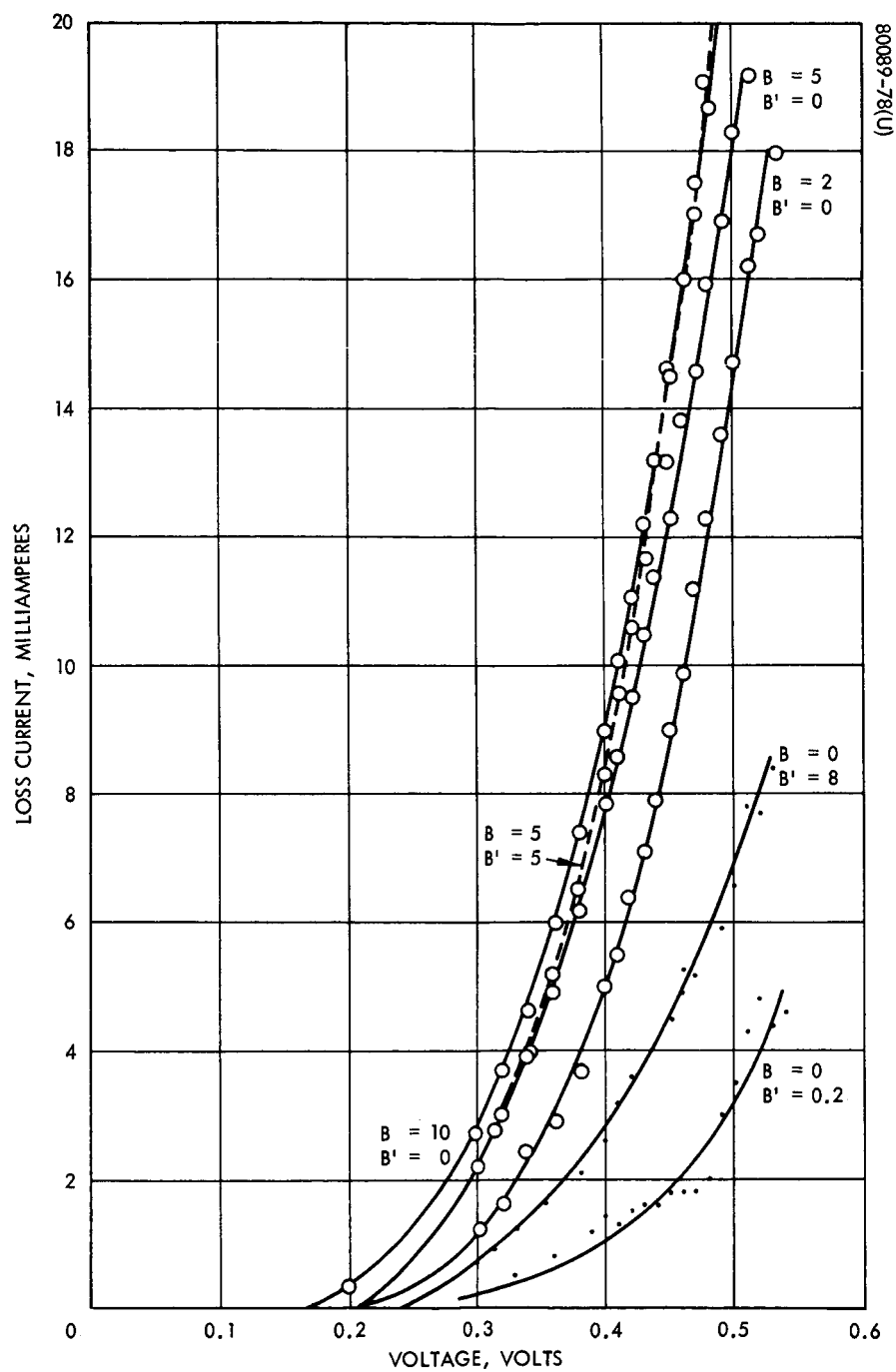


Figure D-15. Loss Function Dependence on Illumination Intensity



a) 10^{13} Proton Spectrum

Figure D-16. Loss Function as Function of Bar Gap
for Texas Instrument Solar Cells



b) 10^{14} Proton Spectrum

Figure D-16. Loss Function as Function of Bar Gap for Texas Instrument Solar Cells (continued)

APPENDIX E. LOW ENERGY PROTON SHIELD INVESTIGATION

From the low energy proton irradiation tests for solar cells with small exposed areas, it was concluded that very small exposed areas of the cell are enough to cause cell damage. To protect these cells with exposed areas, a low energy proton shield is needed which can be applied to the cell assembly. Solar cells with coverglasses, which had large exposed areas of the cell, were chosen for the shield test. Bare cells also were used as a control.

CANDIDATE MATERIALS

Five candidate solutions were chosen for the shield tests and are as follows:

- 1) LMSC solar cell coating
- 2) Black epoxy cell adhesive
- 3) Black epoxy paint, CTL-15 (HP4-112)
- 4) RTV-602
- 5) Polyurethane "Solathane", HP16-130 white

The LMSC solar cell coating is made by Lockheed and the coating of the cells tested was applied by Lockheed. Candidate solutions 2 through 5 were prepared and applied to the cells by Hughes.

TEST PROCEDURES

Proton irradiations for range-energy studies were performed by means of a Van de Graaff generator with variable particle energies up to a maximum of 2.5 mev. A 1200 Å gold foil served to diffuse the proton beam over an area of 1/2 inch by 1/2 inch with only a 0.008-mev loss in proton energy. Measurements indicated a 40-percent drop in proton intensity near the specimen edges. Proton currents of approximately 0.020 microampere

(140 second irradiation period would be required to reach a fluence of 10^{13} protons/cm²) were utilized to reduce heat dissipation to a negligible level of 0.05 watt.

Specimens of relatively uniform thickness were placed in an aluminum holder and the transmitted beam measured by a Faraday cup. Insertion of a second Faraday cup in the 2-inch pipe permitted frequent monitoring of the incident beam intensity. Measurements were made at a number of proton energies to determine the range of protons in specimens of the indicated thickness, with the time required to accumulate 0.243 microcoulomb being recorded.

The Van de Graaff generator of Aerospace Corporation was used to irradiate the solar cells treated with the candidate solutions. These cells were bombarded with a proton spectrum. Photocharacteristics were measured before and after each bombardment, using a tungsten light source.

TEST RESULTS

Table E-1 shows the results after low energy proton bombardment of the LMSC solar cell coating. Unfortunately, the test provides no conclusions for the LMSC coating. The coating suffered no visible damage, although several of the samples were overheated during the cure. It appears that the coating may have been too thin to protect the cells.

Table E-2 shows the results, after low energy proton bombardment, of the Hughes corrective candidate solutions applied to the cells. The definition of the cell type symbols are the same as indicated in Table E-1. Table E-3 is a summary of the proposed solutions with comments as to the application and effectiveness as a low proton shield.

Based on literature data for Mylar, proton range-energy information has been plotted for several of the candidate shield materials in Figure E-1. This Figure shows a transmission threshold of 2.45 mev for 3.3 mil solar cell adhesive. Experimental data, summarized in Figure E-2, indicate a threshold in the range of 2.3 to 2.4 mev. The energy thresholds for all materials, except Sylgard-182, are in the range from 2.3 to 2.6 mev, with variations being largely due to differing mass densities (mg/cm²). Sylgard-182 has an anomalous threshold between 1.9 and 2.1 mev. The range-energy property of Sylgard-182 was investigated at the request of Goddard Space Flight Center. Sylgard-182 was not considered by Hughes as a protective shield for low energy protons because in Hughes experience this material exhibits poor thermal properties.

TABLE E-1. LOCKHEED COATING TEST*†

Cell Type Number	Gap	V_{oc}/V_{oco}	I/I_o at 0.44 volt	Type of Fix and Comments
HS-B	15-right 5-left	0.987	0.930	With coverglass - brush coated gap
HS-215	Bare	0.905	0.884	Bare cell fully coated - overheated during one hour cure - coating cracked
T-7	$B^1 = 5$ $B = 5$	0.987	0.918	With coverglass - fully coated - B^1 partially exposed
T-9	$B^1 = 5$ $B = 5$	0.982	0.882	With coverglass - brush coated gap
H - C	$B^1 = 7$ $B = 20$ Side = 5	0.975	0.883	With coverglass - Fully coated coating 2 - 2.8 mils thick
H - D	$B^1 = 12$ $B = 10$ Side = 5	0.986	0.956	With coverglass brush coated gap - Overheated during one hour cure
C - F	$B = 10$	0.998	0.996	With coverglass - brush coated gap thickness coating
C-188	Bare	0.961	0.872	Fully coated bare cell - overheated during one hour cure - (exposed bar gap ~20-30mil)

*Samples were irradiated with the 10^{14} proton spectrum

†Note: Definition of cell type symbols

HS = Heliotek (1 x 2 cm)
 T = Texas Instrument (1 x 2 cm)
 H = Heliotek (2 x 2 cm)
 C = Centralab (2 x 2 cm)

TABLE E-2. HUGHES CORRECTIVE CANDIDATE SOLUTIONS TEST

Cell Type Number	Gap	Spectrum 10^{13}		Spectrum 10^{14}		Type of Fix	Comments
		Voc/ Voco	I/Io at 0.44 volt	Voc/ Voco	I/Io at 0.44 volt		
C-500	B=20	0.996	0.992	0.991	0.986	Black epoxy cell adhesive	
C-501	B=25	1.0	1.0	0.996	1.0	Black epoxy cell adhesive	
C-502	B=25			1.000	0.999	Black epoxy paint CTL-15	
C-503	B=20			0.996	0.986	RTV-602	Too clear; hard to tell if gap entirely coated
C-504	B=25			0.984	0.998	Solathane HP-16-130 white	Partially exposed bus bar
H-505	B=15 B'=12	1.0	1.0	0.998	0.989	Black epoxy cell adhesive	
H-506	B=20 B'=9	0.995	0.986	0.991	0.965	Black epoxy cell adhesive	Partial exposure of cover-glass to proton beam
H-507	B=20 B'=3			0.989	0.975	Black epoxy paint CTL-15	Partially exposed bus bar caused by cleaning cover-slide and bus bar
H-508	B=17 B'=10			1.0	0.997	RTV-602	
H-509	B=20 B'=7			0.995	0.965	Solathane, HP 16-130 white	Coverslide completely exposed to beam, partially exposed B'
T-510	B=7 B'=0	1.0	0.996	0.987	0.974	Black epoxy cell adhesive	Typical of Texas Instrument - bus bar degradation
T-511	B=10 B'=0	0.996	0.980	0.993	0.967	Black epoxy cell adhesive	Typical of Texas Instrument - bus bar degradation
HS-515	rt. 7 left 10	0.998	0.996	0.996	1.0	Black epoxy cell adhesive	
HS-516	rt. 5 left 11	0.998	0.959	0.991	0.917	Black epoxy cell adhesive	Coverslide completely exposed to beam - 5 mil side gap exposed

TABLE E-3. SUMMARY RESULTS OF EACH OF THE CORRECTIVE SOLUTIONS IRRADIATED WITH LOW ENERGY PROTONS

Proposed Solution	Comments
LMSC solar cell coating	Easy to apply. Coating may have been too thin and therefore ineffective as a low energy proton shield.
Black epoxy cell adhesive	Easy to apply; can be seen easily; would help cell bonding problems.
Black epoxy paint CTL-15 (HP 4-112)	Too thick making it hard to apply accurately; hard to clean off of cell.
RTV-602	Much too clear; hard to tell if cell has been coated properly.
Polyurethane "Solathane" HP 16-130 white	Strings; hard to apply.

CONCLUSIONS

The black epoxy cell adhesive is the best corrective solution to the low energy bombardment on small exposed areas of solar cells for the following reasons:

- 1) Effective low energy proton shield
- 2) Easy to apply
- 3) Can be easily seen, thereby, visually showing that the exposed area of the cell is completely covered
- 4) Would help cell bonding problems

Range-energy measurements with protons show that calculated data give a good estimate of this relationship. 3.3 mils of solar cell adhesive is adequate to stop protons with energies up to 2.3 mev. Sylgard-182 behaves anomalously in range-energy measurements; the cause of this behavior has not been investigated.

Hughes wishes to thank B. S. Marks of Lockheed for both providing and applying the LMSC coating.

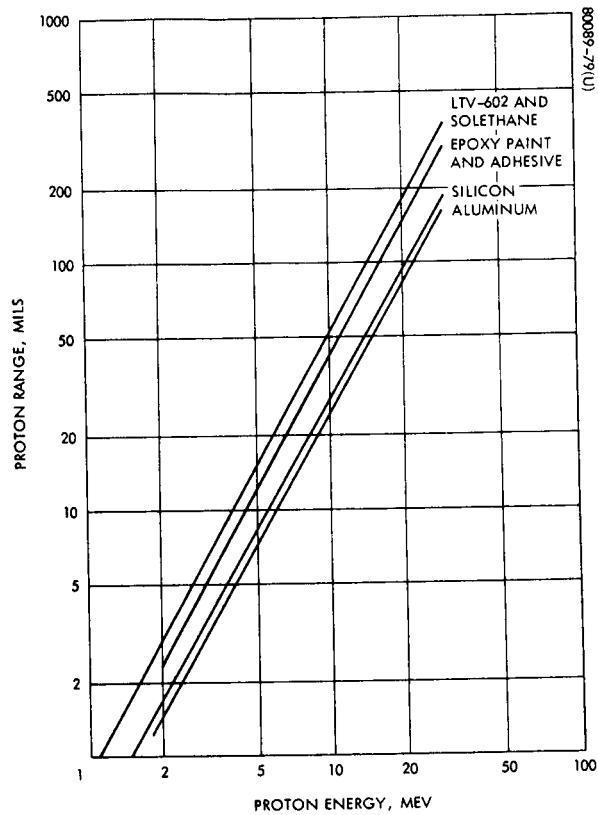


Figure E-1. Range of Protons
in Materials

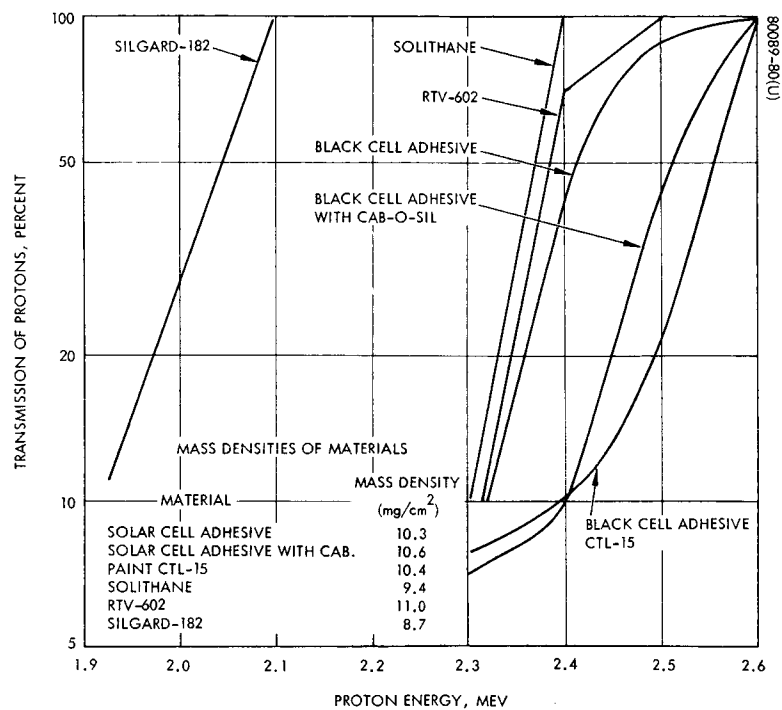


Figure E-2. Experimental Proton Range Data

APPENDIX F. ANGLE OF INCIDENCE EFFECTS ON THE PERFORMANCE OF CYLINDRICAL SOLAR PANELS

Two current degradation mechanisms are considered: degradation due to coverslide transmission losses and degradation due to losses caused by trapped proton radiation. The percent transmission loss in short circuit current is assumed to be directly proportional to the path length through the solar cell coverslide with respect to sun normal. The percent proton loss in short-circuit current is assumed to be inversely proportional to the effective illumination intensity, with respect to sun normal, at the solar cell surface. Given these assumptions, the percent degradation of short circuit current for a cylindrical array is derived as a function of percent transmission loss and percent proton loss.

DERIVATION

Let θ = azimuth angle about the cylindrical array, referenced to the plane containing the spin axis and the sun line

$D_t(0)$ = percent transmission loss at sun normal ($\theta = 0$)

$D_p(0)$ = percent proton loss at sun normal and at $D_t(0) = 0$

Since the percent transmission loss is proportional to the path length through the coverslide, it follows that

$$D_t(\theta) = D_t(0)/\cos \theta.$$

Let $R_T(\theta)$ = the fraction remaining due to transmission loss, hence

$$R_t(\theta) = 1 - \frac{D_t(\theta)}{100} = 1 - \frac{D_t(0)}{100 \cos \theta}$$

The effective normalized intensity with respect to sun normal can be defined as

$$I(\theta) = R_t(\theta) \cos \theta = \left(1 - \frac{D_t(0)}{100 \cos \theta}\right) \cos \theta$$

The percent proton loss is inversely proportional to $I(\theta)$; therefore, it can be defined as

$$d_p(\theta) = D_P(0)/I(\theta) = \frac{100 D_p(0)}{100 \cos \theta - D_t(0)}$$

Let $R_p(\theta)$ equal the fraction remaining after proton loss, hence,

$$R_p(\theta) = 1 - \frac{d_p(\theta)}{100} = 1 - \frac{D_p(0)}{100 \cos \theta - D_t(0)}$$

The fraction remaining due to the combined effects of the proton loss and the transmission loss can be expressed as

$$R_T(\theta) = R_t(\theta) R_p(\theta)$$

or

$$R_T(\theta) = \left[1 - \frac{D_t(0)}{100 \cos \theta} \right] \left[1 - \frac{D_p(0)}{100 \cos \theta - D_t(0)} \right]$$

The cylindrical array short circuit current (I_{sc}) can be calculated from the following integral:

$$I_{sc} = I_o \int_0^{\theta_c} R_T(\theta) \cos \theta d\theta$$

where

$$I_o = I_{sc} \text{ at } \theta = 0, D_t(0) = 0, \text{ and } D_p(0) = 0$$

and

$$\theta_c = \text{the angle at which } R_T(\theta) = 0$$

θ_c can be determined by setting $R_T(\theta) = 0$ and investigating the resulting relationships:

$$0 = 1 - D_t(0)/100 \cos \theta$$

and

$$0 = 1 - D_p(0)/(100 \cos \theta - D_t(0))$$

Solving for θ in each of these equations results in

$$\theta_1 = \cos^{-1} (D_t(0)/100)$$

and

$$\theta_2 = \cos^{-1} \left(\frac{D_t(0) + D_p(0)}{100} \right)$$

Since $D_t(0)$ and $D_p(0)$ are nonnegative, θ_2 is always less than or equal to θ_1 . Then, θ_c can be defined as

$$\theta_c = \theta_2 = \cos^{-1} \left(\frac{D_t(0) + D_p(0)}{100} \right)$$

since the cylindrical array short circuit current is only defined for $R_T(\theta) \geq 0$.

The expression for I_{sc} can be restated as

$$I_{sc}/I_o = \int_0^{\theta_c} \left[\cos \theta - \frac{D_t(0)}{100} \right] \left[1 - \frac{D_p(0)}{100 \cos \theta - D_t(0)} \right] d\theta$$

or

$$\begin{aligned} I_{sc}/I_o = & \int_0^{\theta_c} \cos \theta d\theta - \int_0^{\theta_c} \frac{\cos \theta D_p(0)}{100 \cos \theta - D_t(0)} d\theta \\ & - \int_0^{\theta_c} \frac{D_t(0)}{100} d\theta + \int_0^{\theta_c} \frac{D_t(0) D_p(0)}{100(100 \cos \theta - D_t(0))} d\theta \end{aligned}$$

Let $a = D_t(0)$ and $b = -100$ in the expression for I_{sc}/I_o . Then,

$$I_{sc}/I_o = \sin \theta_c + \frac{a}{b} \theta_c + D_p(0) \int_0^{\theta_c} \frac{\cos \theta}{a+b \cos \theta} d\theta + \frac{D_p(0)a}{b} \int_0^{\theta_c} \frac{d\theta}{a+b \cos \theta}$$

The third term can be reduced by the following integral formula:

$$\int_0^{\theta_c} \frac{\cos \theta d\theta}{a+b \cos \theta} = \frac{\theta_c}{b} - \frac{a}{b} \int_0^{\theta_c} \frac{d\theta}{a+b \cos \theta}$$

Substituting this relationship into the expression for I_{sc}/I_o and simplifying, results in:

$$I_{sc}/I_o = \sin \theta_c + \frac{\theta_c}{b} (a + D_p(0))$$

or

$$I_{sc}/I_o = \sin \theta_c - \frac{\theta_c}{100} (D_t(0) + D_p(0))$$

The short circuit current for a planar array can be expressed as

$$I_{sc}' = I_o R_T(0)$$

Let

$$R = I_{sc}/I_{sc}' = \frac{I_{sc}}{I_o R_T(0)}$$

Then, finally, the percent I_{sc} degradation (P) can be expressed as a function of $D_t(0)$ and $D_p(0)$ as follows:

$$P = (1 - R)100 + (1 - R_T(0))100$$

where

$$R_T(0) = \left[1 - \frac{D_t(0)}{100} \right] \left[1 - \frac{D_p(0)}{100 - D_t(0)} \right]$$

$$R = \frac{1}{R_T(0)} \left[\sin \theta_c - \frac{\theta_c}{100} (D_p(0) + D_t(0)) \right]$$

and

$$(1 - R_T(0))100 = \text{percent } I_{sc}' \text{ degradation.}$$

A plot of P versus $D_p(0)$ for different values of $D_t(0)$ is given in Figure F-1.

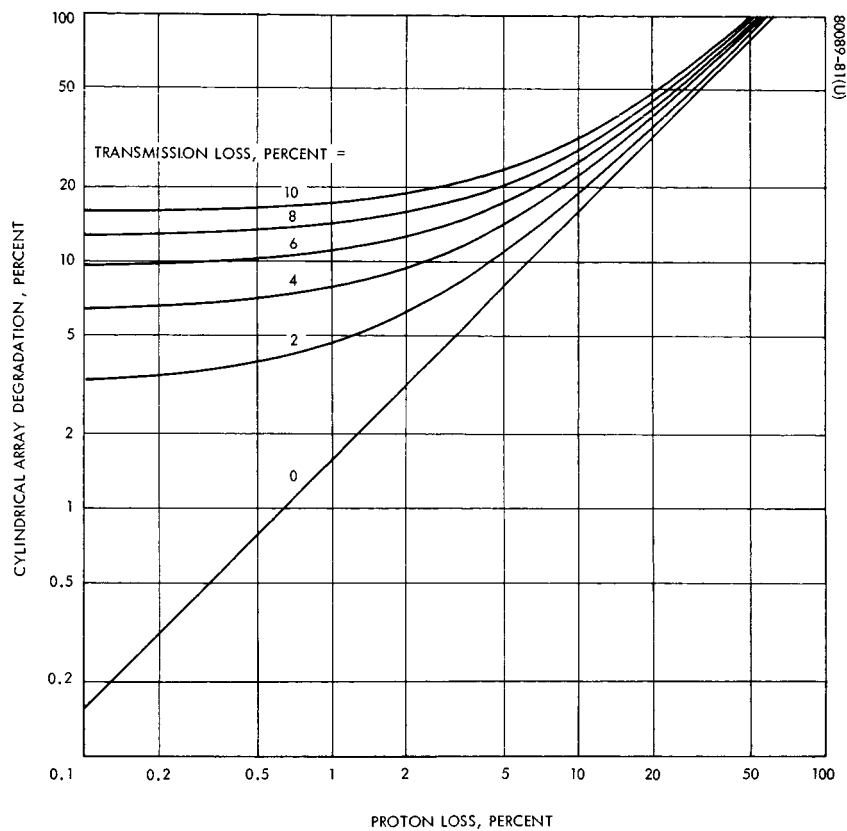


Figure F-1. Total Cylindrical Array Degradation as Function of Transmission Losses and Proton Damage